

**MULTI-SCALE DESIGN FOR DURABLE REPAIR  
OF CONCRETE STRUCTURES**

by

Mo Li

A dissertation submitted in partial fulfillment  
of the requirements for the degree of  
Doctor of Philosophy  
(Civil Engineering)  
in The University of Michigan  
2009

Doctoral Committee:

Professor Victor C. Li, Chair  
Professor Richard E. Robertson  
Associate Professor Jerome P. Lynch  
Assistant Professor Adda Athanasopoulos-Zekkos

© Mo Li

---

All rights reserved  
2009

To Mom and Dad,  
Whom I love more than I can write.

## **Acknowledgements**

This dissertation has been completed under the guidance of my advisor, Professor Victor C. Li. Without his support, inspiration, dedication of time and energy throughout the past five years I could have never completed this work. I owe forever my sincerest gratitude to him, for opening my eyes to the innovative material technology world, and for challenging me with novel research ideas capable of solving real-world problems.

I would like to thank my dissertation committee members, Professor Richard E. Robertson, Professor Jerome P. Lynch, and Professor Adda Athanasopoulos-Zekkos for their intellectual guidance, valuable comments, great patience and encouragement. The research presented in this dissertation is only possible with their help.

I would also like thank Mr. Roger Till at the Michigan Department of Transportation, for his tremendous help and valuable comments that made the development and field implementation of HES-ECC possible, Professor Shuichi Takayama and his graduate students in the Department of Biomedical Engineering, for his selfless sharing of knowledge in fluorescence technology and assistance with the fluorescence microscopic equipments, Professor Erik Schlangen at Delft University of Technology in the Netherlands, for generously providing the software FEMMASSE and guidance of use, Professor Petr Kabele at Czech Technical University in Prague for helpful discussions.

I must acknowledge the National Science Foundation for funding of Materials Use: Science, Engineering, and Society (MUSES) Biocomplexity Grants CMS-0223971 and CMS-0329416, the National Science Foundation for funding of Cyberinfrastructure Training, Education, Advancement, and Mentoring for Our 21<sup>st</sup> Century Workforce (CI-

TEAM) Grant OCI-0636300, the Michigan Department of Transportation, and Metamorphix Global, Inc., all of which supported much of my research.

I would like to thank my colleagues and my friends at the Advanced Civil Engineering Materials Research Laboratory, Dr. Shuxin Wang, Dr. Yun Y. Kim, Dr. Martin Weimann, Dr. Michael D. Lepech, Dr. Shunzhi Qian, Dr. En-Hua Yang, Dr. Andrea Spagnoli, Dr. Yingzi Yang, Dr. Estela Garces, Mr. Jian Zhou, Ms. Lili Kan, Mr. Matthew Fadden, Mr. Ravi Ranade, and Mr. Michael Stults for making my life at ACE-MRL and CEE concrete mixing labs full of inspiration and joy. I would also like to thank Dr. Tsung-Chin Hou for his friendship and great help during my studies.

I am grateful to Ms. Debbie Hemmeter, Ms. Janet Lineer, Ms. Reta Teachout, Ms. Linda Fink, Ms. Kimberly Bonner, Ms. Kimberly Smith, Ms. Jill Miller, Ms. Kimberly Gauss, and Ms. Patricia Mackmiller for unparalleled assistance in administrative matters, and to Mr. Merrick Burch, Mr. Jan Pantolin, Mr. Robert Fischer, and Mr. Robert Spence for their greatly helpful technical support.

To my dearest and best friends for life, Dr. Hao Chen, Zhiyu Luo, Dr. Minhua Shao, Dr. Jiexin Lian, Xiaoqun Huang, Chonglong Fu, and Yan Li, only with their great patience and support was I able to start and enjoy such a wonderful adventure in the U.S.

Finally, I could never have attempted any of this without the love and support of the greatest parents in the world, Ping Gao and Gongda Li. I owe a great deal to Alphonse Anderson. Without his tremendous help and unconditional support I would have never been able to achieve this. I cannot thank you enough Fonz.

## Table of Contents

<b>Dedication</b>	ii
<b>Acknowledgements</b>	iii
<b>List of Tables</b>	x
<b>List of Figures</b>	xiii
<b>Chapter</b>	
<b>1. INTRODUCTION</b>	1
1.1 Deterioration in Concrete Structures – Major Durability Concerns	4
1.1.1 Bridges	5
1.1.2 Highways and Roadways	13
1.1.3 Parking Structures	16
1.2 Limitation of Current Approaches to Improve Durability of Concrete Structures	18
1.2.1 Effectiveness of current material “durability” solutions	19
1.2.2 Compatibility of new repair with existing concrete substrate	22
1.2.3 Some considerations of current repair performance characterization	25
1.3 Proposed Approach	27
1.4 Engineered Cementitious Composites	30
1.5 Research Motivation and Objectives	33
1.6 Research Scope and Dissertation Organization	35
<b>2. Micromechanics Based Design of ECC Repair Materials</b>	63
2.1 High Performance Fiber Reinforced Cementitious Composites	65
2.2 ECC Micromechanics Based Design Theory	67
2.2.1 ECC Design Framework – Scale Linking	67
2.2.2 Conditions for Tensile Strain Hardening	68
2.2.3 Condition for Saturated Multiple Microcracking	71

2.3 High Early Strength Engineered Cementitious Composites	75
2.3.1 Background	75
2.3.2 High Early Strength Requirements	77
2.3.3 Methods of Achieving High Early-Age Compressive Strength	79
2.3.4 Initial Material Composition Selection Based on Strength Requirements	84
2.3.4.1 Experimental Program	84
2.3.4.2 Compression Test Results and Discussion	87
2.3.5 Microstructure Tailoring for Tensile Ductility	90
2.3.5.1 Initial Composite Testing in Uniaxial Tension	90
2.3.5.2 Microstructure Tailoring of Mix 6 for Tensile Ductility	91
2.3.6 HES-ECC Material Characterization	98
2.4 Conclusions	104
<b>3. ECC Processing and Quality Control for Optimized Material Properties and Robustness</b>	145
3.1 Introduction	146
3.2 Effect of Processing on ECC Micromechanical Parameters	149
3.3 Experimental Program	152
3.3.1 Materials	153
3.3.2 Mixing, Testing of Fresh Properties, and Casting	154
3.3.3 Testing of Hardened Tensile Properties	156
3.3.4 Measurement of Fiber Dispersion Coefficient	157
3.4 Experimental Results and Discussion	158
3.5 Rheology Control Concept and Case Study	163
3.6 Conclusions	165
<b>4. Effect of Material Ductility on Restrained Volume Change Induced Cracking and Interfacial Delamination</b>	182
4.1 Introduction	183
4.2 Proposed Approach	188
4.3 Free Shrinkage of HES-ECC	191

4.3.1 Background	191
4.3.2 Materials and Experimental Procedure	194
4.3.3 Experimental Results and Discussion	196
4.4 Restrained Shrinkage Ring Test	197
4.4.1 Materials and Experimental Procedure	197
4.4.2 Experimental Results and Discussion	198
4.5 Restrained Shrinkage Test on a Simulated Repair System	200
4.5.1 Materials	200
4.5.2 Repair Specimen Configuration and Surface Preparation	201
4.5.3 Experimental Results and Discussion	203
4.6 Effects of Surface Preparation on the Repaired System Performance	207
4.6.1 Experimental Procedure	208
4.6.2 Experimental Results and Discussion	209
4.7 Numerical Study on the Simulated Repair System	212
4.7.1 Problem Formulation and FEM Model	212
4.7.2 Numerical Simulation Results	214
4.8 Simplified Analytical Model for the Repair Systems under Restrained Volume Change	216
4.9 Conclusions	220
<b>5. Influence of Material Ductility on Reflective Cracking in Overlay Repairs</b>	<b>252</b>
5.1 Introduction	253
5.2 Ductile ECC Overlay	257
5.3 Experimental Program	259
5.3.1 Specimen Configuration and Loading Conditions	259
5.3.2 Materials and Specimen Preparation	260
5.4 Experimental Results	262
5.4.1 Overlay System Monotonic Flexural Performance	262
5.4.2 Overlay System Fatigue Performance	266
5.5 Conclusions	268

<b>6. Transport Properties of ECC under Chloride Exposure</b>	287
6.1 Steel Corrosion in Concrete Structures	288
6.2 Proposed Approach – ECC Microcracking Phenomenon	290
6.3 Transport Properties of Cementitious Materials	292
6.4 Experimental Program	297
6.4.1 Materials and Mixture Proportions	297
6.4.2 Specimen Preparation and Testing	298
6.5 Experimental Results and Discussion	302
6.6 Conclusions	307
<b>7. Effect of Cracking and Healing on the Durability of ECC under Combined Aggressive Chloride Environment and Mechanical Loading</b>	328
7.1 Introduction	329
7.2 Evidence of Self-Healing of ECC Microcracks and Recovery of Chloride Transport Properties	331
7.3 Experimental Program	334
7.3.1 Testing of Composite Properties	334
7.3.2 Measurement of Micromechanical Properties	335
7.4 Experimental Results and Conclusions	337
7.5 Conclusions	341
<b>8. Large-Scale Processing and Field Demonstration of High Early Strength Cementitious Composites in Bridge Repair</b>	353
8.1 Background	354
8.2 Optimization of HES-ECC Ingredients and Mixing Procedure for Larger Scale Applications	356
8.2.1 Fiber Length Change	356
8.2.2 Hydration Stabilizing Admixtures	358
8.2.3 Batching Sequence	359
8.3 HES-ECC Larger Scale Trial Batching	361
8.3.1 One Cubic Feet Batching	361

8.3.2 Three Cubic Feet Batching and Six Cubic Feet Batching	362
8.4 HES-ECC Material Cost Effectiveness	364
8.5 HES-ECC Patch Repair Demonstration	371
8.6 Long-Term Monitoring of HES-ECC Patch Repair Performance	372
8.7 Conclusions	374
<b>9. Concluding Remarks</b>	<b>402</b>
9.1 Research Overview and Findings	402
9.1.1 Material Engineering for Durable Repair Materials	403
9.1.2 Durability Assessment of ECC/Concrete Repair System	407
9.1.3 Field Application of ECC Repair Materials	415
9.2 Impact of Research	417
9.3 Recommendations for Future Research	420

## List of Tables

Table 2.1	Three phases of ECC microstructure and corresponding micro-parameters.	107
Table 2.2	List of materials used.	108
Table 2.3	Mixing proportions for initial material composition selection based on strength requirements.	109
Table 2.4	Properties of REC 15 PVA fiber from Kuraray, Co, Japan.	109
Table 2.5	Compressive strength of Mix 1 and 2 at different ages.	110
Table 2.6	Compressive strength of Mix 3, 4 and 5 at different ages.	110
Table 2.7	Compressive strength of Mix 6 (w/ and w/o insulation) at different ages.	111
Table 2.8	Mixing proportion of HES-ECC before / after adding artificial flaws.	111
Table 2.9	Mix proportion of HES-ECC.	112
Table 2.10	HES-ECC tensile properties at different ages (mean $\pm$ standard deviation).	112
Table 2.11	HES-ECC compressive properties at different ages (mean $\pm$ standard deviation).	113
Table 2.12	HES-ECC flexural properties at different ages (mean $\pm$ standard deviation).	113
Table 3.1	Mix proportion of materials.	168
Table 3.2	Material fresh and hardened properties.	169
Table 3.3	Mix proportion of WHITE ECC.	169
Table 4.1	General requirements of patch repair materials for structural compatibility.	224
Table 4.2	Mix proportion of the investigated materials.	224
Table 4.3	Mechanical properties of the investigated materials.	225
Table 4.4	HES-ECC tensile properties at different ages.	225

Table 4.5	Theoretical parametric values of the investigated materials.	226
Table 4.6	Restrained drying shrinkage crack width development with age.	226
Table 4.7	Estimated material cracking potentials, RH=45%.	226
Table 4.8	Interface delamination and surface cracking of HES-Concrete, HES-SFRC, and HES-ECC layered repair systems at the age of 60 days.	227
Table 4.9	Material composition, 28-day mechanical properties and cracking potential.	228
Table 4.10	Interface delamination and surface cracking of concrete, SFRC and ECC layered repair systems.	228
Table 4.11	Interface property values in FEM model.	229
Table 5.1	Modulus of rupture of HES-ECC and HES-Concrete overlays under monotonic loading.	270
Table 5.2	Center deflection (upon failure) of HES-ECC and HES-Concrete overlays under monotonic loading.	270
Table 5.3	Interfacial delamination (upon failure, including initial delamination) of HES-ECC and HES-Concrete overlays under monotonic loading.	271
Table 6.1	Permissible crack widths for reinforced concrete under service loads according to ACI Committee 224.	310
Table 6.2	Mixture proportions and properties of ECC and mortar.	310
Table 6.3	Mechanical properties of PVA fiber.	311
Table 6.4	Crack widths, numbers and depths of pre-loaded ECC and mortar prisms.	311
Table 6.5	Chloride ponding test – Effective diffusion coefficient.	311
Table 7.1	Tensile properties of ECC under different combinations of pre-loading and chloride exposure conditions.	343
Table 8.1	ECC material mixing proportions.	377
Table 8.2	Tensile properties of HES-ECC with 0.33 in. (8.4 mm) PVA fiber.	377
Table 8.3	Larger scale HES-ECC mixing proportions and batching weights.	378
Table 8.4	Larger scale HES-ECC batching sequence and time.	378
Table 8.5	Flowability test results from one & six cubic feet (0.03 & 0.17 cubic meter) batching.	379

Table 8.6	Compressive Strength development of HES-ECC from one & six cubic feet (0.03 & 0.17 cubic meter) batching.	379
Table 8.7	Tensile properties of HES-ECC from one & six cubic feet (0.03 & 0.17 cubic meter) batching.	380
Table 8.8	Minimum requirements of HES-ECC material.	380

## List of Figures

Figure 1.1	Concrete Structure Deterioration, Damage, and Defect.	40
Figure 1.2	Deterioration of Kurtsubo Bridge, Japan: (a) Rust signs before the first repair; (b) Tendon corrosion and breakage before the second repair.	41
Figure 1.3	Life cycle cost of Kurtsubo Bridge, Japan.	41
Figure 1.4	Bridge deck transverse cracking.	42
Figure 1.5	Steel corrosion and spalling in concrete bridges in Michigan.	42
Figure 1.6	Pavement overlay reflective cracking.	43
Figure 1.7	Deterioration in parking structures.	43
Figure 1.8	Model of concrete slab restrained against shrinkage and (b) the crack width $w$ controlled by the tension-softening curve.	44
Figure 1.9	Schematic plot of crack width $w$ as a function of shrinkage strain $\epsilon_s$ .	44
Figure 1.10	Integrated Multi-Scale Material & Structural Engineering Framework for durability of repaired concrete structures.	45
Figure 1.11	Disconnected Material Engineering and Structural Engineering Design Philosophies for durability of repaired concrete structures.	46
Figure 1.12	Typical tensile stress-strain curve of ECC.	47
Figure 1.13	Driving surface static friction tester.	48
Figure 1.14	Relative dynamic modulus vs. number of freeze thaw cycles.	48
Figure 1.15	Mihara Bridge with ECC/steel composite deck opened to traffic in April 2005, Japan.	49
Figure 1.16	ECC link slab on the Grove Street Bridge over I-94 opened to traffic in October 2005, Michigan.	49
Figure 2.1	Uniaxial tensile stress-deformation relation of concrete, FRC, and HPCRCC.	114
Figure 2.2	Scale linking in ECC Material Development .	115

Figure 2.3	Typical fiber bridging stress vs. crack opening $\sigma(\delta)$ curve for a tensile strain-hardening composite.	115
Figure 2.4	Steady-state cracking with a constant crack opening .	116
Figure 2.5	Theoretically predicted effect of initial flaw size on the cracking strength of PVA-ECC.	116
Figure 2.6	State and federal compressive strength requirements, and target compressive strength at different ages for HES-ECC.	117
Figure 2.7	Uniaxial compressive test setup.	117
Figure 2.8	Effect of cement type on compressive strength development.	118
Figure 2.9	Effect of water/cement ratio on compressive strength development.	118
Figure 2.10	Effect of accelerator on compressive strength development.	119
Figure 2.11	Effect of curing condition on compressive strength development.	119
Figure 2.12	Uniaxial tensile test setup.	120
Figure 2.13	Dimensions of tensile test specimen.	120
Figure 2.14	Tensile stress-strain curves of Mix 6 at ages of 4h, 24h, 3d, 7d, and 28d.	122
Figure 2.15	Age dependency of tensile strain capacity of Mix 6.	123
Figure 2.16	Age dependency of tensile strength of Mix 6.	123
Figure 2.17	Matrix fracture toughness test set-up.	124
Figure 2.18	Single fiber pull-out test set-up.	124
Figure 2.19	General profile of a single fiber pullout curve.	125
Figure 2.20	Age dependency of matrix fracture toughness.	125
Figure 2.21	Age dependency of matrix/fiber interface chemical bond.	126
Figure 2.22	Age dependency of matrix/fiber interface frictional stress.	126
Figure 2.23	Age dependency of slip hardening coefficient.	127
Figure 2.24	Evolution of tensile strain capacity and $J_b'/J_{tip}$ ratio with age (Mix 6).	128
Figure 2.25	Optimization scheme for pre-existing flaw size distribution in matrix.	129
Figure 2.26	Aggregates used as artificial flaws: polystyrene (PS) beads.	129
Figure 2.27	Age dependent tensile stress vs. strain curve of Mix 7.	131
Figure 2.28	Age dependency of tensile strain capacity.	132
Figure 2.29	Effect of PS beads on compressive strength development.	133

Figure 2.30	HES-ECC tensile strength development with age.	134
Figure 2.31	HES-ECC Young's modulus (E) development with age.	134
Figure 2.32	HES-ECC tensile strain capacity development with age.	135
Figure 2.33	HES-ECC multiple micro-cracking pattern at different ages.	135
Figure 2.34	HES-ECC compressive strength development with age.	136
Figure 2.35	Compressive strength (average value) development of HES-ECC compared with requirements by DOTs and FHWA.	136
Figure 2.36	Third-point bending test setup and specimen dimensions.	137
Figure 2.37	HES-ECC flexural stress – displacement curves at 4 hours, 24 hours, and 28 days.	137
Figure 3.1	Variation in tensile stress vs. strain curves of ECC with same mixing proportion.	170
Figure 3.2	Effect of fiber dispersion on $\sigma(\delta)$ curve and $c_{mc}$ .	170
Figure 3.3	Experimental program.	171
Figure 3.4	Rheology properties tests: (a) Viskomat NT rotational viscometer (b) marsh cone flow rate test (c) mini-slump test.	171
Figure 3.5	Specimen preparation for measuring fiber dispersion at the final failure section.	172
Figure 3.6	Fluorescence imaging technology.	173
Figure 3.7	Fluorescence imaging test setup.	173
Figure 3.8	Marsh cone flow time versus plastic viscosity.	174
Figure 3.9	Mini-slump flow diameter of the seven ECC mixes before/after adding fibers.	174
Figure 3.10	Tensile stress versus strain curves of ECC with different VMA content.	175
Figure 3.11	Tensile strain capacity vs. VMA/cement ratio (error bars describe standard error of the data).	176
Figure 3.12	Tensile strength vs. VMA/cement ratio (error bars describe standard error of the data).	176
Figure 3.13	Fluorescence image of a sample specimen.	177

Figure 3.14	Relation between marsh cone flow time before adding fiber, fiber dispersion coefficient, and tensile strain capacity.	178
Figure 3.15	Effect of rheology control on tensile properties of WHITE ECC.	179
Figure 4.1	Typical deterioration process of concrete repair.	230
Figure 4.2	Schematics of typical failure modes in layered repair system.	231
Figure 4.3	Illustration of the Kelvin Equation.	231
Figure 4.4	Free drying shrinkage test.	232
Figure 4.5	Experimental data and theoretical curves of hygral deformation vs. relative humidity.	232
Figure 4.6	Restrained shrinkage steel ring test.	233
Figure 4.7	Restrained shrinkage crack width development as a function of drying time (at RH = 45 ± 5%).	234
Figure 4.8	Layered repair system test set-up under restrained shrinkage.	235
Figure 4.9	Free shrinkage strain of repair materials at different ages.	235
Figure 4.10	Repair surface cracking at the age of 60 days.	236
Figure 4.11	Interface delamination profiles of repaired systems.	237
Figure 4.12	Specimen end delamination height at different ages.	238
Figure 4.13	FEM model of layered repair system.	239
Figure 4.14	Assumed tensile behavior of (a) HES-Concrete, (b) HES-SFRC, (c) HES-ECC materials, and (d) combined for all three materials.	239
Figure 4.15	Interface model: combined uniaxial stress-strain relation in the normal direction with influence of shear slip.	240
Figure 4.16	Predicted crack width of (a) HES-Concrete, (b) HES-SFRC and (c) HES-ECC repair layer at the age of 60 days.	241
Figure 4.17	Predicted stress distribution ( $\sigma_{xx}$ ) in the (a) HES-Concrete, (b) HES-SFRC and (c) HES-ECC repaired system at the age of 60 days.	242
Figure 4.18	Predicted interface shear stress ( $\sigma_{xy}$ ) of (a) HES-Concrete, (b) HES-SFRC and (c) HES-ECC repaired system.	243
Figure 4.19	Concrete repair subjected to differential shrinkage.	244
Figure 4.20	Simplified tensile stress-strain curve of ECC.	244

Figure 4.21	Analytical model predicted tensile stress in ECC repair $\sigma_{xx}$ , repair/old interfacial tensile stress $\sigma_{yy}$ and shear stress $\sigma_{xy}$ .	245
Figure 5.1	Crack-and-sealed pavement surface.	272
Figure 5.2	Rubblized pavement surface.	272
Figure 5.3	Paving fabric installation.	273
Figure 5.4	HMA interlayer installation.	273
Figure 5.5	Overlay saw and seal.	274
Figure 5.6	Specimen configuration and loading conditions.	274
Figure 5.7	Specimen preparation.	275
Figure 5.8	Concrete substrate surface preparation.	276
Figure 5.9	“Kinking and trapping” mechanism.	276
Figure 5.10	Flexural behavior of HES-ECC and HES-Concrete layered repair system under monotonic loading: (a) smooth interface; (b) rough interface.	277
Figure 5.11	Modulus of rupture (MOR) of HES-ECC and HES-Concrete overlay systems under monotonic loading. (a) Overlay age of 6 hours. (b) Overlay age of 28 days.	278
Figure 5.12	Deflection at failure of HES-ECC and HES-Concrete overlay systems under monotonic loading. (a) Overlay age of 6 hours. (b) Overlay age of 28 days.	279
Figure 5.13	Interfacial delamination upon failure of HES-ECC and HES-Concrete overlay systems under monotonic loading. (a) Overlay age of 6 hours. (b) Overlay age of 28 days.	280
Figure 5.14	Crack pattern of HES-ECC and HES-Concrete overlay systems at overlay age of 28 days. Epoxy glue was spread over the cracking sections of HES-ECC overlays (a) and (b), to better visually reveal multiple microcracking.	281
Figure 5.15	Fatigue stress-fatigue life relation (log) for HES-ECC and HES-Concrete overlay systems.	282
Figure 6.1	Corrosion in Concrete Structures.	312
Figure 6.2	Corrosion process of reinforcing steel according to Tuutti.	313

Figure 6.3	Coefficient of permeability versus crack width for ECC and reinforced mortar series deformed to 1.5% in uniaxial tension.	313
Figure 6.4	Typical tensile stress-strain response of ECC mixture.	314
Figure 6.5	Immersion test. (a) Cylinders were stored under continuous exposure to 3% NaCl solution. (b) One cylinder was taken out, split open, and sprayed with 0.1-N silver nitrate (AgNO <sub>3</sub> ) solution, to measure the chloride penetration depth.	315
Figure 6.6	Four point bending test.	315
Figure 6.7	Salt ponding test on uncracked and cracked beam specimens.	316
Figure 6.8	Typical crack pattern on positive moment surface of ECC beams at 2 mm (0.079 in.) deformation.	317
Figure 6.9	Chloride penetration depth variation measured by immersion test.	317
Figure 6.10	Chloride profiles of uncracked mortar and uncracked ECC prisms after 30 and 90 days in 3% NaCl solution.	318
Figure 6.11	Chloride profiles of mortar and ECC prisms in cracked zone at 30 days exposure.	319
Figure 6.12	Diffusion coefficient versus crack width for mortar deformed under bending load.	320
Figure 6.13	Diffusion coefficient versus number of cracks for ECC.	320
Figure 6.14	Diffusion coefficient versus pre-loading deformation level for ECC and mortar.	321
Figure 6.15	Self-healing products in ECC microcracks before and after salt ponding test at 30 days exposure.	322
Figure 6.16	ESEM micrograph of rehydration products in a self-healed crack.	322
Figure 7.1	Comparison of allowable crack widths under marine exposure.	344
Figure 7.2	Typical pre-cracking tensile stress-strain curves of ECC.	344
Figure 7.3	Tensile stress-tensile strain curves of ECC specimens before and after exposure to 3% NaCl solution.	346
Figure 7.4	Influence of NaCl exposure time and applied strain level on ECC ultimate tensile strength.	347

Figure 7.5	Influence of NaCl exposure time and applied strain level on ECC tensile strain capacity.	347
Figure 7.6	Influence of NaCl solution exposure time on ECC matrix fracture toughness.	348
Figure 7.7	Influence of NaCl solution exposure time on ECC matrix/fiber interfacial chemical bond.	348
Figure 7.8	Influence of NaCl solution exposure time on ECC fiber/matrix interfacial frictional bond.	349
Figure 7.9	Influence of NaCl solution exposure time on ECC PSH Index.	349
Figure 8.1	PVA fiber, 0.5 in. (12.7 mm) and 0.33 in. (8.4 mm).	381
Figure 8.2	Tensile stress-strain curves of HES-ECC with 0.33 in. (8.4 mm) PVA fiber.	381
Figure 8.3	Loss of deformability of HES-ECC with and without hydration stabilizer.	382
Figure 8.4	Gravity mixer with capacity of two cubic feet (0.057 cubic meters).	382
Figure 8.5	HES-ECC one cubic feet (0.03 cubic meter) mixing.	384
Figure 8.6	Loss of deformability of HES-ECC processed in one cubic feet (0.03 cubic meter) batching.	384
Figure 8.7	Compressive strength development of HES-ECC from one cubic feet batching.	385
Figure 8.8	Tensile stress-strain curves of HES-ECC from one cubic feet batching.	385
Figure 8.9	Gravity mixer with capacity of 9 cubic feet (0.25 cubic meters).	386
Figure 8.10	HES-ECC six cubic feet (0.17 cubic meters) mixing.	388
Figure 8.11	Loss of deformability of HES-ECC processed in six cubic feet (0.17 cubic meters) batching.	389
Figure 8.12	Compressive strength development of HES-ECC from 6 cubic feet (0.17 cubic meter) batching.	389
Figure 8.13	Tensile strain capacity development of HES-ECC from 6 cubic feet (0.17 cubic meters) batching.	390
Figure 8.14	Uniaxial tensile test plate dimensions.	390

Figure 8.15	Ellsworth Road Bridge over US-23 (S07 of 81074).	391
Figure 8.16	Bridge deck cracking.	391
Figure 8.17	Partial depth removal.	391
Figure 8.18	Sandblasting of patch area.	392
Figure 8.19	Replacement of damaged reinforcement.	392
Figure 8.20	Completed patch repair preparation.	392
Figure 8.21	Separated patch areas for HES-ECC repair and Thoroc 10-60 repair.	393
Figure 8.22	12 cubic foot (0.34 cubic meter) capacity gas mixer.	393
Figure 8.23	Pouring HES-ECC into wheelbarrow for transportation.	393
Figure 8.24	HES-ECC was poured into patch.	394
Figure 8.25	HES-ECC shows self-compacting property.	394
Figure 8.26	Placement of Thoroc 10-60.	394
Figure 8.27	Comparison of HES-ECC patch repair and Thoroc 10-60 patch repair.	395
Figure 8.28	Completed patch repair work.	395
Figure 8.29	Maximum surface crack width of HES-ECC and Thoroc 10-60 patch repairs.	396
Figure 8.30	Maximum interfacial delamination width of HES-ECC and Thoroc 10-60 patch repairs.	396
Figure 8.31	Surface cracking in HES-ECC patch repair, on September 18, 2009.	397
Figure 8.32	Surface cracking in Thoroc 10-60 patch repair, on September 18, 2009.	398
Figure 8.33	Interfacial delamination between HES-ECC patch repair and existing concrete, on September 18, 2009.	399
Figure 8.34	Interfacial delamination between Thoroc 10-60 patch repair and existing concrete, on September 18, 2009.	399
Figure 8.35	Exposure of aggregates in Thoroc 10-60 patch repair close to the Thoroc 10-60/HES-ECC interface area, on September 18, 2009.	400

## CHAPTER 1

### INTRODUCTION

Concrete infrastructure supports the operation of society, and provides the services and facilities necessary for an economy to function<sup>1</sup>. Concrete is the most heavily used man-made material in the world<sup>2</sup>. It has been the predominant construction material for centuries because of its widely available ingredients (e.g. cement, sand, gravel, water), capacity for taking on different forms, and low cost. Annually, more than one cubic meter of concrete per person on Earth is made<sup>3</sup>, and more than 380 million cubic meters of concrete (almost 1.5 cubic meters per person) are placed every year to support the U.S. infrastructure<sup>4</sup>. The volume of in-place concrete in the U. S. is estimated at 7 billion cubic meters (25 cubic meters per person) and most of the concrete is more than 20 years old<sup>4</sup>.

Concrete infrastructure, both new and repaired, is suffering deterioration, damage, and defects<sup>5, 6, 7, 8</sup> (Figure 1.1). Concrete deteriorates over time under service loading conditions when subjected to combined environmental and mechanical conditions. For

example, saturated concrete exposed to freeze-thaw cycles may experience disintegration; Restrained shrinkage often causes early-age cracking in concrete; Chloride penetration from deicing salts or seawater through cracks, carbonation of concrete, or inadequate concrete cover depth can result in reinforcement corrosion; Expansion of corrosion products can cause spalling and delamination of the concrete cover; Mechanical loading such as fatigue combining with environmental effects will accelerate and aggravate the deterioration process. Concrete damage is normally caused by short-term severe loading conditions such as fire, earthquakes, chemical spills, overloading, or impact. This may result in cracking, immediate spalling, disintegration, or complete failure of the concrete element or structure. Concrete defects are caused by improper detailing or design, construction practices, human error, or materials with improper quality control that result in premature deterioration, aesthetic issues, or inadequate structural capacity. The lack of durability in concrete infrastructure due to deterioration, damage, and defects drives a repair industry that supports researchers, engineers, architects, material manufacturers, equipment suppliers, testing companies, contractors, lawyers, and educators. For owners, the annual cost of concrete repair (including protection and strengthening) is estimated at \$18 billion to \$21 billion in the U.S. alone<sup>9</sup>.

Lack of durability in concrete infrastructure has become a looming threat that could jeopardize the world's prosperity and our quality of life. Although infrastructure deterioration might not be as dramatic as damage from fires or earthquakes, the magnitude of this problem in terms of structural life cycle economic, social, and environmental impacts under service loading conditions dwarfs those associated with failures under severe loading conditions. The economic impacts are associated with the

high cost of maintaining, repairing or replacing deteriorating structures, which is exceedingly burdensome on building owners, departments of transportation, the insurance industry and society. According to the American Society of Civil Engineers (ASCE) 2009 Report Card<sup>10</sup> for U.S. Infrastructure, an average grade of D (poor) was assigned over 12 infrastructure categories. ASCE estimated that USD 2.2 trillion is needed over the next five years for repair and retrofit. Correspondingly, repair and retrofit cost has been estimated to be USD 2 trillion for Asia's infrastructure. In Europe, Japan, Korea, and Thailand, the annual cost for repair has exceeded that for new construction<sup>11</sup>. The social impacts include construction-related congestion, operations interruption, wasted time and fuel cost, vehicle damage due to bad road conditions, and safety concerns. Environmental sustainability, which has become a compelling issue with the current depletion of raw materials and climate change, has been greatly compromised by infrastructure deterioration, repair and reconstruction cycles, which involve significant amounts of raw materials and energy consumption as well as greenhouse gas emissions. To battle these impacts, an effective repair methodology that addresses the underlying concrete durability problems and extends the service life of deteriorating concrete structures is urgently needed.

While countless materials and techniques are used in practice to meet the demand for rapid, inexpensive and durable concrete repairs, few of them target the inherent material shortfall of concrete as a brittle material that cracks and fractures in many applications, leading to further deterioration. It has been estimated that almost half of all concrete repairs fail prematurely<sup>12</sup>. Many undesirable repair behaviours can be observed in the field in the form of early age surface cracking, spalling, or interface delamination

between the repair and the concrete substrate. Delamination and cracking provide routes for chlorides, oxygen, moisture, alkali, and sulphates to penetrate into the repaired system and accelerate further deterioration. Additionally, the loss of structural integrity impairs load transfer between the repair and the concrete substrate. As a result, the repaired concrete structure with unsatisfactory performance and a short service life must be further maintained or repaired, leading to repeated repairs and significantly increased structural life cycle cost.

The Kurtsubo Bridge is a case in point. This bridge, located in a coastal area in Japan, experienced severe corrosion of the post-tensioned tendons<sup>13</sup> due to ingress of chloride through the concrete cover (Figure 1.2). After the first repair the corrosion was not inhibited and the deterioration continued, until severe corrosion and breakage of the tendons necessitated the second repair. After two repairs and one rehabilitation (the latter is more targeted on increasing structural capacity besides restoring serviceability<sup>14</sup>), the bridge was finally replaced. Consequently, after 40 years of service life, the total cost of the prematurely deteriorated bridge was 3.8 times greater than the initial cost of its design and construction (Figure 1.3). The life cycle cost analysis of the Kurtsubo Bridge illustrates that the lack of durability of repairs can result in high maintenance costs that greatly exceed initial construction costs.

## **1.1 Deterioration in Concrete Structures – Major Durability Concerns**

Concrete structure deterioration results from the combined effects of various environmental and mechanical loading conditions throughout the structure's service life. In this section, common deterioration modes in typical concrete structures, i.e. bridges,

roadways and highways, and parking structures, are reviewed. According to Emmons and Sordyl 2006<sup>4</sup>, the total annual cost of repairs, rehabilitation, strengthening, and protection of concrete structures in the U.S. is \$18-21 billion, with \$8 billion, \$4 billion and \$1 billion needed for bridges, highways and roadways, and parking structures, respectively.

### **1.1.1 Bridges**

Repair need and cost for bridges in the U.S. has been rising as the bridge fleet age increases. In the U.S., bridges were typically built with an expected service life of 50 years, and their average age is now 43<sup>15</sup>. According to the U.S. Department of Transportation, of the 600,905 bridges in the U.S. as of December 2008, 12.1% were categorized as structurally deficient, and 14.8% were categorized as functionally obsolete<sup>16</sup>. A structurally deficient bridge may either be closed or restrict traffic due to limited load carrying capacity. Although not unsafe, they pose limits to vehicle speed and weight. A functionally obsolete bridge has outdated design geometries and features. Although not unsafe, they cannot accommodate current traffic volumes, vehicle sizes and weights. These structurally deficient and functionally obsolete bridges require frequent maintenance, repair, and reconstruction, leading to construction-related traffic congestion and lengthy detours, and eventually resulting in significant economic, social, and environmental costs to society<sup>17</sup>. To address bridge needs, AASHTO<sup>18</sup> estimated in 2008 that the repair cost for bridges in the U.S. would amount to \$140 billion – about \$48 billion to repair structurally deficient bridges and \$91 billion to improve functionally obsolete bridges.

### Bridge deck transverse cracking

Transverse cracking (Figure 1.4) in bridge decks is one of the dominant deterioration problems in bridges in many states in the U.S.<sup>19,20,21,23,26,27</sup>. It is estimated that more than 100,000 bridges in the United States have early-age transverse cracks<sup>22</sup>, and these cracks have been observed in most geographical locations on many superstructure types<sup>22</sup>. Some of these cracks form right after construction, and some after the bridge has been opened to traffic for a period of time. Transverse cracks usually form when concrete is set<sup>23,24,25</sup>, and then widen with time. These cracks are typically full depth, are often observed over transverse reinforcement<sup>22,23,25,26,27</sup>, and are spaced 1-3 m apart along the length of the bridge<sup>23,24,28</sup>. These cracks reduce the service life of the bridge deck, and increase maintenance and repair costs during the bridge's life cycle. They accelerate chloride penetration into the concrete and initiate corrosion of reinforcements, especially in marine environments or regions where deicing salts are applied in winter<sup>26,29</sup>. Corrosion damage has even been observed on epoxy coated reinforcing bars in bridge decks with such cracks<sup>29,30</sup>. Furthermore, freeze-thaw cycles of water in cracks and leakage of water to supporting structures may also reduce the service life of a bridge.

The cause of bridge deck transverse cracking is tensile stress induced by restrained volume change of concrete, such as drying shrinkage, autogenous shrinkage, thermal effects, and creep. The magnitude of volume change in concrete depends on its ingredients, composition, and environmental conditions, such as ambient temperature and humidity. The degree of restraint, which is most commonly due to the deck and girder composite behavior, depends on bridge design characteristics, such as boundary

conditions and relative stiffness of the superstructure. Although the relative importance of these factors is not completely quantified yet, drying shrinkage is considered by many studies to be the major cause of concrete deck cracking<sup>22, 23, 31, 32, 33, 34, 35, 36</sup>.

Although transverse cracking in bridge decks has been one of the main concerns of designers and researchers for decades, effective mitigation procedures have not been developed<sup>19,20</sup>. Most research studies on the causes of transverse cracking over the past several decades have focused on three main categories of factors: (i) material and mix design, and their effects on cracking tendency, (ii) construction practices, and (iii) structural design factors.

In terms of material and mix design, it is recommended to: (a) reduce cement content to 385-390 kg/m<sup>3</sup><sup>22, 24, 25, 32, 35, 31, 37</sup>, (b) use AASHTO specification Type II cement for bridge deck construction<sup>22,24,32,33,38</sup> (c) limit the water/cement ratio to 0.4-0.45 and use water reducers to decrease water content<sup>23,25,27,35, 37,39, 40</sup>, (d) use fly ash, (e) avoid using high early strength concrete if “early-opening” is not an issue<sup>22</sup>, (f) use the largest possible aggregate size as specified in ACI-318, use crushed stone as a coarse aggregate, and maximize aggregate content<sup>23, 24, 31, 22, 39, 35, 38</sup>, and (g) increase concrete strength<sup>40</sup>.

In terms of construction practices, it is recommended<sup>22,23,24,27,28,31,35,36,37,38,39,41, 42,43,44,45</sup> to: (a) use the evaporation rate chart proposed by ACI and cast the deck in mild temperatures, (b) start curing immediately after finishing, then cure for at least 7 consecutive calendar days or 14 days if the construction schedule allows, (c) pour the complete deck at one time whenever feasible, within the limitation of the maximum placement length, based on drying shrinkage considerations; if multiple placements must be made and the bridge is continuous span, then place concrete in the center of positive

moment regions first and observe a 72 hour delay between placements; when deck construction joints are created, prime existing interface surfaces with a bonding agent prior to placement of new concrete.

In terms of design factors, the following recommendations<sup>19,40,46,47,48,49,50,51</sup> are made: (a) boundary restraints should be consistent with the design – construction practices should not introduce undue boundary restraints on the girders, (b) minimize the ratio of girder/deck stiffness by adjusting deck thickness, girder spacing, and girder moment of inertia, (c) employ flexible superstructures, and (d) limit the skew angle of bridges to prevent corner cracking. The increase of reinforcement volume above code requirements is discouraged because research<sup>19</sup> shows that it does not help mitigate cracking.

Despite a significant effort among the bridge engineering community to eliminate or at least reduce transverse bridge deck cracking, such cracking still exists and poses a great challenge to engineers and researchers<sup>48,52</sup>. Most of the past efforts have focused on modifying concrete material properties and construction practices to reduce volume change in concrete, especially drying shrinkage. Such efforts, however, have limitations because they don't fundamentally address the inherent brittleness of concrete materials. Therefore, the potential of reducing concrete volume change to a level less than the material's deformation capacity is marginal and unreliable<sup>12,53,54</sup>, resulting in (often “unexpected”) cracks, especially when the combined effects of drying shrinkage, temperature change, and mechanical loading are present. The same brittle material limitation also leads to early-age cracking in partial-depth patching and full-depth concrete repairs of existing bridge decks with transverse cracks<sup>55,56</sup>, which has a major

impact on the long-term durability of a repair system. Early-age cracking often occurs as a result of restrained volume change of the new repair material, due to its dimensional incompatibility with existing concrete<sup>57, 58, 59, 60, 61</sup>. These shortcomings point to an urgent need for developing a new material technology that effectively reduces the cracking potential through removal of the material brittleness, and eventually eliminates restrained volume change induced cracking in new and repaired bridge structures.

### Reinforcing and prestressing steel corrosion

Corrosion of reinforcing or prestressing steel (Figure 1.5) is another pressing deterioration problem in bridge structures and other reinforced concrete structures, demanding significant amounts of repair and rehabilitation<sup>62, 63</sup>. Corrosion starts when chloride ions transport through the sound or cracked concrete cover, reach the steel, and accumulate beyond a critical concentration level (pH falls below 11). At this point the natural protective concrete layer surrounding the steel is depassivated. Corrosion then initiates if oxygen and moisture are present at the steel-concrete interface. The oxidation products generate expansive forces within the concrete, eventually causing the concrete cover to spall<sup>64</sup>. Every year the U.S. spends about \$8.3 billion to directly address corrosion in American highway bridges<sup>65</sup>. Indirect costs related to traffic delays and productivity losses are estimated to exceed 10 times the direct cost of maintenance, repair, and rehabilitation.

According to the FHWA Office of Research, Development & Technology<sup>66</sup>, reinforced concrete bridges functioned reasonably well until the late 1960s, when premature concrete delamination and spalling, which used to be encountered only in coastal areas, became common in many of the reinforced concrete decks in the “snow

belt.” Concrete bridge decks were beginning to require maintenance after being in service for as little as 5 years. The emergence of this type of concrete deterioration, which was first observed in marine structures and chemical manufacturing plants, coincided with the increased application of deicing salts to bridges and roads during winter months. By the mid 1970s, it was recognized that this problem is caused by corrosion of reinforcing steel in concrete, which is induced by the intrusion of even small amounts of chloride from the deicing salts into the concrete. Now it is widely recognized that corrosion of the reinforcing steel has led to premature deterioration of many concrete bridges in the United States before their design life is exceeded. Although corrosion is not the sole cause of all structural deficiencies, it is a significant contributor and has become a major concern to transportation agencies nationwide<sup>67, 68</sup>.

The magnitude of this corrosion problem in transportation infrastructure systems has increased significantly in the last three decades and will continue to increase<sup>69</sup>. Even though the cost of maintaining bridge decks is becoming prohibitively expensive, the benefits to public driving safety provided by deicing salts are so important that their use is not likely to decrease in the future<sup>66</sup>. In fact, the use of road deicing salts, which are extremely corrosive due to the disruptive effects of its chloride ions on protective films on metals, has increased in the first half of the 1990s after leveling off during the 1980s<sup>70</sup>. Although an effective alternative deicing agent, calcium magnesium acetate (CMA), is available and less corrosive, its high price greatly limits its wide-spread application<sup>71, 72</sup>. Therefore, it can be expected that the road environment will likely remain corrosive. In response to the tremendous economic burden that corrosion of reinforcing steel in concrete bridges placed on the national economy, the Structure Division of FHWA has

placed emphasis on finding effective and economical solutions that can be easily implemented by state and local transportation agencies.

Compared to reinforcing steel, corrosion of prestressing steel and its impact on structural performance can be more severe. Prestressed concrete technology was only applied to bridges relatively recently. Therefore, the existing prestressed concrete members in bridges are still relatively young, and the corrosion and concrete deterioration problems associated with prestressed concrete members didn't become evident until the early 1980s<sup>73</sup>. Although prestressed concrete members were generally manufactured with higher strength concrete, time has shown that they are subject to the same adverse effects of reinforcement corrosion as reinforced concrete members<sup>74</sup>. Because the cross section of each prestressing wire or strand is relatively small and is already under significant stress, a very small cross sectional loss from corrosion will cause the wire or strand to debond from the concrete and eventually break<sup>75</sup>. Since prestressed concrete members rely on the tensile strength of the strands to resist loads, loss of even a few strands per member can be catastrophic<sup>76, 77</sup>. Additionally, because the strands are subjected to high stress, corrosion effects can be accelerated<sup>78</sup>. Even small corrosion pits may cause a strand to fracture, as compared to non-prestressed reinforcing steel that will literally rust away before breaking. Documented cases of prestressing strands breaking as a result of corrosion make this a pressing problem.

The rapid premature deterioration of many concrete bridge decks in the late 1960s raised concern among state highway agencies. As a result, the use of non-corroding fusion bonded epoxy-coated reinforcement has become a standard practice since the late 1970s<sup>79</sup>. For additional protection, low-permeability concrete, such as low water-cement

ratio Portland cement concrete, latex-modified concrete, and other specialty concrete began to be used, along with increased concrete cover thickness over coated reinforcing steel<sup>80</sup>. Additionally, the use of waterproof membranes over concrete decks<sup>81</sup>, in conjunction with an asphalt overlay, has produced mixed results and been adopted sparingly. A few states have used epoxy-coated rebars in conjunction with a waterproof membrane and asphalt overlay on bridge decks.

FHWA research and field data have indicated that the use of overlays, waterproof membranes, and sealers only marginally extend the life of a structure, to a variable extent<sup>66</sup>. On the other hand, cathodic protection has proven to be successful at retarding and controlling chloride-induced corrosion in reinforced concrete bridge components<sup>82,83,84,85,86,87,88</sup>. In addition, electrochemical chloride extraction is another alternative rehabilitation technique that is being explored by a number of state highway agencies<sup>89</sup>. More research is under way to bring this technology up to par with cathodic protection.

Current approaches to preventing steel reinforcement corrosion in concrete bridges have mixed results<sup>66</sup>. These approaches include the use of good construction design and procedures, adequate concrete cover depth, corrosion-inhibiting admixtures, and the adoption of low-permeability concrete. The reason for the limited success is due to the fact that concrete is brittle and tends to crack in a variety of combined mechanical and environmental loads. In fact, it has been observed recently that the new low permeability concrete (high-performance concrete), which is made from partial substitution of Portland cement with silica fume or fly ash, has a more pronounced tendency than conventional concrete to crack<sup>66,90,91</sup>. As a result, a faster, gravity-assisted

flow of salt-laden water channels through the cracks, rather than a slow diffusion of chloride through the uncracked concrete. Corrosion-inhibiting admixtures for concrete will not be useful once concrete cracks<sup>92</sup>, and the reinforcing steel solely relies on itself as the last line of defense against corrosion. In this situation, the use of a barrier system on the reinforcing steel, such as an epoxy coating or other organic coating, becomes more critical in abating corrosion. However, it is likely that there may never be an organic coating that can resist the extreme combination of constant wetting, high temperature, and high humidity that reinforcing steel is exposed to in marine environments, especially in the splash zone in coastal regions<sup>66</sup>. Epoxy-coated steel bars will have to be used in conjunction with sound, crack-free concrete in bridge decks<sup>89</sup> where the concrete is not constantly wet and the other exposure conditions are not as severe. The limitations of current approaches to reducing steel corrosion in concrete calls for a fresh approach in tackling this problem – a new methodology that addresses the intrinsic brittleness of concrete material for the purpose of enhancing structural durability.

### **1.1.2 Highways and Roadways**

Highway and roadway infrastructure involve enormous material consumption, energy usage, and capital investment. Currently, the U.S. consumes more than 35 million metric tons of asphalt and 48 million metric tons of cement annually, at a cost of nearly \$65 billion in the transportation infrastructure system alone. Repair and reconstruction of deteriorated and aging highway and roadway infrastructure in the United States leads to significant economic cost, environmental burdens, and social costs, which motivate sustainable engineering initiatives. Highway and roadway systems should provide a safe,

reliable, efficient, and comfortable driving environment. While the transportation of people and goods has expanded significantly in recent decades due to the existence of an extensive highway and roadway system in the U.S., deteriorating and aging highway and roadway pavement systems have become a burden to society. Poor road conditions lead to excessive wear and tear on motor vehicles and increased numbers of crashes and delays, and cost U.S. motorists \$67 billion (\$333 per motorist) annually in vehicle repair and operating costs. Currently, 33% of America's major roads are in poor or mediocre condition and 36% of the nation's major urban highways are congested<sup>93</sup>. The current spending level of \$70.3 billion for highway capital improvements<sup>94</sup> is well below the estimated \$186 billion needed per year to substantially improve the nation's highways<sup>95</sup>.

Typical deterioration mechanisms in highways and roadways include transverse cracking, longitudinal cracking, D-cracking, and alkali silica reaction<sup>9,96,97</sup>. Transverse cracking results from restrained volume change, such as drying shrinkage and temperature gradient, similar to the causes of transverse cracking in bridge decks<sup>98,99</sup>. These environmental effects, combined with repeated vehicle loading, aggravate the deteriorated area and further increase cracking and spalling. Longitudinal cracks are caused by a combination of repeated heavy loading, loss of foundation support, and curling and warping stresses, or by improper construction of longitudinal joints. Durability, or "D", cracking manifests as a "closely spaced crescent-shaped hairline cracking pattern", and occurs near joints, cracks, and free edges<sup>100</sup>. D-cracking is caused by freeze-thaw expansion of some types of coarse aggregate, and occurs frequently with limestone in Midwestern states in the United States. The alkali silica reaction occurs between alkali hydroxyl ions in Portland cement and certain siliceous minerals found in

the aggregate, such as opaline chert, and strained quartz. This reaction produces a gel that surrounds the aggregate in the concrete matrix. With the introduction of moisture, the gel expands and causes cracking and distress of the pavement<sup>101</sup>.

In developed countries such as the U.S., much of the highway and roadway construction activities involve maintenance, repair, and reconstruction of existing pavements. Three main types of repair methods have been used: (i) partial-depth patching (partial-depth repair), (ii) full-depth repair, and (iii) unbonded concrete overlay or hot mixed asphalt (HMA) overlay.

Partial-depth patching is a pavement restoration technique that repairs surface distress and localized failures that do not extend to the bottom of the slab, re-establishes well-defined joint reservoirs, or reduces impact loading at transverse joints, with the goal of extending pavement service life<sup>102</sup>. More specifically, it is used for mid-slab surface cracking and spalling, joint spalling, localized scaling, and localized distress from corroding steel reinforcement. Partial-depth patching improves the rideability of concrete pavement, and reduces intrusion of moisture, chloride, or incompressibles into cracks or joints.

Full-depth repair is for joint deterioration larger than 1/3 of slab depth, severe transverse cracking, longitudinal cracking, and broken slabs or corner breaks<sup>103</sup>. Partial-depth and full-depth repairs are subjected to restrained volume change induced cracking and debonding from existing concrete, which are most frequently caused by inappropriate selection of repair materials with higher cracking tendency, material variation, poor construction practice and quality control, late curing, and lack of bond between the repair and the existing concrete.

Concrete or HMA overlay is one of the major rehabilitation methods used for severely deteriorated pavements<sup>104</sup>. Reflective cracking is often the ultimate failure mode that limits the overlay service life<sup>105,106,107</sup>. Reflective cracking is characterized as new cracks reflected through the overlay from pre-existing cracks or joints in the substrate (Figure 1.6) under repeated traffic loads. Current methods to abate reflective cracking include the use of a bond-breaking layer, i.e. HMA, between the concrete overlay and the substrate, to release stress concentration at the source of reflective cracking, rubblization (breaking the substrate pavement into a well graded high modulus aggregate base material), or extensive repair of existing pavement deterioration before overlaying. Currently, none of these approaches has been able to effectively eliminate reflective cracking in rigid (concrete) pavement overlays, mainly due to the brittle nature of the overlay material.

### **1.1.3 Parking Structures**

Apart from bridge decks and highway pavements, parking structures represent another category of structures that suffers early deterioration (Figure 1.7). A combination of parking lot, building, and bridge structures, the modern parking structure<sup>108</sup> is designed to meet an ever-expanding array of criteria to support vehicular traffic loads while enduring challenging environmental conditions. A parking structure frame can be made of cast-in-place concrete, pre-cast concrete, or steel. A parking structure deck is commonly cast-in-place or pre-cast concrete. The concrete members are either reinforced or pre-stressed<sup>109</sup>. Cast-in-place decks are usually a single, continuous reinforced concrete deck spanning between steel or concrete framing. This type of deck is generally

more prone to deterioration from restrained shrinkage cracking, chloride attack, and corrosion induced spalling<sup>110, 111, 112</sup>. Therefore, performance of this type of deck is directly related to provisions that mitigate chloride attack<sup>113</sup>. While there is no substitute for good design and materials, combating chloride attack has become a challenge over the years<sup>114, 115, 116</sup>. Current protection methods include reinforcement coating, adding corrosion indicators to concrete, applying sealers and densifiers to the concrete surface, and using traffic bearing membranes<sup>117, 118, 119, 120</sup>. For decks that are left unprotected, maintenance dollars are spent chasing defects<sup>121</sup>.

Pre-cast deck elements are cast in a factory and use dense and high quality concrete produced with strict quality control methods. Therefore, they are expected to have higher resistance to chloride penetration<sup>108</sup>. Because these members are typically pre-stressed in compression, shrinkage cracking should not be of concern. However, maintenance requirements for pre-cast parking garages can be far more demanding than for cast-in-place parking garages. This is because pre-cast elements are often thinner and have a low tolerance against construction caused defects. They tend to crack when restrained from thermal expansion and contraction<sup>122, 123</sup>. Cracks, once formed, pose a serious threat to the pre-cast elements as they allow a direct path for chloride to penetrate through and reach the reinforcement, despite the dense microstructure of pre-cast members. As the pre-cast members typically use wire that is thinner than the reinforcement bar used for cast-in-place decks, a relatively small amount of corrosion can cause a significant loss of load carrying capacity. Even worse, repair of these thin elements is often difficult and costly<sup>123</sup>. Moreover, pre-cast members typically require sealant joints as connections. These joints, extending around each pre-cast member, can

very quickly add up to miles of sealant that must be maintained and replaced periodically. Water migration through failed joints can cause problems for cars below and accelerate deterioration of the pre-cast members<sup>124</sup>.

In summary, water leakage through cracks and joints, chloride ingress, and freeze-thaw cycles are common mechanisms that cause reinforcement corrosion, spalling, and other distress in parking structures. The risk associated with deterioration in parking structures is severe, and the threat of costly and time-consuming lawsuits associated with driving and tripping hazards is substantial. Current repair methods include use of waterproofing membranes, joint sealants to control water intrusion, strengthening systems to correct design and construction errors, surface repair systems for spalling damage, and slab replacement.

## **1.2 Limitation of Current Approaches to Improve Durability of Concrete Structures**

Summarizing from the previous discussion, early-age cracking due to restrained volume change, reflective cracking, chloride penetration, corrosion, spalling, and alkali silica reaction are major deterioration phenomena in new and repair concrete structures. At the root of these durability concerns is the inherent brittleness of concrete materials. Concrete tends to crack and spall under applied structural loads, restrained volume change (shrinkage, thermal deformation, etc.), and stress concentration induced by existing cracks in the substrate concrete. Once cracked, wider crack width tends to exacerbate water, gas, and chloride ion transport and accelerate the deterioration mechanisms mentioned above. The factors driving wider crack width include the level of

deformation (determined by ambient environmental conditions and structural loading conditions), constraints (determined by boundary conditions), member geometry, and material characteristic length. Crack width has a direct influence on transport properties. Large cracks easily allow water and corrosives into the material and accelerate deterioration, such as leeching, steel corrosion, spalling, sulfate attack and freezing-and-thawing damage.

Current methods to increase durability of concrete structures include (a) increasing density of concrete material microstructure through well-graded particle size distribution to reduce permeability and transport of corrosives to the steel<sup>125, 126</sup>, (b) increasing concrete compressive strength, (c) modifying the concrete matrix by adding entrained air, sulfate resistance cements, and corrosion-inhibiting admixture, and (d) adding cracking-control reinforcement. These methods, except (d), do not target the inherent brittleness and cracking behavior of concrete, and instead rely upon the concrete to remain uncracked within a structure throughout its service life so that the denser concrete matrix is able to resist penetration of aggressive agents. As discussed above, concrete cracking behavior and crack width play the most important role in a majority of the concrete durability problems in the field. Therefore, a fundamental solution, which reduces the brittle nature of concrete and controls crack width while maintaining cost effectiveness and ease of application, is necessary.

### **1.2.1 Effectiveness of current material “durability” solutions**

It is often perceived that the solution to the repair durability problem is improving the compressive strength of the repair material or accelerating its strength gain at material

early ages. This misconception encourages the seeking of various expensive, high strength repair materials that do not behave as expected, or sometimes even worse in the field<sup>12</sup>. High strength concrete (with 50-140 MPa compressive strength), for example, is often believed to be a highly durable material because of its very dense microstructure, which lowers permeability and reduces transport of corrosives to the steel<sup>125,126</sup>. This is achieved with low water/cement ratios<sup>127</sup>, silica fume and fly ash<sup>128</sup>, and a well-graded particle size distribution<sup>129</sup>. This concept, however, is based on the assumption that high strength concrete remains uncracked throughout the structure's expected service life, so that it can resist the ingress of water, chloride ions, oxygen, and other aggressive agents through its dense microstructure.

In reality, however, high strength concrete is particularly susceptible to cracking due to its high brittleness and small creep deformation<sup>130</sup>. Containing more finely ground particles than regular concrete, high strength concrete typically has increased early age shrinkage and thermal volume change. Restrained volume change induces large tensile stress in the high strength concrete because of its high elastic modulus and small creep deformation, consequently resulting in cracking. Cracks provide paths for the aggressive agents to penetrate into the high strength concrete, and ultimately lead to steel corrosion, freezing and thaw disintegration, alkali or sulfate attack<sup>12</sup>.

The higher cracking tendency of high strength concrete can be explained using fracture mechanics theory. Stang and Li<sup>131</sup> investigated the cracking stability of concrete material under restrained shrinkage conditions using a simple model of a concrete slab of length  $L$ , restrained on both ends as shown in Figure 1.8. When the shrinkage strain  $\epsilon_{\text{shrink}}$  stays below concrete's elastic tensile strain capacity  $\epsilon_t$ , no cracking occurs,

although tensile stress develops in the restrained direction. Once  $\varepsilon_t$  is exceeded, the magnitude and stability of the crack opening depend on the brittleness of the material. For an ideally brittle material, the crack width will instantly jump from zero to a crack width equal to the shrinkage strain times the length of the slab, as shown in Figure 1.9. If the concrete material has tension softening behavior, then the predicted crack width is dependent on the material characteristic length  $l_{ch}$  through Equation 1.1.

$$w = \frac{L(\varepsilon_{shrink} - \varepsilon_t)}{(1 - L/2l_{ch})} \quad (1.1)$$

where  $w$  is the crack width,  $L$  is the length of the restrained member,  $\varepsilon_{shrink}$  is the shrinkage strain,  $\varepsilon_t$  is the elastic tensile strain capacity, and  $l_{ch}$  is the characteristic length as defined by Hillerborg et al.<sup>132</sup> in Equation 1.2.

$$l_{ch} = \frac{EG_f}{f_t^2} \quad (1.2)$$

where  $l_{ch}$  is the characteristic length,  $E$  is the modulus of elasticity,  $G_f$  is the fracture energy, and  $f_t$  is the tensile strength.

Figure 1.9 suggests that the crack width will grow from zero linearly proportional to the excess of shrinkage strain over the tensile strain capacity ( $\varepsilon_s - \varepsilon_t$ ). This slope has two limits. As characteristic length drops to  $L/2$ , the slope becomes infinity and the material behaves as an ideally brittle material by conforming immediately to the  $L\varepsilon_s$  line. As characteristic length increases to infinity, the slope approaches  $L$ . This demonstrates that for the same shrinkage potential ( $\varepsilon_s - \varepsilon_t$ ), a material with small characteristic length (i.e. very brittle with low toughness) will show larger crack widths. The development of cracks also tends to be unstable, as indicated by the infinite slope of the line. A material with higher toughness and characteristic lengths will have smaller crack widths and more

stable crack development. Cracking of a quasi-brittle material will fall between these two limits. Characteristic length values for ordinary Portland cement concrete and high strength concretes are calculated to be about 190 and 120 mm (7.5 and 4.7 in.), respectively<sup>131</sup>. Because high strength concrete has lower material characteristic lengths, it should exhibit larger cracks after early age shrinkage. This is supported by field evidence of very early age cracking of bridge decks constructed using high strength concrete in Colorado and California<sup>133, 134, 135</sup>, highlighting the susceptibility of high strength concretes to early age cracking due to restrained volume change.

Based on the above discussion, the effectiveness of current solutions for concrete structure and repair durability is questionable. Instead, material durability should be highly dependent on its cracking resistance and cracking stability. A material with high tensile strain capacity (ductility) will be able to accommodate restrained volume change due to shrinkage, temperature effects, structural loading, etc., and relieve the tensile stress buildups in the repair without cracking failure.

### **1.2.2 Compatibility of new repair with existing concrete substrate**

Unlike new structures, the durability of a repaired system highly depends on the compatibility of the repair material with existing concrete<sup>136</sup>. Compatibility is defined as:

“a balance of physical, chemical and electrochemical properties, and dimensions between a repair material and the existing substrate that will ensure that the repair can withstand all the stresses induced by volume changes and chemical and electrochemical effects without distress and deterioration over a designated period of time.”<sup>4</sup>

Dimensional compatibility, which is the most important among these considerations, is the ability of the repair to withstand restrained volume change without cracking and loss

of bond. It also refers to the ability of the repair to diffuse stress concentration from existing cracks in the substrate concrete without reflective cracking. These types of cracking, either due to restrained volume change or reflective cracking, are the main causes of reduction in service lives of bridges, highways and roadways, parking structures, and other concrete structures, as discussed earlier in Section 1.1.

Dimensional compatibility includes drying shrinkage, thermal expansion or contraction, creep, modulus of elasticity, and repair geometry. An ideal repair material should undergo zero shrinkage, and the same amount of thermal expansion or contraction, creep, and modulus of elasticity as the existing surrounding concrete. In reality, shrinkage always takes place in a new repair as soon as it is installed, and is restrained by existing reinforcements and the surrounding old concrete, which already underwent shrinkage years ago. Restrained shrinkage results in tensile stress in the repair, and tensile and shear stresses at the repair/old interface. These stresses are the cause of repair cracking and interfacial debonding. In such a situation, a relatively larger creep strain and lower elastic modulus are actually preferred for repair materials, as they aid in relieving the stress buildup in the repair and at the repair/old interface.

It should also be noted that the interaction between the new repair and the existing concrete is a time-dependent process. Repair material shrinkage, creep, elastic modulus, tensile strength, and the repair/old interfacial bond are all age-dependent properties, and develop at different rates once the new repair is installed. Cracking and interfacial debonding time and extent are determined by competition among these age-dependent parameters. In the past years, there have been many efforts made on improving repair material properties by reducing repair material shrinkage, increasing its

compressive/tensile strength, or enhancing its bond strength with concrete. These efforts, although meaningful, have resulted in only marginal improvements. For example, increasing repair material strength may delay repair cracking, as long as the restrained shrinkage induced tensile stress remains below the material tensile strength over time. However, it poses an elevated risk of interfacial debonding because higher levels of shear and tensile stress build-up at the new/repair interface, which could have otherwise been relieved through cracking in the repair layer. On the other hand, accelerating interfacial bond development may delay the debonding process, but makes the repair more prone to cracking because debonding reduces the level of constraints and partially relieves the tensile stress in the repair. Reducing repair material shrinkage seems to be the most effective method. However, considering the low deformation capacity (elastic strain capacity  $\approx 0.01\%$ ) for most of the currently available concrete repair materials, most efforts can only reduce the shrinkage to a small amount below 0.01%. In reality, shrinkage is not the only factor that contributes to the deformation of concrete repairs. When thermal effects, structural loading, and other factors are combined, it is highly possible that the total imposed deformation of the repair will surpass its deformation capacity, and cracking and/or debonding will inevitably follow.

To ensure dimensional compatibility within the repaired system, the repair material should be able to deform to an extent that fully accommodates the imposed deformation due to a combination of many factors, without debonding or cracking locally. These criteria should be satisfied at all ages throughout the repair's life. In this sense, a repair material can be considered truly dimensionally compatible with existing concrete if the following characteristics are satisfied at all ages: (a) high tensile ductility

(deformation capacity), (b) adequate bonding with concrete, (c) similar thermal coefficient and creep as concrete, and (d) same or lower elastic modulus as concrete.

### **1.2.3 Some considerations of current repair performance characterization**

The technical guideline published by the International Concrete Repair Institute (ICRI)<sup>137</sup> provides a standardized protocol for testing and reporting data for inorganic concrete repair material. In this guideline, test methods for characterizing repair materials contain three main categories: (a) mechanical properties (i.e., compressive, flexural, splitting tensile and direct tensile strength), (b) dimensional compatibility (i.e., modulus of elasticity, bond strength, length change, compressive creep, and coefficient of thermal expansion), and (c) durability (i.e., freezing and thawing resistance, scaling resistance, rapid chloride permeability, chloride ponding, sulfate resistance, chemical resistance, and cracking resistance). While these test methods provide standardized characterization of repair material properties, and insights on material selection for the objective of improving durability of concrete repairs, appropriate adoption of these test methods and adequate interpretation of the test results require special consideration of a number of issues detailed below.

The performance and durability of concrete repairs and new concrete structures should not be evaluated in the same way. New structures are typically well-defined structural systems that have been designed and put into service. Therefore, it is not necessary to consider pre-existing cracks. However, in repair and rehabilitation, pre-existing conditions such as cracking, delamination, and spalling are already present from the beginning of the repair system's service life. As an example, concrete substrate

cracks can act as stress concentrators in the repair layer, resulting in reflective cracking and shortening of service life. These pre-existing conditions should be accounted for when laboratory testing is conducted to measure repair performance.

In addition, the repair may experience cracking shortly after placement due to restrained shrinkage or other factors, which would affect repair durability. One example of the inadequate measurement of repair performance is the permeability test, the results from which are widely used as durability indicators of repair materials. This method, conducted using uncracked laboratory specimens, fails to take the early-age cracking that usually occurs in repairs due to restrained volume change into consideration. Moreover, permeability is a measurement of the transport of water under a hydrostatic pressure head, and is not the only parameter that describes the transport properties of repair materials. For surface repairs of bridge decks or road pavements, for example, the diffusion of chloride ions under an applied concentration gradient is the governing transport process that impairs the durability of the repair, and should be measured using the saltwater ponding test on uncracked as well as cracked specimens.

Another example of tests that may result in inadequate performance characterization of repaired systems is the free shrinkage test. This test is generally used to measure shrinkage strain of repair materials. Repair materials with lower shrinkage strain are considered to have higher resistance to shrinkage cracking, and therefore are believed to be more durable. However, the shrinkage cracking potential of a repair is determined by a combination of different factors, including the repair material's shrinkage strain, tensile strain capacity, creep, elastic modulus, and tensile strength at all ages. A repair material with relatively low shrinkage strain, but low creep strain, low

tensile strain capacity, and high elastic modulus can be more susceptible to shrinkage cracking. Therefore, a restrained shrinkage test such as ASTM C1581 “Standard Test Method for Determining Age at Cracking and Induced Tensile Stress Characteristics of Mortar and Concrete under Restrained Shrinkage”<sup>138</sup> will be more meaningful than a free shrinkage test for evaluating a repair material’s resistance to shrinkage cracking.

### **1.3 Proposed Approach**

The challenges posed by deteriorating concrete structures and widely-observed repair failures require an effective and practical approach that breaks down the concrete deterioration process, which typically begins with restrained volume change induced cracking or reflective cracking, followed by penetration of aggressive agents, and eventually results in concrete spalling, disintegration, and loss of structural capacity. This dissertation research focuses on the development and implementation of an innovative material technology based on an integrated multi-scale material/structural engineering framework, as illustrated in Figure 1.10. This framework begins with material microstructure tailoring at the micrometer scale, links to repaired system durability assessment through composite material properties at the centimeter scale, and ultimately relates construction processes and performance evaluation at the meter scale of the repaired infrastructure. To achieve the holistic durability of such engineered systems, durability concepts are interwoven across all material engineering, system durability assessment, and structural application scales.

At the material engineering scale, innovative cementitious composite materials are developed to have desired material properties through microstructure tailoring and

processing techniques. The critical target material properties are large tensile strain capacity and tight self-controlled crack width, which are essential to address the major causes of concrete repair deterioration, e.g. lack of dimensional compatibility, cracking due to restrained volume change, reflective cracking, and penetration of aggressive agents. In this way, the typical deterioration process in concrete repairs can be disrupted. Additionally, the materials proposed herein are designed with special functionalities favorable for specific repair applications, without sacrificing durability. These functionalities include workability, high early-age strength, lightweightness, greenness, and cost effectiveness.

At the repaired system durability assessment scale, repair material properties are linked to repaired system durability through the interaction between the repair and the existing concrete. Experimental measurements are designed to take into consideration the interaction between new repair and old concrete as well as the presence of cracks. The durability performance of the repaired systems is investigated under various environmental and mechanical loading conditions. This work bridges the gap of translation from the properties of repair material properties to the durability of a repaired system, which has not been fully understood through previous approaches.

The structural application stage focuses on bringing repair materials designed and tested in the laboratory to full-scale field applications. Before the newly developed repair materials can be considered a viable construction material for use in concrete repairs, they must be capable of processing and placement with controlled quality at a larger scale using commercial batching equipment common within the repair industry. This is achieved through further tailoring of the composite ingredients and processing procedure

for larger scale mixing, scaled up trial batches, and workability measurements and control. The ability of full-scale processing and placement of a newly developed repair material is demonstrated in a bridge patch repair project in Michigan. Monitoring the long-term durability of the HES-ECC repair further validates the applicability of the repair technology.

At the core of this integrated multi-scale material/structural engineering framework is Engineered Cementitious Composites (ECC), which is a unique class of high-performance fiber-reinforced cementitious composites (HPFRCC). The tailorability of ECC at the microstructure level for prescribed material properties and structural performance lends itself towards easy adoption with the integrated multi-scale material/structural engineering philosophy.

In contrast to the presently proposed approach to durable repair development, current practice can be illustrated by Figure 1.11, which shows the disconnect between material engineering and structural engineering in current concrete repair practices. Within this philosophy, material engineering is often focused on developing new repair materials or modifying currently available repair materials to achieve desired properties, such as higher compressive strength, a denser matrix, low permeability, and low shrinkage. These “durable” materials, once available, are adopted in concrete structural repair applications for “durable performance”. However, without bridging the gap between “repair material properties” and “repaired structure performance” through appropriate durability assessment that addresses the interaction between repair and existing concrete, the transferability between the two concepts is questionable. Furthermore, the disconnected philosophy hinders the ability of performance-based

material development through microstructure tailoring for target concrete repair performance (e.g. cracking resistance, corrosion prevention, early re-opening, etc.). This disconnect may be seen as a major reason why current concrete repair technology has not been satisfactory. This thesis attempts to address this technological gap from an integrated material/structural system viewpoint.

#### **1.4 Engineered Cementitious Composites**

Engineered Cementitious Composites (ECC) is a unique class of high-performance fiber-reinforced cementitious composites (HPFRCC) that features high intrinsic tensile ductility and moderate fiber content<sup>139,140</sup>. ECC exhibits tensile strain-hardening behavior through multiple microcracking with self-controlled crack width, leading to fracture toughness similar to aluminum alloys<sup>141</sup>. Tensile strain capacity in the 3-5% range, which is around 300-500 times that of concrete and fiber reinforced concrete (FRC), has been demonstrated in ECC materials using polyethylene fibers and polyvinyl alcohol (PVA) fibers with fiber volume fraction no greater than 2%<sup>142,143</sup>. A typical uniaxial tensile stress-strain curve for ECC is shown in Figure 1.12, along with crack width development at different loading stages. The tensile strain-hardening behavior, i.e. increasing load capacity with increasing straining without localizing into a fracture plane, distinguishes ECC from FRC, which shows tension-softening after first cracking. ECC materials also feature high ductility when subjected to large shear stress<sup>144</sup> and impact loading<sup>145,146</sup>, and exhibit high damage resistance to fracture failure under severe stress concentrations induced by steel/concrete interactions<sup>147, 148</sup>.

Due to its unique high tensile ductility as well as compatibility with ordinary Portland cement concrete in other respects, such as compressive strength and thermal properties, ECC possesses characteristics sought by engineers for improving performance of civil infrastructure, such as buildings, bridges and pipes<sup>149</sup>. The high tensile ductility and toughness of ECC material greatly elevates the mechanical performance of reinforced ECC (R/ECC) structures by preventing brittle failure and loss of structural integrity, which are common in traditional reinforced concrete (R/C) structures under excessive loading. It has been demonstrated experimentally that R/ECC structural members, such as beams<sup>150</sup>, columns<sup>151</sup>, walls<sup>152</sup>, and connections<sup>153</sup> surpass normal R/C structural members in structural load carrying capacity, deformability, and energy absorption capacity under monotonic and reverse cyclic loading.

An extensive body of literature exists on the durability of ECC materials. A brief review of durability characteristics of ECC under abrasion and wear, freezing and thawing, and hot and humid environments, is given below. ECC resistance to chloride penetration will be a focus of the present thesis (Chapter 6). A review of other durability related studies on ECC, including salt scaling resistance, permeability, and absorption, can be found in Chapter 6 as well.

To evaluate ECC's abrasion and wear resistance for roadway applications, surface friction and wear track testing according to Michigan Test Method 111 was conducted in conjunction with MDOT<sup>154</sup> using a static friction tester (Figure 1.13). These tests were conducted on a wet pavement surface with vehicle tires operated at 65 kph (40 mph). Initial friction forces between the tire and the ECC surfaces were determined. The ECC specimens were then subjected to 4 million tire passes to simulate long-term wear. After

wearing, friction forces were again determined to evaluate deterioration or surface polishing during wearing. These final measured frictional forces are called the Aggregate Wear Index (AWI). AWI values for the textured ECC samples range from 1.6kN to 2.3kN, which are higher than the required minimum AWI of 1.2kN for Michigan trunkline road surfaces. The test results show that ECC has good abrasion and wear resistance to heavy traffic.

Freeze and thaw testing was conducted on ECC and normal concrete specimens based on ASTM C666A<sup>155</sup> (Figure 1.14). In addition, a series of ECC tensile specimens were also subjected to freeze-thaw exposure to evaluate the effect on ECC's tensile strain capacity. Testing of non-air-entrained ECC and concrete prisms was conducted concurrently over 14 weeks. After 5 weeks (110 cycles), the concrete specimens had severely deteriorated, requiring removal from the test. However, ECC specimens survived 300 cycles with no degradation of dynamic modulus. The computed durability factor of ECC was 100, far larger than the value of 10 for the non-air-entrained concrete. The uniaxial tension tests performed on freeze and thaw exposed ECC specimens after 200 cycles showed no significant drop in strain capacity (3%).

Hot water immersion tests, performed on single fibers embedded in ECC matrix, and on composite ECC material specimens, were conducted to simulate hot and humid environments<sup>156</sup>. After immersion in hot water at 60°C for 26 weeks, little change was seen in fiber properties. Interfacial properties, however, experienced significant changes, particularly between 13 and 26 weeks of immersion, resulting in a drop of ultimate composite strain capacity from 4.5% at early age to 2.8% after 26 weeks of hot water immersion. The residual strain capacity of ECC after exposure to this accelerated

weather environment (equivalent to more than 70 years of natural weathering) was still over 250 times that of normal concrete.

ECC is currently emerging in full-scale structural applications, including the composite deck of a cable-stayed bridge in Japan<sup>157</sup> (Figure 1.15). This bridge employed an estimated 800 cubic meters of ECC for the 38 mm (1.5 in.) thick ECC/Steel composite deck. In the United States, the first full-scale ECC link slab has been constructed in Michigan<sup>158,159</sup>, as shown in Figure 1.16.

The combination of high performance and moderate fiber content is achieved by micromechanics-based composites optimization<sup>149, 160</sup> (also see Chapter 2). Micromechanics provides guidance in selection and tailoring of the type, size, amount, and properties of ingredients at micrometer and nanometer scales. The fibers, matrix, and interface interact synergistically, thus resulting in a composite material with controlled multiple microcracking when overloaded in tension, as well as other target functionalities. The ECC micromechanics-based design framework elevates the cementitious materials design from conventional trial-and-error empirical combination of individual constituents to systematic material “engineering”. Its ability to suppress localized fracture modes through controlled microcracking, and its micromechanics-based design philosophy and tailor-ability, differentiates ECC from other fiber reinforced cementitious composites.

## **1.5 Research Motivation and Objectives**

The huge flow of material driven by concrete global production and consumption and the lack of durability of concrete infrastructure has created large economic, social

and environmental impacts, and poses great challenges for the civil engineering profession. Presently it is very difficult to meet this challenge of durable development with traditional concrete materials, which have inherently low resistance to cracking. Also, the limitations of currently available repair materials and technologies are widely evident in the common occurrence of early deterioration of repairs, which fail to address the underlying concrete deterioration problems and prolong the service life of concrete structures. Moreover, the current disconnect between material engineering, system durability assessment, and structural application often causes breakdowns within the overall design.

This research looks to develop and demonstrate an integrated multi-scale material/structural engineering approach for improving durability of concrete structures. This will be accomplished through the establishment of links between the development, assessment, and implementation of an innovative material technology that fundamentally tackles major concrete deterioration problems. Specifically, the deterioration mechanisms of concrete repairs under various environmental and mechanical loading conditions should be understood first. Through identifying causes and effects of each deterioration stage, the critical repair material properties that influence each stage need to be accurately determined. These properties should be designed into special versions of ECC materials, with other functionalities that are preferred for specific repair applications, through constituent ingredients screening, micromechanical tailoring of matrix and fiber/matrix interfacial properties, and laboratory testing. Repair systems containing the developed repair material should be properly evaluated under various environmental exposure and mechanical loading conditions. The influence of material properties on the

interaction between the repair and the existing concrete as well as the durability of the repair system should be fully addressed. Finally, the performance and practicality of this material technology should be justified not only in laboratory studies, but also in full-scale field applications.

## **1.6 Research Scope and Dissertation Organization**

Within this dissertation, the development, evaluation, and implementation of an innovative ductile repair technology on all three levels of the integrated multi-scale material/structural engineering framework will be addressed, namely material engineering, repair system durability assessment, and field application (Figure 1.10). Within each of these levels, the tailoring of ECC materials is highly focused on meeting specific structural performance requirements while adhering to additional system constraints (i.e. cost, processing, material availability, existing cracks, etc.). A variety of micromechanics based tools, along with carefully designed experiments and finite element methods, are employed to understand and optimize ECC materials development for specific repair applications. In addition to laboratory development and experimental studies, the newly-developed ductile repair technology is transferred to field implementation by optimizing workability and processing techniques, accommodating traditional large-scale mixing equipment, and demonstrating in a bridge repair project in Southern Michigan.

In Chapter 2 the ECC micromechanical design theory is introduced, and the development of special versions of ECC materials for concrete repair applications will be presented. The development of high-early-strength ECC (HES-ECC) is first discussed.

This material is designed for fast and durable repair of transportation infrastructure (e.g. bridges, roadways and highways), or other types of concrete structures, which prefer a minimal interruption of operations and are often exposed to challenging environmental and mechanical loading conditions. The material design begins with matrix screening for strength and workability requirements, and the initially selected mixing proportion is further tailored to achieve the target tensile ductility.

Chapter 3 focuses on maximizing ECC material properties (e.g. tensile strain capacity, tensile strength) and minimizing material variation through processing technique. ECC laboratory testing and application in construction projects will rely on the capacities to consistently produce ECC materials with controlled quality. To address this need, this work develops a simple and practical quality control method for ECC processing. The influence of fresh material processing on the microstructure of ECC composites is first discussed. Through measurement of ECC mortar rheological parameters, fiber dispersion, and ECC tensile properties, the correlation between the three is established. The optimal range of marsh cone flow rate, an indicator of plastic viscosity of ECC mortar, was then indentified and used to guide ECC quality control. By controlling the plastic viscosity of ECC mortar within this optimal range, the ECC material can achieve optimized material properties as originally designed through the micromechanical methodology described in Chapter 2. Collectively, Chapters 2 and 3 comprise the “material engineering” portion of the integrated material/structural engineering framework shown in the bottom triangle in Figure 1.10.

Chapters 4, 5, 6 and 7 shift the focus from “material engineering” to “repair system durability assessment” (the middle triangle in Figure 1.10). Chapter 4 addresses

one of the major durability concerns in concrete repairs, i.e. repair cracking and repair/old interfacial delamination due to restrained volume change and lack of dimensional compatibility. Experimental and numerical studies are conducted on a simulated repair system, which consists of a layer of old concrete substrate and a layer of new repair material, under restrained shrinkage conditions. The influence of repair material ductility on the durability of the repaired system is identified. The effect of substrate surface preparation on the repair performance is also investigated. Experimental and numerical results verify that when adequate interfacial bonding is present, the high tensile ductility of HES-ECC can relieve shrinkage induced stresses in the repair layer and at the repair/old interface, thereby simultaneously suppressing large repair surface cracks and interface delamination. This research departs from the traditional emphasis on high compressive strength repair materials, and moves toward balancing strength, ductility and the repair material's compatibility with the old surrounding concrete. This concept of translating the ductility of the repair material to the durability of the repair system, when subjected to restrained volume change, can be widely applied to concrete structure repair applications for minimizing maintenance requirements and reducing repair costs.

Chapter 5 addresses the reflective cracking issues prevalent in concrete repairs, especially overlay repairs. As discussed in Section 1.1, reflective cracking and restrained volume change induced cracking are two major cracking mechanisms affecting concrete repair service life. Experimental studies are conducted on an overlay repair system, which consists of a layer of overlay repair cast on a concrete substrate with an existing crack and small amount of interfacial debonding. This overlay repair system is subjected to monotonic flexural loading to measure its load carrying capacity, and fatigue flexural

loading to measure its S-N curve. The influence of repair material ductility on the load carrying capacity and service life of the repaired system is investigated. Findings verify that the tensile ductility of ECC effectively diffuses the stress concentration in the zone above the existing crack, therefore preventing reflective cracking. Through this mechanism, the ECC repaired system exhibits 100% increased load carrying capacity and significantly prolonged fatigue life, compared to the control concrete repaired system. This methodology of suppressing reflective cracking through material ductility can be generalized as translating the ductility of the repair material to the durability of the repair system, when it is subjected to stress concentration from existing cracks.

Chapter 6 addresses the chloride penetration stage in a typical repair deterioration process, before and after cracking occurs at different straining levels. Chloride diffusion driven by a chloride concentration gradient, which is the predominant mechanism of chloride transport for most of the concrete structures exposed to deicing salts and airborne chloride ions, is considered in this study. Experiments are conducted under combined mechanical (flexural) and environmental (3% chloride solution ponding) conditions, to simulate actual conditions experienced by a structural member when it is subjected to both structural loading and chloride exposure. Influences of material tensile strain capacity, crack width, and applied deformation level on the effective chloride diffusion coefficient are investigated. The results conclude that ECC is effective at slowing down the diffusion process of chloride ions under combined mechanical and environmental loading, by virtue of its ability to achieve a self-controlled tight crack width, even under large applied straining levels. This study verifies the concept of

improving repaired system durability with the built-in crack self-controlling mechanism of ECC repair materials.

Chapter 7 investigates the influence of cracking and self-healing on the durability of ECC under aggressive chloride exposure combined with mechanical loading conditions. The results show that after various levels of pre-applied deformation and time-lengths of chloride exposure, the reloaded ECC still remains its large tensile ductility accompanied by multiple microcracking behavior. Recovery of ECC mechanical properties in term of stiffness, tensile strain capacity, and tensile strength was observed, indicating strong evidences of self-healing of the microcracked ECC material under chloride exposure. This study confirms that ECC, whether uncracked or microcracked, remains durable under severe marine environment.

Chapter 8 shifts the focus from “repair system durability assessment” to the “structural application” portion of the integrated engineering methodology (upper triangle in Figure 1.10). Efforts are made to transfer innovative ECC repair technology from the laboratory to field implementation through a bridge patch repair demonstration project. Large-scale processing and construction of an HES-ECC repair using commercial facilities are realized through optimization of the HES-ECC ingredients and mixing procedure, trial batches, and quality control methods. The long-term durability of the HES-ECC patch repair under field conditions is monitored. Through this work, the linkages between material engineering, repair system durability assessment, and structural application are further forged.

Overall conclusions from this study are summarized in Chapter 9, and some future works worthy of further investigation are outlined.



Deterioration due to steel corrosion,  
concrete cracking and spalling



Damage caused by earthquake



Defect associated with improper detailing  
and construction practice

Figure 1.1 – Concrete Structure Deterioration, Damage, and Defect.

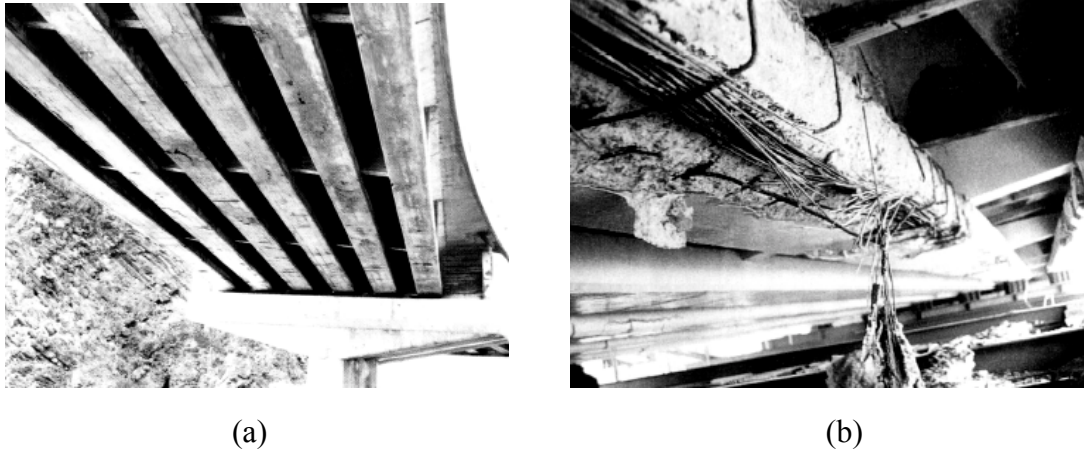


Fig. 1.2 – Deterioration of Kurtsubo Bridge, Japan: (a) Rust signs before the first repair; (b) Tendon corrosion and breakage before the second repair.

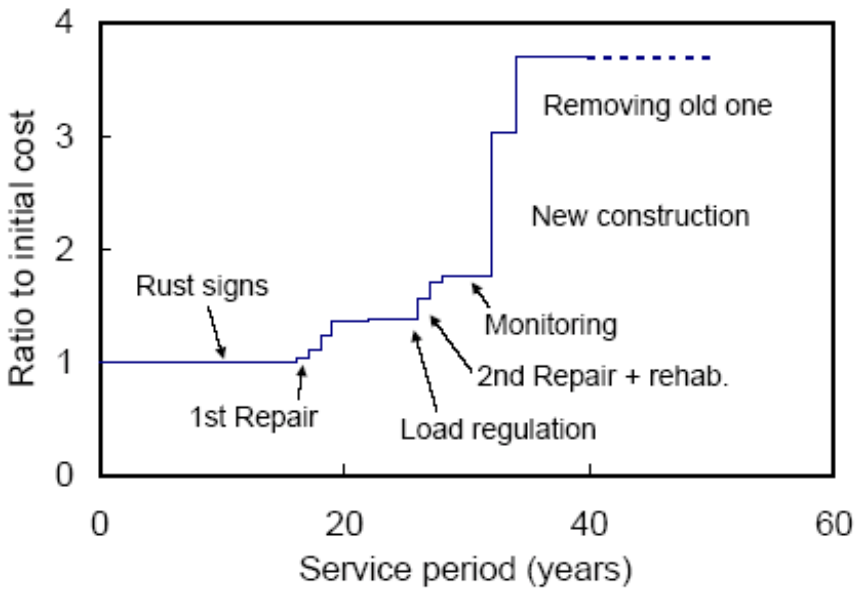


Figure 1.3 – Life cycle cost of Kurtsubo Bridge, Japan.



(a)



(b)

Figure 1.4 – Bridge deck transverse cracking. (a) Transverse cracking of a normal strength concrete deck in Ontario. Cracks 0.5 mm wide spaced at 200 mm. (b) Early-age transverse cracking of a high strength concrete deck in Colorado. Cracks 0.4 mm wide while construction is being completed (concrete < 2 months old).



Figure 1.5 – Steel corrosion and spalling in concrete bridges in Michigan (Courtesy of MDOT).



Figure 1.6 – Pavement overlay reflective cracking.



(a)



(b)

Figure 1.7 – Deterioration in parking structures. (a) Cracking in concrete slab. (b) Corrosion and spalling of the pans and ribs on a parking deck soffit.

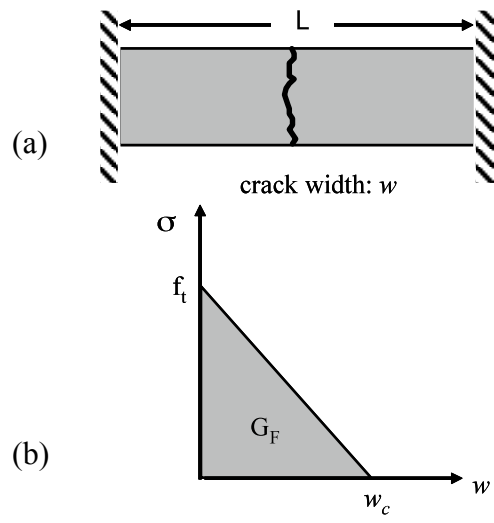


Figure 1.8 – (a) Model of concrete slab restrained against shrinkage and (b) the crack width  $w$  controlled by the tension-softening curve.

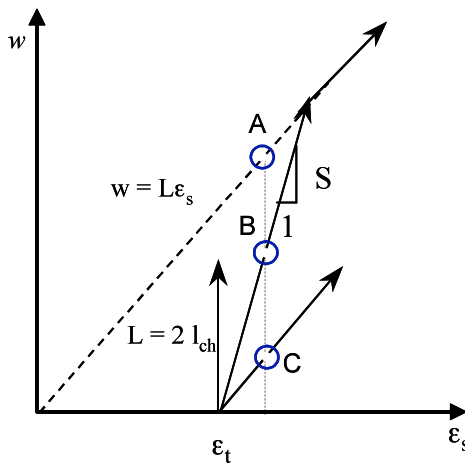


Figure 1.9 – Schematic plot of crack width  $w$  as a function of shrinkage strain  $\epsilon_s$ . The crack width development is shown for three materials with varying toughness.

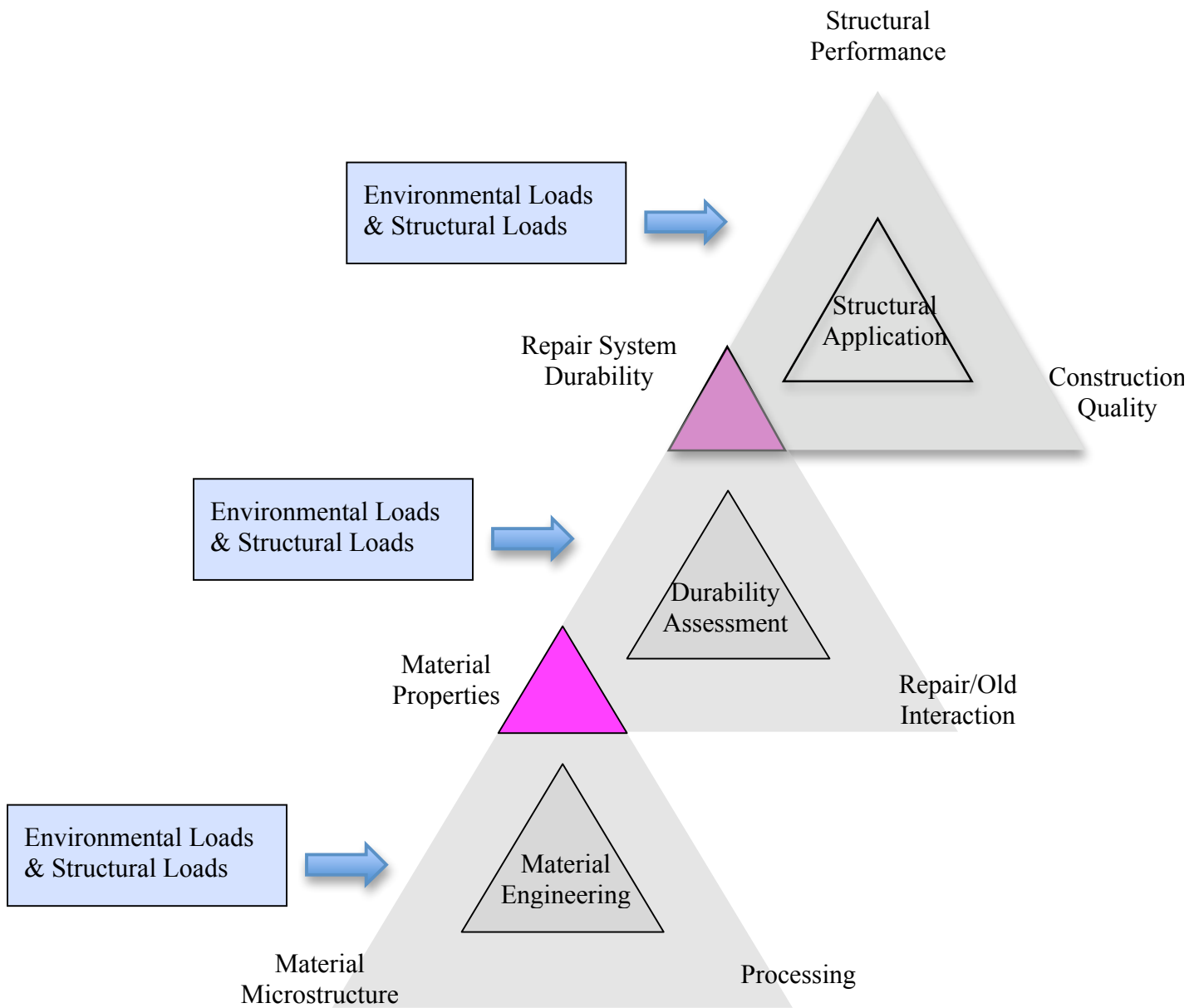


Figure 1.10 – Integrated Multi-Scale Material & Structural Engineering Framework for durability of repaired concrete structures.

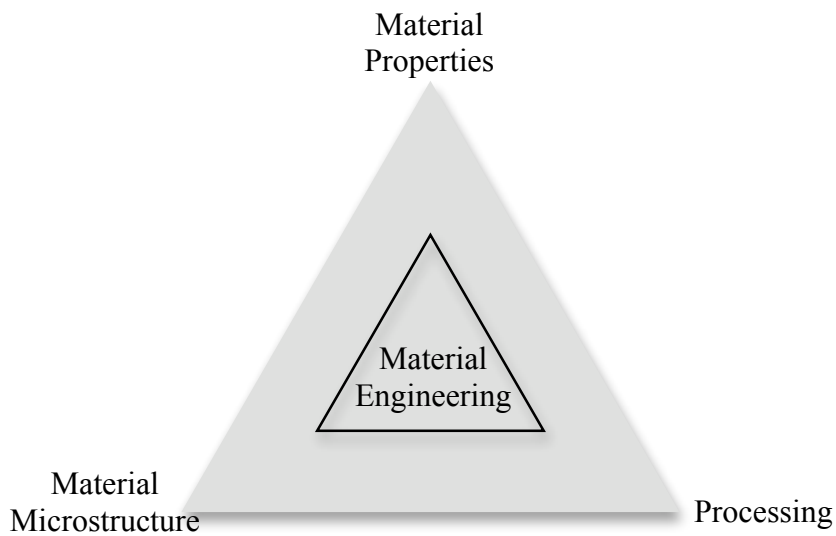
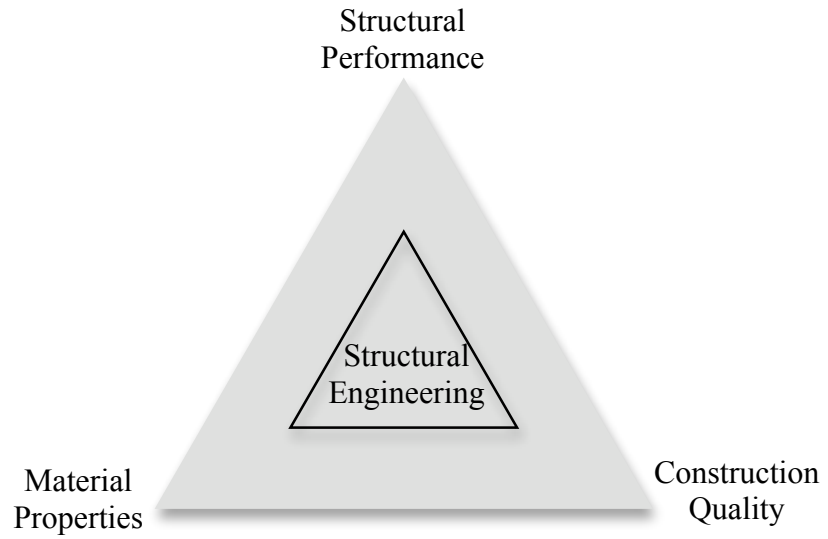


Figure 1.11 – Disconnected Material Engineering and Structural Engineering Design Philosophies for durability of repaired concrete structures.

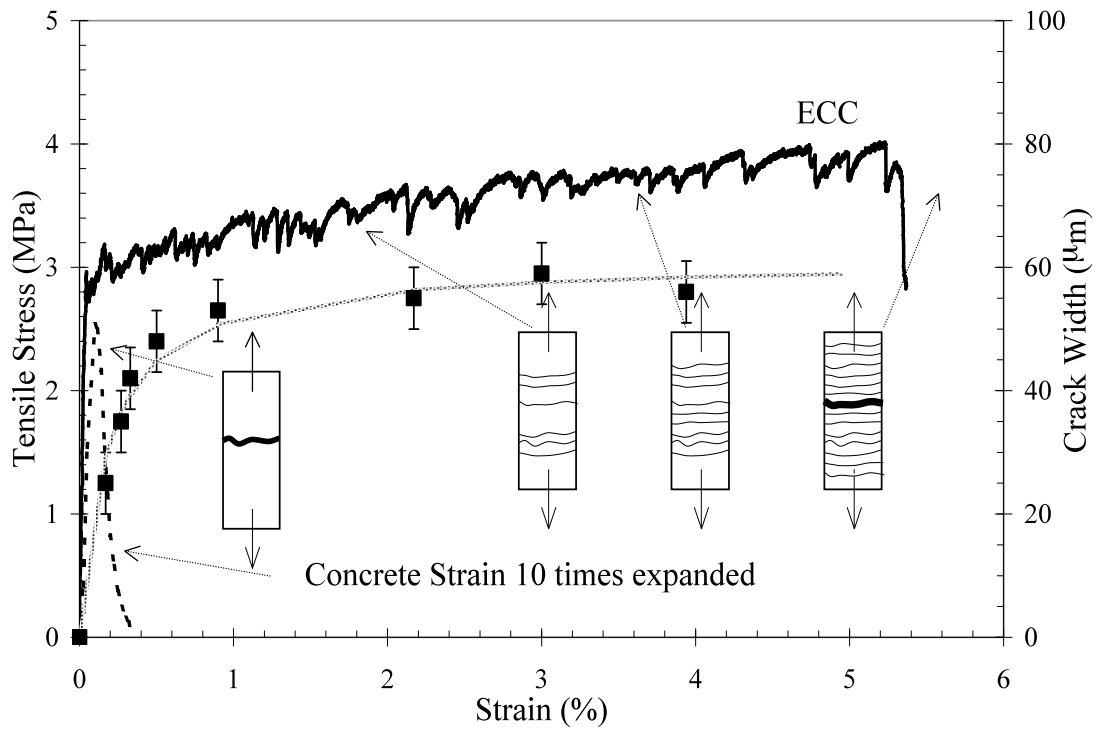


Figure 1.12 – Typical tensile stress-strain curve of ECC. Above 3 MPa, ECC shows a distinct strain-hardening response up to about 5% strain. In contrast, normal concrete fails at 0.01% strain.



Figure 1.13 – Driving surface static friction tester.

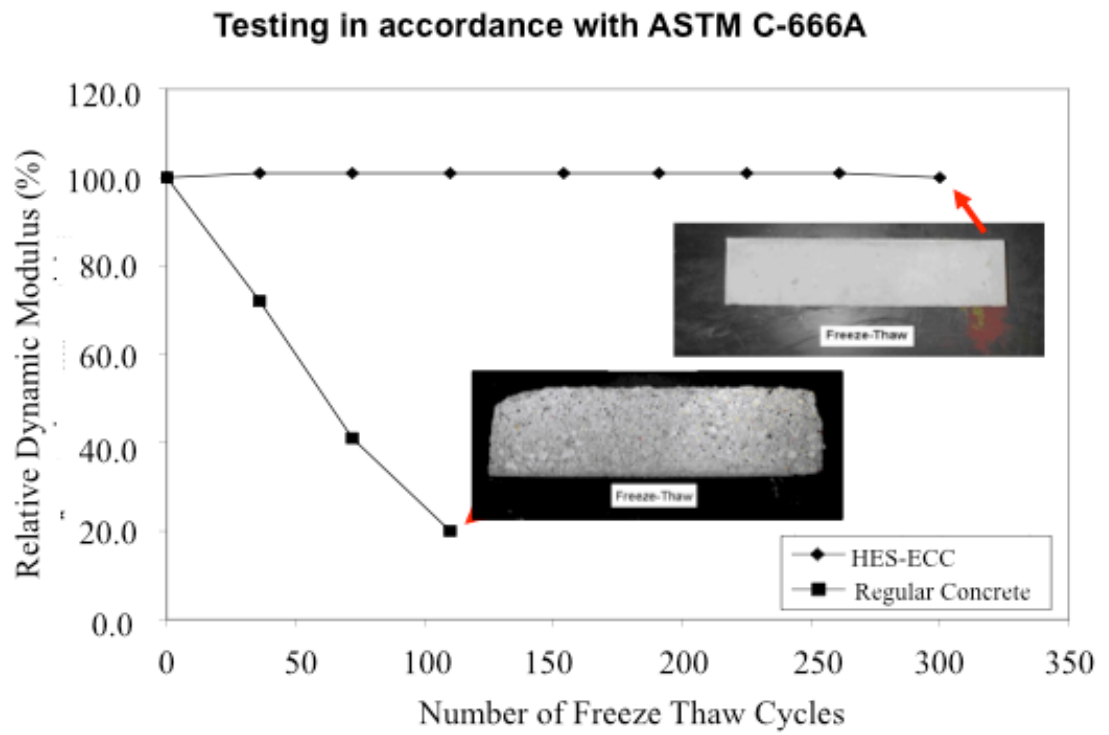


Figure 1.14 – Relative dynamic modulus vs. number of freeze thaw cycles.



Figure 1.15 – Mihara Bridge with ECC/steel composite deck opened to traffic in April 2005, Japan.

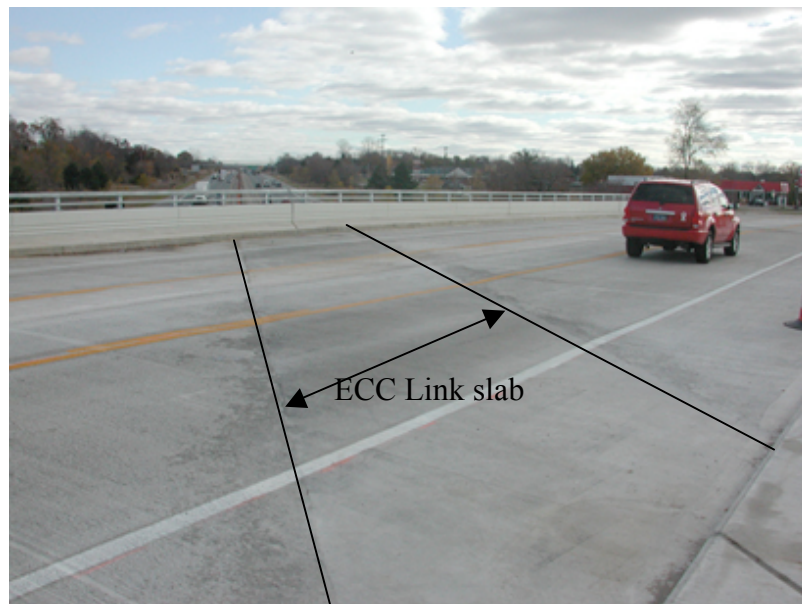


Figure 1.16 – ECC link slab on the Grove Street Bridge over I-94 opened to traffic in October 2005, Michigan.

## References:

- 
- <sup>1</sup> Infrastructure, Online Compact Oxford English Dictionary, [http://www.askoxford.com/concise\\_oed/infrastructure](http://www.askoxford.com/concise_oed/infrastructure), accessed on June 24, 2009.
- <sup>2</sup> Lomborg, B., *The Skeptical Environmentalist: Measuring the Real State of the World*, 2001, pp. 138.
- <sup>3</sup> “Minerals Commodity Summary – Cement – 2007”, <http://minerals.usgs.gov/minerals/pubs/commodity/cement/index.html>, accessed on June 24, 2009.
- <sup>4</sup> Emmons, P. H., and Sordyl, D. J., “The State of the Concrete Repair Industry, and a Vision for its Future,” *Concrete Repair Bulletin*, July/August 2006.
- <sup>5</sup> Frangopol, D. M., and Furuta, H., *Proceedings of the US-Japan Workshop on Life-Cycle Cost Analysis and Design of Civil Infrastructure Systems*, Honolulu, Hawaii, 2000.
- <sup>6</sup> Narayan, W., “Infrastructure, Climate Change, Sustainability: The Challenge of Design – Strength or Durability,” *Concrete*, Vol. 41, No. 9, October 2007, pp. 31-33.
- <sup>7</sup> Mays, G., *Durability of Concrete Structures: Investigation, Repair, Protection*, 1992.
- <sup>8</sup> “Identifying and Evaluating Concrete Defects”, [http://www.cement.org/tech/cct\\_con\\_design\\_defects.asp](http://www.cement.org/tech/cct_con_design_defects.asp), accessed July 10, 2009.
- <sup>9</sup> Vision 2020: A Vision for the Concrete Repair Protection and Strengthening Industry, the Strategic Development Council (SDC). 2006. [http://www.concretesdc.org/\\_pdfs/Vision2020-Version1.0\\_%20May2006.pdf](http://www.concretesdc.org/_pdfs/Vision2020-Version1.0_%20May2006.pdf)
- <sup>10</sup> Report Card for America’s Infrastructure. 2009. <http://www.infrastructurereportcard.org/>
- <sup>11</sup> Li, V. C., “Engineered Cementitious Composites”, *Proceedings of ConMat’05*, Vancouver, Canada, August 22-24, 2005, CD-documents/1-05/SS-GF-01\_FP.pdf.
- <sup>12</sup> Vaysburd, A. M., Brown, C. D., Bissonnette, B., and Emmons, P. H., ““Realcrete” versus “Labcrete””, *Concrete International*, Vol. 26 No.2, pp 90-94, 2004.
- <sup>13</sup> Tanaka, Y., Kawano, H., Watanabe, H and Nakajo, T., “Study on required cover depth of concrete highway bridges in coastal environment”, *17th U.S. – Japan Bridge Engineering Workshop*, Tsukuba, 2001.
- <sup>14</sup> Federal Highway Administration, “Pavement Preservation Definitions,” <http://www.fhwa.dot.gov/pavement/preservation/091205.cfm>, accessed on August 13, 2009.

- 
- <sup>15</sup> The American Association of State Highway and Transportation Officials (AASHTO), “America’s Top Five Transportation Headaches – and Their Remedies,” January 2009, [www.tripnet.org/Transportation\\_Headaches\\_Report\\_Jan\\_2009.pdf](http://www.tripnet.org/Transportation_Headaches_Report_Jan_2009.pdf).
- <sup>16</sup> Report Card for America’s Infrastructure. <http://www.infrastructurereportcard.org/factsheet/bridges>
- <sup>17</sup> Keoleian, G.A., Kendall, A., Dettling, J.E., Smith, V.M., Chandler, R.F., Lepech, M.D. and Li, V.C., “Life Cycle Modeling of Concrete Bridge Design: Comparison of ECC Link Slabs and Conventional Steel Expansion Joints,” *Journal of Infrastructure Systems*, ASCE, March 2005, pp.51-60.
- <sup>18</sup> American Association of State Highway and Transportation Officials (AASHTO). Bridging the Gap. July 2008. <http://www.transportation1.org/BridgeReport/frontpage.html>
- <sup>19</sup> Saadeghvaziri, M. A., and Hadidi, R., “Transverse Cracking of Concrete Bridge Decks: Effects of Design Factors,” *ASCE Journal of Bridge Engineering*, Vol. 10, No. 5, September/October 2005, pp. 511-519.
- <sup>20</sup> Hadidi, R., and Saadeghvaziri, M. A., “Transverse Cracking of Concrete Bridge Decks: State-of-the-Art,” *ASCE Journal of Bridge Engineering*, Vol. 10, No. 5, September/October 2005, pp. 503-510.
- <sup>21</sup> Cady, P. D, and Carrier, R. E., “Final Report on Durability of Bridge Deck Concrete: Part 1: Effect of Construction Practice on Durability,” *PennDOT Contract No. 31057-H*, Dept. of Civil Engineering, Pennsylvania State Univ., University Park, PA, 1971.
- <sup>22</sup> Krauss, P. D., and Rogalla, E. A., “Transverse Cracking in Newly Constructed Bridge Decks,” *NCHRP Rep. No. 380*, Transportation Research Board, National Research Council, Washington, D. C., 1996.
- <sup>23</sup> Portland Cement Association (PCA), “Durability of Concrete Bridge Decks – A Cooperative Study,” *Final Rep., III*, 1970.
- <sup>24</sup> Kosel, H. C., and Michols, K. A., “Evaluation of Concrete Deck Cracking for Selected Bridge Deck Structures of Ohio Turnpike,” Rep., Ohio Turnpike Commission, Construction Technology Laboratory, Ohio Department of Transportation, Columbus, Ohio, 1985.
- <sup>25</sup> Iowa Department of Transportation (Iowa DOT), “A Study of Transverse Cracks in the Keokuk Bridge Deck,” *Final Rep.*, Ames, Iowa, 1986.
- <sup>26</sup> McKeel, W. T., “Evaluation of Deck Durability on Continuous Beam Highway Bridges.” *Rep. No. VHTRC 85-R32*, Virginia Highway and Transportation Research Council, Charlottesville, VA, 1985.

- 
- <sup>27</sup> Ramey, G. E., Wolff, A. R., and Wright, R. L., "Structural Design Actions to Mitigate Bridge Deck Cracking," *Practice Periodical on Structural Design and Construction*, Vol. 2, No. 3, pp. 118-124, 1997.
- <sup>28</sup> Cheng, T. T., and Johnson, D. W., "Incidence Assessment of Transverse Cracking in Bridge Decks: Construction and Material Consideration," *Rep. No. FHWA/NC/85-002*, Federal Highway Administration, Washington, D. C., Vol. 1, 1985.
- <sup>29</sup> Perfetti, G. R., Johnson, D. W., and Bingham, W. L., "Incidence Assessment of Transverse Cracking in Concrete Bridge Decks: Structural Considerations," *Rep. No. FHWA/NC/85-002*, Vol. 2, Federal Highway Administration, Washington, D. C., 1985.
- <sup>30</sup> Perragaux, G. R., and Brewster, D. R., "In-Service Performance of Epoxy Coated Steel Reinforcement in Bridge Decks," *Final Technical Rep. No. 92-3*, New York State Department of Transportation, Albany, N. Y., 1992.
- <sup>31</sup> Babaei, K., and Hawkins, N. M., "Evaluation of Bridge Deck Protective Strategies," *NCHRP Rep. No. 297*, Transportation Research Board, National Research Council, Washington, D. C., 1987.
- <sup>32</sup> La Fraugh, R. W., and Perenchio, W. F., "Phase I Report of Bridge Deck Cracking Study West Seattle Bridge," *Rep. No. 890716*, Wiss, Janney, Elstner Associates, Northbrook, Ill, 1989.
- <sup>33</sup> Babaei, K. and Purvis, R., "Prevention of Cracks in Concrete Bridge Decks: Report on Laboratory Investigation of Concrete Shrinkage," *Research Project No. 89-01*, Pennsylvania Department of Transportation, Harrisburg, PA, 1994.
- <sup>34</sup> Ducrete, J., Lebet, J. , and Monney, C., "Hydration Effect and Deck Cracking During the Construction of Steel Concrete Composite Bridges," *Proc. ICOM-Construction Metallique*, Article 359, 1997.
- <sup>35</sup> French, C., Eppers, L., Le, Q., and Hajjar, J. F., "Transverse Cracking in Concrete Bridge Decks," *Transportation Research Record 1688*, Transportation Research Board, Washington, D. C., 1999, pp. 21-29.
- <sup>36</sup> Frosch, R. J., Radabaugh, R. D., and Blackman, D. T., "Investigation of Transverse Deck Cracking," *Proc. Structures Congress*, ASCE, Reston, VA, 2002.
- <sup>37</sup> Schmitt, T. R., and Darwin, D., "Cracking in Concrete Bridge Decks," *Rep. No. K-TRAN:KU-94-I*, Kansas Department of Transportation, Topeka, KAN, 1995.
- <sup>38</sup> Horn, M. W., Stewart, C. F., and Boulware, R. L., "Factors Affecting the Durability of Concrete Bridge Decks: Construction Practice," *Interim Rep. No. 3, CA-DOT-ST-4101-4-75-3*, Bridge Department, California Division of Highways, Sacramento, California, 1975.

- 
- <sup>39</sup> Kochanski, T., Parry, J., Pruess, D., Schuchardt, L., and Ziehr, J., "Premature Cracking of Concrete Bridge Decks Study," *Final Rep.*, Wisconsin Department of Transportation, Madison, Wisconsin, 1990.
- <sup>40</sup> Ramey, G. E., Wolff, A. R., and Wright, R. L., "Structural Design Actions to Mitigate Bridge Deck Cracking," *Practice Periodical on Structural Design and Construction*, Vol. 2, No. 3, 1997, pp. 118-124.
- <sup>41</sup> Meyers, C., "Survey of Cracking on Underside of Classes B-1 and B-2 Concrete Bridge Decks in District 4," *Investigation No. 82-2*, Division of Material and Research, Missouri Highway and Transportation Department, Jefferson City, Mo, 1982.
- <sup>42</sup> Stewart, C. F., and Gunderson, B. J., "Factors Affecting the Durability of Concrete Bridge Decks," *Interim Rep. No. 2*, Research and Development Section of Bridge Department, California Department of Transportation, Sacramento, California, 1969.
- <sup>43</sup> American Concrete Institute (ACI), "Hot Weather Concreting," ACI 305 R, Committee 305, Detroit, 1999.
- <sup>44</sup> New York State Department of Transportation (NYDOT), "The State of the Art Bridge Deck," *Final Rep.*, The Bridge Deck Task Force, NYDOT, Albany, N. Y., 1995.
- <sup>45</sup> Issa, M., "Investigation of Cracking in Concrete Bridge Decks at Early Ages," *Journal of Bridge Engineering*, Vol. 2, No. 2, 1999, pp. 116-124.
- <sup>46</sup> Hadidi, R., Saadeghvaziri, M. A., and Hsu, C. T., "Practica Tool to Accurately Estimate Tensile Stresses in Concrete Bridge Decks to Control Transverse Cracking," *Practice Periodical on Structural Design and Construction*, Vol. 8, No. 2, 2003, pp. 74-82.
- <sup>47</sup> Houde, J., "Study of Force-Displacement Relationship for the Finite Element Analysis of Reinforced Concrete," *Rep. No. 72-3*, Department of Civil Engineering and Applied Mechanics, McGill University, Montreal, 1973.
- <sup>48</sup> Saadeghvaziri, M. A., and Hadidi, R., "Cause and Control of Transverse Cracking in Concrete Bridge Decks," *Final Rep.*, FHWA-NJ-2002-19, 2002.
- <sup>49</sup> Yam, L. C. P., and Chapman, J. C., "The Inelastic Behavior of Simply Supported Composite Beam of Steel and Concrete," *Proc.-Inst. Civ. Eng.*, Vol. 41, 1969, pp. 651-683.
- <sup>50</sup> Gilani, A. and Jansson, P., "Link Slabs for Simply Supported Bridges." *MDOT Report Number MDOT SPR-54181*, Structural Research Unit, Construction and Technology Support Area, Michigan Department of Transportation. Lansing, Michigan, 2004.
- <sup>51</sup> Fu, G., Feng, J., Dimaria, J., and Zhuang, Y., "Bridge Deck Corner Cracking on Skewed Structures," *MDOT Report RC-1490*, Sept. 2007.

- 
- <sup>52</sup> CTC & Associates LLC, WisDOT Research & Library Unit, “Early Concrete Cracking on Bridge Decks and Overlays,” prepared for WHRP Structures Technical Oversight Committee, January 30, 2008.  
<http://on.dot.wi.gov/wisdotresearch/database/tls/tlsdeckcracking.pdf>.
- <sup>53</sup> Li, M., and Li, V. C., "Behavior of ECC/Concrete Layered Repair System under Drying Shrinkage Conditions", *Journal of Restoration of Buildings and Monuments*, Vol. 12, No. 2, 2006, pp143-160.
- <sup>54</sup> Li, V.C., “High Performance Fiber Reinforced Cementitious Composites as Durable Material for Concrete Structure Repair,” *Proc. of ICFRC Int’l Conference on Fiber Composites, High Performance Concretes, and Smart Materials*, Ed. By V.S. Parameswaran, Pub. Allied Publishers Private Limited, New Delhi, India, 2004, pp. 57-74.
- <sup>55</sup> Beushausen, H. D., and Alexander, M. G., “Performance of Concrete Patch Repair Systems,” *Advances in Construction Materials*, 2007, No. 255-262.
- <sup>56</sup> Simpson, J. M., and Burdett, E. G., “Predicting Thermal Cracking in Bridge Deck Repairs,” Publication #C02C067, Copyright © 2002 Hanley-Wood, LLC.,  
<ftp://imgs.ebuild.com/woc/C02C067.pdf>.
- <sup>57</sup> Czarnecki, L., Garbacz, A., Lukowski, P., and Clifton, J. R., “Polymer Composites for Repairing Portland Cement Concrete: Compatibility Project,” *Technical Report NISTIR 6394*, National Institute of Standards and Technology, 1999.
- <sup>58</sup> Emmons, P. H., Vaysburd, A. M., Poston, R. W., and McDonald, J. E., “Performance Criteria for Concrete Repair Materials, Phase II, Field Studies,” *Technical Report REMR-CS-60*, U. S. Army Waterways Experiment Station, Vicksburg, MS, September 1998.
- <sup>59</sup> Pigeon, M. and Bissonnette, B., “Bonded Concrete Repairs: Tensile Creep and Cracking Potential,” *Concrete International*, Vol. 21, No. 11, November 1999, pp. 31-35.
- <sup>60</sup> Vayburd, A. M., “Research Needs for Establishing Material Properties to Minimize Cracking in Concrete Repairs, Summary of a Workshop,” *ICRI Publication No. Y320001*, 1996.
- <sup>61</sup> Vaysburd, A. M., Emmons, P. H., McDonald, J. E., Poston, R. W., and Kesner, K. E., “Performance Criteria for Concrete Repair Materials, Phase II Summary Report,” *Technical Report REMR-CS-62*, U. S. Army Engineers Waterways Experiment Station, Vicksburg, MS, March 1999.
- <sup>62</sup> Batis, G., Pantazopoulou, P., and Routoulas, A., “Corrosion Protection Investigation of Reinforcement by Inorganic Coating in the Presence of Alkanolamine-Based Inhibitor,” *Cement and Concrete Composites*, Vol. 25, 2003, pp. 371-377.

- 
- <sup>63</sup> Elsener, B., "Macrocell Corrosion of Steel in Concrete – Implications for Corrosion Monitoring," *Cement & Concrete Composites*, Vol. 24, 2002, pp. 65-72.
- <sup>64</sup> Scheissl, P., "Corrosion of Steel in Concrete," *RILEM Report*. Chapman and Hall. London. 1988.
- <sup>65</sup> Bavarian, B., and Reiner, L., "Migrating Corrosion Inhibitors for Steel Rebar in Concrete," *Materials Performance*, February 2003, pp. 3-5.
- <sup>66</sup> Virmani, Y. P., and Clemena, G. G., "Corrosion Protection – Concrete Bridges," *FHWA-RD-98-088*, US Department of Transportation Federal Highway Administration, Research and Development Turner-Fairbank Highway Research Center, VA, September 1998.
- <sup>67</sup> The State of the Nation's Highway Bridges: Highway Bridge Replacement and Rehabilitation Program and National Bridge Inventory," *Thirteenth Report to the United States Congress*, Federal Highway Administration, Washington, D. C., May 1997.
- <sup>68</sup> Hime, W. G., "The Corrosion of Steel – Random Thoughts and Wishful Thinking," *Concrete International*, Vol. 15, No. 10, 1993, pp. 54-57.
- <sup>69</sup> Lewis, D. A., "Some Aspects of the Corrosion of Steel in Concrete," *Proceeding of the First International Congress on Metallic Corrosion, London, 1962*, pp. 547-555.
- <sup>70</sup> Berman, H. A., "The Effects of Sodium Chloride on the Corrosion of Concrete Reinforcing Steel and on the PH of Calcium Hydroxide Solution," *Report No. FHWA-RD-74-1*, Federal Highway Administration, Washington, D. C., 1974.
- <sup>71</sup> Santagata, M. C., and Collepardi, M., "The Effect of CMA Deicers on Concrete Properties," *Cement and Concrete Research*, Vol. 30, No. 9, September 3000, pp. 1389-1394.
- <sup>72</sup> Dunn, S. A., and Schenk, R., "Alternate Highway Deicing Chemicals," *Publication No. FHWA-RD-79-108*, Federal Highway Administration, Washington, D. C., October 1979.
- <sup>73</sup> Novokshchenov, V., "Salt Penetration and Corrosion in Prestressed Concrete Members," *Report No. FHWA-RD-88-269*, Federal Highway Administration, Washington, D. C., July 1989.
- <sup>74</sup> Whiting, D., Stejskal, B., and Nagi, M., "Condition of Prestressed Concrete Bridge Components: Technology Review and Field Surveys," *Report No. FHWA-RD-93-037*, Federal Highway Administration, Washington, D. C., 1993.
- <sup>75</sup> Lankard, D. R., Thompson, N., Sprinkel, M., and Virmani, Y. P., "Grouts for Post-Tensioned Concrete Construction: Protecting Prestressed Steel in Concrete," *ACI Materials Journal*, September/October, 1993, pp. 406-413.

- 
- <sup>76</sup> Ghorbanpoor, A., “Evaluation of Post-Tensioned Concrete Bridge Structures by the Impact-Echo Technique,” *Report No. FHWA-RD-90-096*, Federal Highway Administration, Washington, D. C., 1993.
- <sup>77</sup> Wagner, J., Young, W., Scheirer, S., and Fairer, P., “Cathodic Protection Development for Prestressed Concrete Components – Interim Report,” *Report No. FHWA-RD-92-056*, Federal Highway Administration, Washington, D. C., March, 1993.
- <sup>78</sup> Funahashi, M., Wagner, J., and Young, W. T., “Cathodic Protection Developments for Prestressed Concrete Components,” *Report No. FHWA-RD-94-001*, Federal Highway Administration, Washington, D. C., July, 1994.
- <sup>79</sup> Virmani, Y. P., Clear, K. C., and Pasko, T. J., “Time-to-Corrosion of Reinforcing Steel in Concretes, Vol. 5: Calcium Nitrite Admixture or Epoxy-Coated Reinforcing Bars as Corrosion Protection Systems,” *Report No. FHWA/RD-83/012*, Federal Highway Administration, Washington, D. C., 1983.
- <sup>80</sup> Hay, R. E., and Virmani, Y. P., “North American Experience in Concrete Bridge Deterioration and Mechanism,” *Proceeding of the Concrete Society*, United Kingdom, September, 1985.
- <sup>81</sup> Manning, D. G., National Research Council (U. S.), Transportation Research Board, National Cooperative Highway Research Program, American Association of State Highway and Transportation Officials (U. S.), Federal Highway Administration, “Waterproofing Membranes for Concrete Bridge Decks,” No. 220, 1995.
- <sup>82</sup> Stratfull, R. F., “Experimental Cathodic Protection of a Bridge Deck,” *Transportation Research Record No. 500*, 1974, pp. 1-15.
- <sup>83</sup> Fromm, H. J., “Electrically Conductive Asphalt Mixes for the Cathodic Protection of Concrete Bridge Decks,” Presented at the 1976 Meeting of the Association of Asphalt Paving Technologists, New Orleans, February, 1976.
- <sup>84</sup> Fontana, J. J., Reams, W., and Elling, D., “Conductive Overlay in Conjunction with an Active Cathodic Protection System,” *Report No. FHWA-RD-88-145*, Federal Highway Administration, Washington, D. C., 1989.
- <sup>85</sup> Clemena, G. G., and Jackson, D. R., “Performance of a Conductive-Paint Anode in Cathodic Protection Systems for Inland Concrete Bridge Piers in Virginia,” *Report No. FHWA/VTRC 98-R7*, Virginia Transportation Research Council, Charlottesville, Virginia, 1997.
- <sup>86</sup> Whiting, D., Nagi, M., and Broomfield, J. P., “Evaluation of Sacrificial Anode for Cathodic Protection of Reinforced Concrete Bridge Decks,” *Report No. FHWA-RD-95-041*, Federal Highway Administration, Washington, D. C., May, 1995.

- 
- <sup>87</sup> Hartt, W., Joubert, E., and Kliszowski, S., “Long-Term Effects of Cathodic Protection on Prestressed Concrete Bridge Components,” *Report No. FHWA-RD-96-029*, Federal Highway Administration, Washington, D. C., November, 1996.
- <sup>88</sup> Bennett, J. E., and Shue, T. J., “Field Evaluation of Cathodic Protection on Prestressed Concrete Bridge Members: Final Report,” *Report No. FHWA-RD-97-153*, Federal Highway Administration, Washington, D. C., 1997.
- <sup>89</sup> Clemena, G. G., and Jackson, D. R., “Pilot Applications of Electrochemical Chloride Extraction on Concrete Piers in Virginia – Interim Reports,” *Report No. VTRC-96-IR4*, Virginia Transportation Research Council, Charlottesville, Virginia, 1996.
- <sup>90</sup> Mehta, P.K., “Durability–Critical Issues for the Future”, *Concrete International*, Vol. 19, No. 6, 1997, pp. 27-33.
- <sup>91</sup> Xi, Y., B. Shing, N. Abu-Hejleh, A. Asiz, A. Suwito, Z. Xie, A. Ababneh, “Assessment of the Cracking Problem in Newly Constructed Bridge Decks in Colorado,” Colorado Department of Transportation Research Branch. Denver, Colorado. CDOT-DTD-R-2003-3. March, 2003.
- <sup>92</sup> Kondratova, I., and Bremner, T. W., “Field and Laboratory Performance of Epoxy-Coated Reinforcement in Cracked and Uncracked Concrete,” Presented at the 77th Annual Meeting of the Transportation Research Board, Washington, D. C., 1998.
- <sup>93</sup> The Road Information Project (TRIP), Key Facts About America's Road and Bridge Conditions and Federal Funding, updated August 2008
- <sup>94</sup> U.S. Department of Transportation, Status of the Nation's Highways, Bridges and Transit: Conditions and Performance, 2006.
- <sup>95</sup> Report of the National Surface Transportation Policy and Revenue Study Commission - Transportation for Tomorrow, December 2007. Volume II.
- <sup>96</sup> Al-Qadi, I. L., Scarpas, T., and Loizos, A., *Pavement Cracking*, 2008, p. 930.
- <sup>97</sup> Delatte, N. J., *Concrete Pavement Design, Construction, and Performance*, 2007, p. 372.
- <sup>98</sup> Huang, Y. H., *Pavement Analysis and Design (2<sup>nd</sup> Edition)*, 2003, p. 792.
- <sup>99</sup> Miller, J. S., and Bellinger, W. Y., Distress Identification Manual for the Long-Term Pavement Performance Program (Fourth Revised Edition), *FHWA-RD-03-031*, June 2003.
- <sup>100</sup> Schwartz, D. R., and Brown, B. C., “D-Cracking of Concrete Pavements,” National Transportation Research Board, 1987, p. 34.
- <sup>101</sup> Carpenter, A. J., and Cramer, S. M., “Mitigation of Alkali-Silica Reaction in Pavement Patch Concrete that Incorporates Highly Reactive Fine Aggregate,”

---

Transportation Research Record, Annual Meeting of the Transportation Research Board, No. 78, 1999, pp. 60-67.

<sup>102</sup> U.S. Department of Transportation, Federal Highway Administration, Partial-Depth Repairs, <http://www.fhwa.dot.gov/pavement/concrete/index.cfm>.

<sup>103</sup> U.S. Department of Transportation, Federal Highway Administration, Full-Depth Repairs, <http://www.fhwa.dot.gov/pavement/concrete/full.cfm>.

<sup>104</sup> MDOT, Pavement Design and Selection Manual, Michigan Department of Transportation, Lansing, Michigan, 2005, p. 65.

<sup>105</sup> Tayabji, S. D. and Okamoto, P. A., "Thickness Design of Concrete Resurfacing," Proc., *3<sup>rd</sup> Int'l Conf. on Concrete Pavement Design and Rehabilitation*, 1985, pp. 367-379.

<sup>106</sup> ERES Consultants, Inc., NCHRP Report 415, Evaluation of Unbonded Portland Cement Concrete Overlays, Transportation Research Board, Washington, D. C., 1999.

<sup>107</sup> Huang, Y. H., *Pavement Analysis and Design*, 2<sup>nd</sup> edition, Pearson Education, Upper Saddle River, NJ 07458.

<sup>108</sup> Keenan, L. E., and Soden, B. R., "Parking Structure Maintenance: Early Detection, Early Cure," *Journal of Architectural Technology* published by Hoffmann Architects, Vol. 19, No. 2, Feb. 2001.

<sup>109</sup> Peterson, C. A., "Designing and Building Durable Parking Structures," *Aberdeen's Concrete Construction*, Vol. 40, No. 3, March 1999.

<sup>110</sup> Bhuyan, S. (Walker Parking Consultants, Inc.), Sabnis, G. M., Shiu, K. N., "A Systematic Approach to Extending Service Life of Parking Structures," *Indian Concrete Journal*, Vol. 75, No. 1, January 2001, pp. 58-64.

<sup>111</sup> Bhuyan, S. (Walker Parking Consultants & Restoration Engineers, Kalamazoo, MI, USA), "Repairing Concrete Parking Structure," *Concrete Construction – World of Concrete*, Vol. 33, No. 2, February 1998.

<sup>112</sup> O'Connor, J. P., and Olson, C. A., "Deterioration in Precast Prestressed Concrete Parking Garage," *Concrete International*, Vol. 12, No. 11, Nov 1990, pp. 52-54.

<sup>113</sup> Bickley, J. A., "Deterioration of Parking Structures," *Annals of Biomedical Engineering*, 1980.

<sup>114</sup> Ma, R., Xiao, Y., "Full-Scale Testing of a Parking Structure Column Retrofitted with Carbon Fiber Reinforced Composites," *Construction and Building Materials*, Vol. 14, No. 2, pp 63-71, March 30, 2000.

- 
- <sup>115</sup> Aalami, B. O., Swanson, D. T., “Innovative Rehabilitation of a Parking Structure,” *Concrete International*, Vol. 10, No. 2, February 1988, pp. 30-35.
- <sup>116</sup> Brainerd, M. L., “Evaluation and Rehabilitation of Deteriorated Parking Structures,” *Construction Specifier*, Vol. 42
- <sup>117</sup> Litvan, G. G., “Waterproofing of Parking Garage Structures with Sealers and Membranes: The Canadian Experience,” *Construction and Building Materials*, Vol. 10, No. 1 Spec. Iss., February 1996, pp. 95-100.
- <sup>118</sup> Ojha, S. K., “Rehabilitation of a Parking Garage,” *Concrete International*, Vol. 8, No. 4, 1986, pp. 24-28.
- <sup>119</sup> Meyers, M., “Structures at Risk. Preparing and Repairing Parking Garages,” *Public Works*, Vol. 121, No. 9, 1990, pp. 46-47.
- <sup>120</sup> Steele, M., “Protecting Concrete Parking Structures: From Asphaltics to Polyurethanes,” *Journal of Protective Coatings and Linings*, Vol. 23, No. 11, 2006, pp. 52-55.
- <sup>121</sup> Tighe, M. R., Hembra, D., “Industry Faces the Parking Problem,” *Civil Engineering* New York, N. Y., Vol. 60, No. 11, November 1990, pp. 65-66.
- <sup>122</sup> Delaney, T. J., “Repairing Post-Tensioned Parking Structures,” *Aberdeen’s Concrete Repair Digest*, Vol. 7, No. 4, Aug-Sep 1996, pp. 186-189.
- <sup>123</sup> Nehil, T. E., “Rehabilitating Parking Structures with Corrosion-Damaged Button-Headed Post-Tensioning Tendons,” *Concrete International*, Vol. 13, No. 10, Oct 1991, pp. 66-73.
- <sup>124</sup> Anon, “Avoid Joint Deterioration in Concrete Parking Structures,” *Aberdeen’s Concrete Construction*, Vol. 36, No. 8, Aug 1991, pp. 616-618.
- <sup>125</sup> Beeldens, A., and Vandewalle, L., “Durability of high strength concrete for highway pavement restoration,” *In CONSEC '01: Third International Conference on Concrete under Severe Conditions*, Vancouver, BC, Canada, 2001, pp. 1230-1238.
- <sup>126</sup> Oh, B.H., Cha, S.W., Jang, B.S. & Jang, S.Y., “Development of high-performance concrete having high resistance to chloride penetration,” Elsevier Science SA, *Nuclear Engineering and Design* (Switzerland), Vol. 212, No. 1-3, 2002, pp. 221-231.
- <sup>127</sup> Mehta, P. K., *Concrete: Structure, Properties, and Materials*, Prentice-Hall, Englewood Cliffs, New Jersey, 1986, pp. 353-367.
- <sup>128</sup> Chang, P. K., Peng, Y. N., and Hwang, C. L., “A Design Consideration for Durability of High-Performance Concrete,” *Cement & Concrete Composites*, Vol. 23, No. 4-5, Aug. – Oct. 2001, pp. 375-380.

- 
- <sup>129</sup> Hwang, C. L., Liu, J. J., Lee, L. S., and Lin, F. Y., “Densified Mixture Design Algorithm and Early Properties of High Performance Concrete,” *Journal of the Chinese Institute of Civil and Hydraulic Engineering*, Vol. 8, No. 2, 1996, pp. 217-229.
- <sup>130</sup> Shah, S. P., Wang, K., and Weiss, W. J., “Is High Strength Concrete Durable?” *Concrete Technology for a Sustainable Development in the 21<sup>st</sup> Century* Eds. O. E. Gjorv and K. Sakai, 2000, pp. 102-114.
- <sup>131</sup> Li, V. C., and Stang, H., “Elevating FRC Material Ductility to Infrastructure Durability,” *Proceedings of 6<sup>th</sup> RILEM symposium on FRC*, Varenna, Italy, 2004, pp. 171-186.
- <sup>132</sup> Hillerborg, A., Mod er, M., and Petersson, P.E. “Analysis of Crack Formation and Crack Growth in Concrete By Means of Fracture Mechanics and Finite Elements.” *Cement and Concrete Research*, Vol. 6, No. 6, 1976, pp. 773-782.
- <sup>133</sup> Mehta, P.K., “Durability–Critical Issues for the Future”, *Concrete International*, Vol. 19, No. 6, 1997, pp. 27-33.
- <sup>134</sup> Mehta, P.K. and R.W. Burrows, “Building durable infrastructures in the 21st century.” *Concrete International*, Vol. 23, No. 3, 2001, pp. 57-63.
- <sup>135</sup> Xi, Y., B. Shing, N. Abu-Hejleh, A. Asiz, A. Suwito, Z. Xie, A. Ababneh “Assessment of the Cracking Problem in Newly Constructed Bridge Decks in Colorado” *Colorado Department of Transportation Research Branch*. Denver, Colorado. CDOT-DTD-R-2003-3. March 2003.
- <sup>136</sup> Morgan, D. R., “Compatibility of Concrete Repair Materials and Systems,” *Construction and Building Materials*, Vol. 10, No. 1, 1996, pp. 57-67.
- <sup>137</sup> International Concrete Repair Institute, “Guideline for Inorganic Repair Material Data Sheet Protocol,” *Guideline No. 03740*, 2003.
- <sup>138</sup> ASTM C1218/C1218M “Standard Test Method for Water-Soluble Chloride in Mortar and Concrete” Vol. 4.02.
- <sup>139</sup> Li, V. C., “Reflections on the Research and Development of Engineered Cementitious Composites (ECC),” *Proceedings of the JCI International Workshop on Ductile Fiber Reinforced Cementitious Composites (DFRCC) – Application and Evaluation (DRFCC-2002)*, Takayama, Japan, Oct. 2002, pp. 1-21.
- <sup>140</sup> Li, V.C., “Integrated Structures and Materials Design,” *RILEM J. of Materials and Structures*, Vol. 40, No. 4, 2007, pp. 387-396.
- <sup>141</sup> Maalej, M., Hashida, T., and Li, V.C., "Effect of Fiber Volume Fraction on the Off-Crack Plane Energy in Strain-Hardening Engineered Cementitious Composites," *Journal of American Ceramics Society*, Vol. 78, No. 12, 1995, pp. 3369-3375.

- 
- <sup>142</sup> Li, V. C., “Engineered Cementitious Composites – Tailored Composites Through Micromechanical Modeling,” *Fiber Reinforced Concrete: Present and the Future*, N. Banthia, A. A. Bentur, and A. Mufti, eds., Canadian Society for Civil Engineering, Montreal, Quebec, Canada, 1998, pp. 64-97.
- <sup>143</sup> Li, V. C., Wu, C., Wang, S., Ogawa, A., and Saito, T., “Interface Tailoring for Strain-Hardening Polyvinyl Alcohol-Engineered Cementitious Composites (PVA-ECC),” *ACI Materials Journal*, Vol. 99, No. 5, Sept.-Oct. 2002, pp. 463-472.
- <sup>144</sup> Fischer, G., and Li, V. C., “Deformation Behavior of Fiber-Reinforced Polymer Reinforced Engineered Cementitious Composites (ECC) Flexural Members under Reversed Cyclic Loading Conditions,” *ACI Structural Journal*, Vol. 100, No. 1, Jan-Feb. 2003, pp. 25-35.
- <sup>145</sup> Zhang, J., Maalej, M. and Quack, S. T., “Hybrid Fiber Engineered Cementitious Composites (ECC) for Impact and Blast-Resistant Structures,” *Proceedings of the First International Conference on Innovative Materials and Technologies for Construction and Restoration-IMTCR04*, Lecce, Italy, Vol. 1, June 2004, pp. 136-149.
- <sup>146</sup> Maaley, M., Quack, S. T., and Zhang, J., “Behavior of Hybrid-Fiber Engineered Cementitious Composites Subjected to Dynamic Tensile Loading and Projectile Impact,” *ASCE Journal of Materials in Civil Engineering*, Vol. 17, No. 2, 2005, pp. 143-152.
- <sup>147</sup> Qian, S., Lepech, M. D., Kim, Y. Y., and Li, V. C., “Introduction of Transition Zone Design for Bridge Deck Link Slabs Using Ductile Concrete,” *ACI Structural Journal*, Vol. 106, No. 1, Jan. 2009, pp. 96-105.
- <sup>148</sup> Qian, S. and Li, V. C., “Influence of Concrete Material Ductility on Headed Anchor Pullout Performance,” *ACI Materials Journal*, Vol. 106, No. 1, Jan. 2009, pp. 72-81.
- <sup>149</sup> Li, V. C., “Engineered Cementitious Composites,” *Proceedings of ConMat'05*, Vancouver, Canada, August 22-24, 2005, CD-documents/1-05/SS-GF-01\_FP.pdf.
- <sup>150</sup> Li, V.C., and Wang, S., “Flexural Behavior of GFRP Reinforced Engineered Cementitious Composites Beams,” *ACI Materials Journal*, Vol. 99, No.1, 2002, pp.11-21.
- <sup>151</sup> Fischer, G., and Li, V.C., "Effect Of Matrix Ductility On Deformation Behavior of Steel Reinforced ECC Flexural Members Under Reversed Cyclic Loading Conditions," *ACI Structural Journal*, Vol. 99, No. 6, 2002, pp.781-790.
- <sup>152</sup> Kesner, K., and Billington, S. L., "Experimental Response of Precast Infill Panels Made with DFRCC," *DFRCC-2002 International Workshop*, Takayama, Japan, 2002, pp. 289-298.
- <sup>153</sup> Parra-Montesinos, G., and Wight, J.K., "Seismic Response of Exterior RC Column-to-Steel Beam Connections," *Journal of Structural Engineering*, Vol. 126, No. 10, 2000, pp. 1113-1121.

- 
- <sup>154</sup> Li, V.C. & Lepech, M. 2004. "Crack resistant concrete material for transportation construction," In TRB 83rd Annual Meeting, Washington, D.C., CD ROM, Paper 04-4680.
- <sup>155</sup> Li, V.C., Fischer, G., Kim, Y.Y., Lepech, M., Qian, S., Weimann, M. & Wang, S., "Durable Link Slabs for Jointless Bridge Decks Based on Strain-Hardening Cementitious Composites," *Report for MDOT RC-1438*. 2003.
- <sup>156</sup> Li, V.C., Horikoshi, T., Ogawa, A., Torigoe, S. & Saito, T., "Micromechanics-based Durability Study of Polyvinyl Alcohol-Engineered Cementitious Composite (PVA-ECC)," *ACI Materials Journal*, Vol. 101, No. 3, 2004, pp. 242-248.
- <sup>157</sup> Kunieda, M., and Rokugo, K., "Recent Progress on HPCFRCC in Japan," *Journal of Advanced Concrete Technology*, Vol. 4, No. 1, 2006, pp.19-33.
- <sup>158</sup> Li, V.C., Lepech, M., and Li, M., "Field Demonstration of Durable Link Slabs for Jointless Bridge Decks Based on Strain-Hardening Cementitious Composites," *Michigan DOT Report RC-1471*, Dec. 2005.
- <sup>159</sup> Li, V. C., Li, M., Lepech, M., "High Performance Material for Rapid Durable Repair of Bridges and Structures," *Michigan DOT Report RC-1484*, Dec. 2006.
- <sup>160</sup> Lin, Z., and Li, V. C., "Crack Bridging in Fiber Reinforced Cementitious Composites with Slip-Hardening Interfaces," *Journal of Mechanics and Physics of Solids*, Vol. 45, No. 5, 1997, pp. 763-787.

## CHAPTER 2

### **Micromechanics Based Design of ECC Repair Materials**

Within the material engineering phase of the Integrated Material and Structural Engineering framework, shown in Figure 1.10, microstructure tailoring and material processing converge to ultimately produce composite materials with desired combinations of properties. This chapter focuses on the microstructure tailoring portion of this framework through the development of a new version of ECC material called HES-ECC, specifically for fast and durable repair applications. Besides tensile ductility, HES-ECC also possesses high early-age strength properties, which are not achieved by ordinary type I Portland cement based ECC (e.g. ECC M45). High early-age strength is necessary for repaired structures to be able to return to service with minimum operations interruption; tensile ductility is crucial for the repaired structures to be durable with minimum repair and maintenance frequency during their service lives.

Wang and Li, 2006<sup>1</sup> first introduced the idea of simultaneously designing tensile ductility and high early strength into cementitious materials. Their work mainly focused

on the micromechanical design of HES-ECC based on proprietary rapid-hardening cement binders. Although other binder systems (i.e. Type I Portland cement and Type III Portland cement) were also included in the study, the emphasis was on composite scale, and a detailed study of the effects of these binder systems on micromechanical parameters was not reported. Type III Portland cement, however, is more widely available, less expensive, more compatible with existing commercially available admixtures, and more familiar to the construction industry compared to proprietary rapid-hardening cement. Driven by these reasons, the research described in this chapter focuses on the detailed micromechanical design and material characterization of HES-ECC based on Type III Portland cement binder systems.

Within this chapter, the ECC design philosophy and scale linking are described first, followed by a review of strain-hardening criteria and conditions for saturated multiple cracking. After the initial mix design to meet the target early-age strength and workability requirements, effects of the Type III Portland cement binder system on the age dependency of the micromechanical parameters (i.e. matrix, fiber/matrix interfacial properties) and the pseudo strain-hardening index (PSH) were investigated. Based on these factors, the initial mix was then further tailored through introducing artificial flaws to maximize multiple-cracking behavior and tensile strain capacity while maintaining self-controlled crack width below 100  $\mu\text{m}$ . Finally, this new Type III Portland cement based HES-ECC was characterized based on composite traits such as tensile, compressive, and flexural properties to provide a database for future structural applications. Durability of this material, such as shrinkage properties, was also investigated and will be reported in later chapters.

## 2.1 High Performance Fiber Reinforced Cementitious Composites

In the past decade great strides have been made in developing high performance fiber reinforced cementitious composites (HPFRCC). HPFRCC were first classified by Naaman and Reinhardt<sup>2</sup> as materials that achieved different degrees of tensile ductility, often accompanied by a macroscopic pseudo-strain hardening response after first cracking. Under this definition, HPFRCC is distinguished from an ordinary Fiber Reinforced Concrete (FRC) that has a tension-softening response. Figure 2.1 compares the uniaxial tensile stress-deformation relation of concrete, FRC, and HPFRCC. For concrete, crack formation results in a sudden drop in load carrying capacity. For FRC, after cracking occurs, tensile load capacity drops at a relatively slow rate as the single crack enlarges. This is called “tension-softening”. For HPFRCC, after the first crack forms, tensile load capacity continues to rise with increasing strain (“strain-hardening”) through formation of multiple cracks. The deformation during the elastic and strain-hardening stages in HPFRCC can be treated as “volumetric straining” rather than “localized crack opening”<sup>3</sup>.

Efforts to design tensile ductility into cementitious materials started in the 1970s, and have mainly focused on using continuous aligned fibers or large-volume discontinuous fibers. Aveston et al., 1971<sup>4</sup> and Krenchel and Stang, 1989<sup>5</sup> achieved tensile ductility hundreds of times that of normal concrete using continuous aligned fibers in concrete materials. Textile reinforced concrete materials, representing the modern version of continuous fiber reinforced concrete, were developed by Curbach and Jesse, 1999<sup>6</sup>, and Reinhardt et al, 2003<sup>7</sup>. Moreover, pultruded continuous fiber reinforced concrete was recently developed by Mobasher et al, 2006<sup>8</sup>. Additionally, cementitious

composite materials using discontinuous fibers at high dosage (4-20%) in cement laminates<sup>9</sup> or in SIFCON (Slurry Infiltrated Fiber Concrete)<sup>10,11</sup> attain higher tensile strength and strain capacity than normal concrete, but much lower tensile ductility than continuous fiber and textile reinforced cementitious materials.

The HPFRCC materials described above have so far found limited field applications. This is due to their considerable cost and difficulty in processing, especially in on-site construction. Considering the huge consumption of materials in the construction industry, cost effectiveness and construction efficiency are of foremost importance. These requirements can hardly be met using aligned fiber or large-volume discontinuous fiber materials. Various methods have been proposed for overcoming processing difficulties. For example, Shah et al. employed an extrusion process to produce HPFRCC with tensile strain capacity below 1%, at greater than 4% fiber volume content. Most of these research efforts have focused on approaches to embed a large volume of fibers in order to attain high composite performance. The market, however, demands low cost and ease of processing.

In recent years, a new class of HPFRCC has emerged. ECC (Engineered Cementitious Composites), originally developed at the University of Michigan<sup>12</sup>, features high ductility with a moderate amount (no more than 2 vol%) of short discontinuous fibers. Despite its apparent similarity in composition (e.g. cementitious binder, fine aggregates, water, and fiber) compared with other HPFRCC materials, ECC's design principle is quite distinct. Instead of relying on a high fiber content to achieve strain-hardening behavior, the development approach for ECC is to design synergistic interactions between the fiber, matrix, and fiber/matrix interface to maximize tensile

ductility of the composite through formation of closely spaced multiple microcracks while minimizing fiber content. Through this micromechanics and fracture mechanics based material design approach, ECC can achieve tensile strain capacities of 3-5%, approximately 300-500 times that of concrete or FRC, with 2 vol% or less discontinuous polymer fibers. The theoretical framework of ECC material design is reviewed in the next section.

## **2.2 ECC Micromechanics Based Design Theory**

### **2.2.1 ECC Design Framework – Scale Linking**

Micromechanics based design theory of ECC was first established in the early 90's<sup>13,14</sup>. This theory links the measurable constituent parameters to the cracking propagation mode, and then to conditions for composite tensile strain-hardening. Scale linking (Figure 2.2) is a fundamental characteristic of the ECC design approach, in which understanding and tailoring of microscale constituent parameters are the keys to achieving target macroscale composite behavior.

The scale linking between ECC microstructure and composite tensile behavior is illustrated in Figure 2.2. As a composite material, ECC contains three main phases: fibers, matrix (including pre-existing flaws), and fiber/matrix interface. Each phase can be defined by a set of micro-parameters as shown in Table 2.1. Under uniaxial tension, ECC composites exhibit tensile strain hardening behavior at the macroscale (mm – cm) through a multiple cracking process. Steady-state crack propagation is a necessary condition to ensure multiple cracking, which is governed by the fiber bridging properties across cracks at the mesoscale ( $\mu\text{m}$  – mm). The fiber bridging spring law across a crack,

quantified by the fiber bridging stress vs. crack opening relationship  $\sigma(\delta)$ , is the integration of the bridging force contributed by every single fiber bridging the crack. For an individual fiber, its bridging force for a given crack opening is determined by its pullout behavior from the surrounding matrix, and governed by fiber and interface properties at the microscale (nm –  $\mu\text{m}$ ), as well as by fiber embedment length and inclination angle between the fiber axis and the crack face normal. In summary, the micromechanics model links microscale constituent parameters to fiber bridging constitutive behavior on the mesoscale; steady-state crack analysis links fiber bridging properties to tensile strain-hardening behavior on the composite macroscale. Once established, the model-based linking provides a systematic framework for optimizing composite tensile properties with the minimum amount of fibers by strategically tailoring the microstructure at the smallest scales.

### **2.2.2 Conditions for Tensile Strain Hardening**

The tensile strain-hardening behavior of ECC is realized by tailoring the synergistic interaction between the fibers, matrix, and fiber/matrix interface using micromechanics theory. As a fiber reinforced brittle mortar matrix composite, ECC's pseudo strain-hardening behavior is achieved through sequential formation of matrix multiple cracking. The fundamental requirement for matrix multiple cracking is that steady-state flat crack propagation prevails under tension, which was first characterized by Marshall and Cox<sup>15</sup> for continuous aligned fiber-reinforced ceramics, and extended to discontinuous fiber-reinforced cementitious composites by Li and Leung<sup>13</sup>. To ensure steady-state cracking, the crack tip toughness  $J_{\text{tip}}$  must be less than the complementary

energy  $J_b$  calculated from the fiber bridging stress  $\sigma$  versus crack opening  $\delta$  curve, as illustrated in Figure 2.3 and shown in Equations 2.1 and 2.2.

$$J_{tip} \leq \sigma_0 \delta_0 - \int_0^{\delta_0} \sigma(\delta) d\delta \equiv J'_b \quad (2.1)$$

$$J_{tip} = \frac{K_m^2}{E_m} \quad (2.2)$$

where  $\sigma_0$  is the maximum bridging stress corresponding to the opening  $\delta_0$ ,  $K_m$  is the matrix fracture toughness, and  $E_m$  is the matrix Young's modulus. Equation 2.1 employs the concept of energy balance during flat crack extension between external work ( $\sigma_0 \delta_0$ ), crack flank energy absorption through fiber/matrix interface debonding and sliding ( $\int_0^{\delta_0} \sigma(\delta) d\delta$ ), and crack tip energy absorption through matrix breakdown ( $J_{tip}$ ). This energy-based criterion determines whether the crack propagation mode is steady-state flat cracking or Griffith cracking<sup>16</sup>, as illustrated in Figure 2.4.

The fiber bridging stress versus crack opening relationship  $\sigma(\delta)$ , which can be viewed as the constitutive law of fiber bridging behavior, is analytically derived from fracture mechanics, micromechanics, and probabilistics tools. In particular, the energetics of tunnel crack propagation along the fiber/matrix interface is used to model the debonding process of a single PVA fiber from the surrounding cementitious matrix. After debonding is complete the fiber pullout stage begins, and is modeled as slip-hardening behavior with the assumption that non-linear frictional stress increases with slip distance. By these means, the full debonding-pullout process of a single fiber, with given embedment length, is quantified as the fiber bridging force vs. fiber displacement relationship<sup>13</sup>. Probabilistics is then introduced to describe the randomness of fiber

location and orientation with respect to a crack plane, with the assumption of uniform random fiber distribution<sup>17</sup>. The random orientation of the fibers also necessitates the accounting of the mechanics of interaction between an inclined fiber and the matrix crack. In addition, the snubbing coefficient  $f$  and strength reduction factor  $f'$  are introduced to account for the interaction between fiber and matrix, as well as the reduction of fiber strength when pulled at an inclined angle. As a result, the  $\sigma(\delta)$  curve is expressible as a function of micromechanics parameters, including: fiber volume content  $V_f$ , fiber diameter  $d_f$ , fiber length  $L_f$ , fiber Young's modulus  $E_f$ , matrix Young's modulus  $E_m$ , interface chemical bond  $G_d$ , interface frictional bond  $\tau_0$ , and slip-hardening coefficient  $\beta$ , as well as  $f$  and  $f'$ .

Apart from the energy criterion (Equation 2.1), another condition for pseudo strain-hardening is that the matrix tensile cracking strength  $\sigma_c$  must not exceed the maximum fiber bridging strength  $\sigma_0$ .

$$\sigma_c < \sigma_0 \tag{2.3}$$

where  $\sigma_c$  is determined by the matrix fracture toughness  $K_m$  and pre-existing internal flaw size  $a_0$ . While the energy criterion (Equation 2.1) governs the crack propagation mode, the strength-based criterion (Equation 2.3) controls the initiation of cracks. Satisfaction of both Equation 2.1 and Equation 2.3 is necessary to achieve ECC strain-hardening behavior; otherwise, the composite behaves as a normal fiber reinforced concrete (FRC) and tension-softening behavior results.

### 2.2.3 Condition for Saturated Multiple Microcracking

For ECC materials with pseudo strain-hardening behavior, high tensile strain capacity results from saturated formation of multiple microcracks. Material tensile strain capacity increases as the number of microcracks increases. While the steady-state cracking criteria ensures the occurrence of multiple cracking, it is not directly related to the intensity of multiple cracking. Aveston et al.<sup>18</sup> and later Wu and Li<sup>19</sup> derived minimum crack spacing  $x_d$  for aligned continuous fiber and short discontinuous fiber reinforced composites respectively, assuming that the matrix cracking strength is uniform at each section. Under this assumption, crack spacing between  $x_d$  and  $2x_d$  is predicted after crack saturation. The minimum crack spacing is determined by the distance necessary for transferring load from the bridging fibers at one crack back into the matrix through the fiber/matrix interface shear, so that the next crack can be formed. However, in ECC uniaxial tension specimens, a wide distribution far exceeding two times the minimum crack spacing is often observed, due to the variation in ECC matrix properties and non-uniform fiber dispersion. Large crack spacing means that the potential of reinforcing fibers is not effectively utilized, and maximum tensile strain capacity is not achieved.

Once the steady-state cracking criteria is satisfied, the number of microcracks that can be developed is determined by (i) the maximum fiber bridging stress  $\sigma_0$ , and (ii) the matrix properties, in particular the pre-existing flaw size distribution, and the matrix fracture toughness. Considering that ECC is a non-homogenous brittle-matrix composite, first-cracking strength is determined by the largest flaw size in the section where the first microcrack is initiated. Its ultimate tensile strength is determined by the "weakest"

section, where the fiber bridging capacity (maximum bridging stress  $\sigma_0$ ) is the lowest among all sections subjected to the same level of stress. Therefore, the maximum fiber bridging stress  $\sigma_0$  at the "weakest" section imposes a lower bound of critical flaw size  $c_{mc}$ , so that only those flaws larger than  $c_{mc}$  can be activated and contribute to multiple cracking. There also exists a minimum crack spacing controlled by interface properties, which imposes an upper bound for the density of multiple cracking.

#### Matrix randomness – flaws

Matrix imperfections, e.g. random distribution of pre-existing flaws, is one cause of the variation in crack spacing and tensile strain capacity. In ECC composites with a quasi-brittle matrix, cracks initiate from pre-existing flaws in the matrix. Most of the flaws have sizes below 4 mm, and their existence reduces the cracking strength of the cementitious matrix. Li and Wang, 2005<sup>20</sup> computed the effect of initial flaw size on the theoretical cracking strength of an infinite two-dimensional ECC plate under uniaxial tension. The ECC contains poly-vinyl-cohol (PVA) fiber at a volume content of 2%. As shown in Figure 2.5, the theoretical tensile strength of the composite without macrodefects is assumed to be 6.5 MPa. If the composite contains an initial crack 1 mm wide, the matrix tensile cracking strength is reduced to 5.4 MPa. A larger initial crack with 4 mm width reduces the cracking stress to 4.8 MPa. This reduction in matrix tensile cracking strength is important to make Equation 2.3 hold, because the matrix tensile cracking strength  $\sigma_c$  must be lower than the maximum fiber bridging strength  $\sigma_0$ , which is 5.5 MPa for this particular PVA-ECC theoretical specimen, to satisfy the strength-based strain-hardening criterion. Therefore, the critical flaw size  $c_{mc}$  can be determined as the

flaw size that corresponds to the cracking stress 5.5 MPa ( $\sigma_c = \sigma_0 = 5.5\text{MPa}$ ). The critical flaw size is what separates inert and active flaws – only flaws larger than  $c_{mc}$  can be activated and contribute to multiple cracking. The pre-existing flaws in ECC can be entrapped air pores, weak boundaries between phases, and cracks induced by material differential shrinkage, which all possess a random nature and strongly depend on processing details and environmental effects. The number of cracks that can form before reaching the maximum fiber bridging stress may therefore be limited, and can vary significantly from batch to batch. Therefore, a large number of flaws slightly larger than  $c_{mc}$  (flaws much larger than  $c_{mc}$  will lead to a reduction in the net cross section and fiber bridging stress at the crack section) are preferred for saturated multiple cracking and high tensile strain capacity.

#### Fiber dispersion non-uniformity

Fiber dispersion non-uniformity is another contributor to the variation in tensile strain capacity and unsaturated multiple cracking. With a fixed fiber volume percentage, the maximum fiber bridging stress  $\sigma_0$  at the weakest section is determined by the degree of fiber dispersion uniformity in the composite. Fiber dispersion uniformity is directly influenced by the rheology characteristics of the fresh ECC during processing. The uniformity of fiber dispersion determines the maximum bridging stress  $\sigma_0$ , the shape of the  $\sigma(\delta)$  curve at the weakest section, and the critical flaw size  $c_{mc}$ . Non-uniform fiber dispersion leads to a reduction of the value of  $\sigma_0$  at the weakest section, which increases the critical flaw size  $c_{mc}$ . Therefore, less pre-existing flaws with sizes larger than  $c_{mc}$  can be triggered and contribute to multiple cracking, resulting in a relatively lower tensile

strain capacity. Non-uniform fiber dispersion also shifts the  $\sigma(\delta)$  curve downwards, and may reduce complementary energy  $J_b'$  to less than  $J_{tip}$ . In this case, the steady-state criteria are violated and tension-softening behavior results. ECC then loses its ductile behavior and becomes a regular FRC material. Ideally, processing of ECC should optimize fiber dispersion to achieve a uniform random distribution state, therefore minimizing the probability of creating “weak” sections with lower fiber content. By these means, the largest possible tensile strain capacity can be achieved by maximizing multiple cracking behavior.

The random nature of pre-existing flaw size and fiber distribution in ECC leads to variation in  $J_b'$  and  $J_{tip}$ . A large margin between  $J_b'$  and  $J_{tip}$ , and between  $\sigma_0$  and  $\sigma_c$ , is preferred to increase the tendency toward saturated multiple cracking. The pseudo strain-hardening (PSH) performance index is used to quantitatively evaluate the margin, and is defined as follows (Equation 2.4).

$$\begin{aligned}
 PSH_{energy} &= \frac{J_b'}{J_{tip}} \\
 PSH_{strength} &= \frac{\sigma_0}{\sigma_c}
 \end{aligned}
 \tag{2.4}$$

The micromechanics-based strain-hardening criteria, Equation 2.1 and 2.3, are used to guide ECC design in the following sections. The evaluation of PSH is helpful in quantifying the saturation of multiple cracking and the robustness of tensile ductility for the newly developed ECCs.

## **2.3 High Early Strength Engineered Cementitious Composites**

### **2.3.1 Background**

There is an increasing demand for fast and durable repair of concrete structures (e.g. bridge decks, highway pavements, parking structures, and airport runways), where the least disruption of operations is needed. This requires that repair materials be able to gain strength rapidly during early ages, and also remain durable throughout the repaired structure's service life. For example, rapid concrete pavement repairs, including full-depth repairs and patch repairs, have become common on many busy highways throughout North America<sup>21</sup>. Highway transportation authorities often require the repair job to be completed in 6-8 hours at night so that the lane can be reopened to traffic the next morning. Overnight closures are complicated by the fact that these pavements typically carry heavy traffic, and heavy delays and user costs are induced by construction. For freeway and toll roads it is very often that only overnight closures are permitted<sup>22</sup>. Overnight construction is also common for airport pavements<sup>23,24</sup>, especially for bridging areas where taxiways cross, high traffic volume apron areas, and runaway intersections<sup>25</sup>. Very fast setting concrete is used in such circumstances. Beside short closure time, low maintenance and repair frequency are similarly important to avoid operations interruption. This requires the repair to be durable under combined environmental and structural loading conditions. Therefore, high early-age strength as well as durability (e.g. resistance to cracking, chloride penetration, disintegration due to ASR, etc.) are critical characteristics desired for concrete repair materials. Additionally, the repair materials should be cost effective and easy to be processed and placed for various construction situations.

Over the past two decades, high early strength concrete materials have been successfully developed by academic and industry groups with various strength (compressive and flexural) gain rates, depending on the types of cement binders and accelerating admixtures used<sup>26, 27, 28, 29, 30, 31, 32, 33</sup>. While possessing the desired high early strength properties, these materials have been perceived to be more prone to early-age cracking due to their higher thermal and autogenous shrinkage, caused by faster early-age hydration and heat release<sup>34, 35, 36</sup>. Cracking leads to early deterioration and great reduction in the service life of these repairs. Additionally, reduced freeze-thaw resistance<sup>28</sup> has also been found in some very high early strength concrete mixes, limiting their applications in cold regions. Achieving high early-age strength and preventing early-age cracking are conflicting goals that must be carefully balanced through new material technology to achieve acceptable performance of concrete repairs.

This work targets on designing an innovative repair material, called HES-ECC (High Early Strength Engineered Cementitious Composites), based on the ECC micromechanical design theory discussed in Section 2.2. Conventional ECC mixes use Type I ordinary portland cement (OPC), and have relatively slow strength development. The new HES-ECC material should have the high early-age strength desired for rapid repair applications, while possessing large tensile ductility and self-controlled tight crack width below 100  $\mu\text{m}$  during the strain-hardening stage. Wang et al.<sup>37</sup> reported that as crack width increases from 100  $\mu\text{m}$  to 500  $\mu\text{m}$ , the permeability coefficient increases nearly seven orders of magnitude, from  $1.0 \times 10^{-11}$  m/sec to  $1.0 \times 10^{-4}$  m/sec. However, for crack widths under 100  $\mu\text{m}$ , the permeability coefficient remains nearly identical to that of uncracked concrete, suggesting that for crack widths below this threshold there is

no significant increase in permeability after cracking. The tensile ductility and self-controlled crack width of repair materials are essential for achieving repair durability by preventing cracking and penetration of aggressive agents, which has been validated in this dissertation work and will be discussed in Chapters 4, 5, and 6. Besides high early-age strength and tensile ductility, the HES-ECC material should also be cost-effective, and possess workability that make it easy to be applied in different construction applications.

### **2.3.2 High Early Strength Requirements**

When a repair material is applied to a structure, such as a highway overpass, the strength gain rate during early age determines when the repaired structure can be reopened to traffic. Different repair applications have different minimum strength requirements, which must be reached before the structure can be returned to service. For example, large deck patches are typically given a 24 hour cure; small deck patches generally use fast setting mortar and open to traffic after 4 to 6 hours; and for prestressed concrete beam end repairs, both the early age strength and the 28 day strength are specified; for airport runway spall repairs, overnight closure is often preferred. Selection of a repair material depends on the ability of the material to meet early age strength performance targets.

Currently, there is no general standard for minimum high early strength. The California Department of Transportation (Caltrans) specifies a minimum flexural strength of 400 psi (2.8 MPa) prior to opening to highway traffic for full depth highway pavement repairs<sup>38</sup>. The New Jersey State Department of Transportation (NJDOT) specifies a

minimum compressive strength of 3000 psi (20.7 MPa) in 6 hours, and a minimum flexural strength of 350 psi (2.4 MPa) in 6 hours for the “Fast-tract mix” developed in the mid-90’s<sup>39</sup>. The Michigan Department of Transportation (MDOT) specifies minimum compressive strengths of 2000 psi (13.8 MPa) in 2 hours, 2500 psi (17.2 MPa) in 4 hours, and 4500 psi (31.0 MPa) in 28 days (higher for prestressed concrete applications) for prepackaged hydraulic fast-set materials used in structural concrete repairs<sup>40</sup>. Moreover, Parker et al.<sup>41</sup> suggested a minimum compressive strength of 2000 psi (17.2 MPa) for road patching repair to prevent damage when initially reopened to traffic. An FHWA national research program report<sup>42</sup> on high performance concretes designates three categories based on strength: (a) very early strength, (b) high early strength, and (c) very high strength. The very early strength concretes have strength of at least 3000 psi (20.7 MPa) within 4 hours after placement. The high early strength concretes have a compressive strength of at least 5000 psi (34.5 MPa) within 24 hours. In addition, the FHWA<sup>43</sup> recommends a minimum compressive strength of 1000 psi (6.9 MPa) at 3 hours and 3000 psi (20.7 MPa) at 24 hours for rapid-setting cementitious concretes. To meet these various requirements, the target compressive strength for HES-ECC is prescribed as below:

- > 2500 psi (17.2 MPa) at 4 hr
- > 3000 psi (20.7 MPa) at 6 hr
- > 5000 psi (34.5 MPa) at 24 hr
- > 7000 psi (48.3 MPa) at 28 d

The minimum compressive strength of 2500 psi (17.2 MPa) at 4 hr and 3000 psi (20.7 MPa) at 6 hr enables the repaired bridge or structure to be opened to traffic within

4-6 hours after placement. Consequently a fast repair can be done at night, and then reopened to traffic the next morning. The early age strength gain rate within 24 hours is considered sufficient for repair jobs in heavy traffic areas. The minimum compressive strength of 7000 psi (48.3 MPa) at 28 days should be adequate for prestressed concrete applications. As shown in Figure 2.6, the target compressive strength at different ages for HES-ECC serves as an envelope of the requirements by the DOTs and FHWA. Besides compressive strength requirements, a minimum 15 minutes working time is required for repair handling and placement.

### **2.3.3 Methods of Achieving High Early-Age Compressive Strength**

High early strength of concrete materials is mostly attained by using traditional concrete ingredients and concreting practices, although sometimes special materials or techniques are needed. Depending on the age at which the specified strength must be achieved and on application conditions, high early strength can be achieved by using one or a combination of the following:

- a) Type III Portland Cement
- b) Proprietary rapid hardening cements
- c) High cement content
- d) Low water/cementing materials ratio
- e) Chemical admixtures (accelerator, superplasticizer, retarder, etc.)
- f) Silica fume (or other supplementary cementing materials)
- g) Insulation to retain heat of hydration
- h) Higher freshly mixed concrete temperature

- i) Higher curing temperature
- j) Steam or autoclave curing

Type III Portland Cement is widely used in construction where a more rapid rate of strength gain is desirable. Type III Portland Cement and Type I Ordinary Portland Cement (OPC) are both normal Portland cement, and the same manufacturer will produce each with the same composition. The strength gain of normal Portland cement is mainly contributed by the hydration of Tricalcium Silicate ( $C_3S$ ) and Dicalcium Silicate ( $C_2S$ ), which produces a calcium silicate hydrate (C-S-H). By grinding the cement more finely compared with Type I cement ( $540 \text{ m}^2/\text{kg}$  vs.  $370 \text{ m}^2/\text{kg}$ ), the resultant cement surface area in contact with water will increase, leading to faster hydration and more rapid development of strength. By this method, Type III cement can develop strength much faster than Type I cement – within the first 3-8 hours. The amount of strength gain of Type III cement over the first 24 hours almost doubles that of Type I cement<sup>44</sup>.

Proprietary rapid hardening cements such as magnesium phosphate-based cement, gypsum-based cement, and calcium aluminate cement have also been used to obtain very high early strength in some concrete mixes<sup>26,27,28,29,30</sup>. However, many proprietary rapid hardening cements often perform unpredictably under various conditions. For example, magnesium phosphate based cement is extremely sensitive to water content, and its strength can be severely reduced by a very small amount of extra water<sup>45</sup>; concrete containing gypsum-based cement may lose durability in freezing weather or when exposed to moisture<sup>46</sup>, and the presence of sulfates in its mixture may promote embedded steel corrosion<sup>45</sup>; calcium aluminate cement may lose strength at high curing temperature due to chemical conversion<sup>43</sup>. Furthermore, most commercially available proprietary

rapid-hardening cements are expensive compared with ordinary type III cement. Due to the unpredictable performance and higher cost, proprietary rapid-hardening cements will not be considered in this research, unless HES-ECC based on Type III cement fails to achieve the target strengths.

Chemical admixtures play a key role in producing high early strength concrete mixtures that meet strength and workability criteria; they include water-reducing admixtures, accelerating admixtures, and hydration controlling admixtures. Water-reducing admixtures increase early strength by lowering the quantity of water required while increasing the workability for appropriate concrete placement and finishing techniques, and increase strength at later ages by dispersing the cement to allow more efficient hydration. Accelerating admixtures aid early strength development and reduce initial setting times by increasing the rate of hydration. Hydration controlling admixtures allow time for transportation of the concrete from the ready-mix plant to the jobsite, and provide time for adequate placement and finishing. Chemical admixtures and their potential effects on material performance are reviewed below.

#### Water-reducing admixtures

As high cement content and a low water/cement ratio are favorable for achieving high early strength, a water-reducing admixture should be necessary to effectively lower the water/cement ratio in HES-ECC by reducing the water required to attain a given slump. Consequently, it improves the strength and impermeability of the cement matrix. The strength increase can be observed in as early as one day if excessive retardation does not occur<sup>47</sup>. Furthermore, since the cement is dispersed and a more uniform

microstructure is developed, the compressive strength can be as much as 25% greater than that achieved by the decrease in w/c alone<sup>48</sup>.

Water-reducing admixtures are often observed to increase the rate of shrinkage and creep of concrete, depending on the cement type and the particular admixture. However, after 90 days of drying, there is little difference in shrinkage compared to a control concrete<sup>49, 50</sup>. The shrinkage properties of the developed HES-ECC including the use of water-reducing admixture and related durability issues will be investigated in Chapter 4.

#### Accelerating admixtures:

Accelerating admixtures accelerate the normal strength development and processes of setting. Regular accelerators are used to speed construction by permitting earlier attainment of sufficient strength to allow removal of formwork and to carry construction loads. Quick-setting admixtures provide setting times of only a few minutes. They are generally used in shotcreting applications and for emergency repair in general, where very rapid development of rigidity is required. Accelerators are also beneficial during winter concreting because they can partially overcome the slower rate of hydration due to low temperatures, and shorten the period for which protection against freezing is required<sup>51, 52</sup>.

Accelerating admixtures can be divided into three groups: (1) soluble inorganic salts, (2) soluble organic compounds, and (3) miscellaneous solid materials<sup>53</sup>. Many soluble inorganic salts, including chlorides, bromides, nitrites, nitrates, fluorides, carbonates, thiosulfates, silicates, aluminates, and alkali hydroxides, can accelerate the

setting and hardening of concrete to some degree, calcium salts generally being the most effective. Soluble carbonates, aluminates, fluorides, and ferric salts have quick-setting properties and they are commonly used in shotcreting applications. Calcium chloride is the most widely used because it is the most cost effective, in terms of giving more strength acceleration at a particular rate of addition when compared to other accelerators<sup>54</sup>. However, the use of calcium chloride will increase the rate of corrosion of metals embedded in concrete. The ACI Building Code places limits on the chloride content of concrete that preclude its use for both prestressed and reinforced concrete. Chloride-free accelerators should be used in such cases.

Organic compounds for most commercial uses include triethanolamine, calcium formate<sup>55</sup>. Calcium acetate, calcium propionate, oxalic acid, lactic acid and various ring compounds are also in this group. These compounds accelerate the hydration of tricalcium aluminate and produce more ettringite at early age. The reaction of triethanolamine with Portland cement is complex. However, excessive amounts of these compounds can result in retardation effects<sup>56</sup>.

Solid materials such as calcium fluoroaluminate or calcium sulfoaluminate can be used to obtain rapid-hardening characteristics. In certain instances, finely ground silicate minerals and hydrated Portland cement itself have been found to act as accelerators due to the effects of seeding. Also, introduction of small amounts of calcium-aluminate cement can significantly shorten the setting time of Portland cement concrete<sup>55, 57, 58, 59</sup>.

Solid materials are not often used in concrete materials for accelerating hydration.

Although accelerating admixtures can be expected to increase early strength, the increase diminishes with time, and later strengths (at 28 days or more) are likely to be

lower than the strength of concretes without an accelerating admixture<sup>60</sup>. This reduction in later strength is more pronounced when the initial accelerating effects are large. Accelerating admixtures may also increase the rate of drying shrinkage and creep, although the ultimate values are not affected<sup>61</sup>. The early shrinkage leads to high tensile stresses in restrained repair material, often resulting in cracking or interface delamination. The undesirable effects of accelerating admixture use on concrete material performance negate many of its benefits.

### **2.3.4 Initial Material Composition Selection Based on Strength Requirements**

The material development of HES-ECC contains three phases. The first phase is matrix design for high early strength (Section 2.3.4). In this phase, the main factors that affect early strength gain rate, including cement type, water/cement ratio, accelerator, and curing conditions, are experimentally investigated. The second phase is composite tailoring for saturated multiple cracking and high tensile ductility (Section 2.3.5). The third phase is detailed characterization of mechanical properties, including tensile, compressive, and flexural properties, of the developed HES-ECC composite material (Section 2.3.6).

#### **2.3.4.1 Experimental Program**

The ingredient materials used in this study are listed in Table 2.2 with information on product name, manufacturer, chemical composition and particle size. The trial mixes for initial material composition selection are listed in Table 2.3. Two types of cements were investigated. Type III Portland cement has the same composition as Type I

Ordinary Portland Cement (OPC), except that it is finely ground. ASTM class F fly ash is a pozzolantic material that is an integrated part of conventional ECC. It is eliminated from some of the mixes in this study to improve early age compressive strength.

Fine silica sand is the main aggregate in ECC, with a maximum particle size of 270  $\mu\text{m}$  and average size of 110  $\mu\text{m}$ . Polystyrene (PS) bead is another type of aggregate that forms a very weak bond with the cementitious matrix so that it behaves as an artificial flaw under tensile loading. As the uniaxial tensile test described in Section 2.3.5 shows, the initially selected mix was not able to meet the target tensile strain capacity requirements, so polystyrene beads were deliberately introduced into the mix to control initial flaw size and distribution at the material tailoring stage. By these means, the composite material can develop saturated multiple microcracks during the strain-hardening stage, leading to a large tensile strain capacity.

The chemical admixtures used in this study include accelerating admixture and superplasticizer. The accelerating admixture is Pozzolith<sup>®</sup> NC 534 from Master Builders, Inc. The accelerating species in this brand of admixture are calcium nitrate and sodium thiocyanate. The recommended maximum effective dosage of Pozzolith<sup>®</sup> NC 534 is 4 wt% to cement. Superplasticizer is necessary to achieve sound workability when the mixing composition has a low water/cement ratio. The superplasticizer used in this research project was Glenium<sup>®</sup> 3200 HES from Master Builders Inc. Glenium<sup>®</sup> 3200 HES is a late generation superplasticizer with powerful dispersion capacity at low water/cement ratios. It can better facilitate hydration of cement particles, resulting in a stronger accelerating effect. Due to combined electrostatic and steric repulsion forces,

Glenium® 3200 HES requires a lower dosage than other types of superplasticizer, such as melamine formaldehyde based ML330, to achieve the same workability.

The fiber in this study is REC15 Polyvinyl-alcohol (PVA) fiber from Kuraray Co., Japan, used at a moderate volume fraction of 2% in ECC materials. PVA fiber possesses great potential as a reinforcing fiber because of its high strength, high modulus of elasticity, and relatively low cost. However, directly applying commercially available PVA fiber has resulted in composites with low tensile strain capacities, on the order of 0.5-1.0%, even when as much as 4% fiber by volume is used<sup>62</sup>. This poor composite performance can be attributed to the hydrophilic behavior of PVA fiber, that leads to excessive chemical bonding (i.e. interface debonding fracture energy  $G_d$ ) with cementitious hydrates and strong slip-hardening response during pullout, which consequently results in premature rupture of the fibers<sup>63, 64</sup>. In order to maximize  $J_b'$ , the micromechanical models suggested that the fiber/matrix interfacial bond should be significantly reduced. This leads to the adjusted fiber manufacturing process that applies a 1.2% oil agent content coating to the fiber surface<sup>65</sup>. This interfacial modifying process reduces both chemical bond  $G_d$  and frictional bond  $\tau_0$ , and increases  $J_b'$ . The dimensions of the PVA fiber are 12 mm in length and 39  $\mu\text{m}$  in diameter, on average. The nominal tensile strength of the fiber is 1620 MPa and the density of the fiber is 1300  $\text{kg}/\text{m}^3$ . The detailed properties of REC 15 PVA fiber are listed in Table 2.4.

A Hobart mixer with 13L capacity was used in preparing all ECC mixtures. Solid ingredients, including cement, fly ash, and sand, were first mixed for approximately 1 minute. Water and superplasticizer were slowly added into the dry mixture and mixed for another 3 minutes. Once a consistent and uniform state of mortar was reached, fibers

were slowly added into the mortar matrix and mixed until they were evenly dispersed. The mixture was then cast into molds. Accelerating admixture, if used, was added after the fiber and just before casting. The molds were covered with plastic sheets and cured in air at room temperature ( $20\pm 3^{\circ}\text{C}$ ). The specimens were demolded at the earliest possible testing age, ranging from 4 hours to 24 hours.

Compressive testing was carried out according to ASTM C39 “Standard Test Method for Compressive Strength of Cylindrical Concrete Specimens” on standard cylinders measuring 75 mm (3 in.) in diameter and 150 mm (6 in.) in length. The ends of the specimens were capped with a sulfur compound to ensure a flat and parallel surface, and better contact with the loading device. Tests were conducted on a FORNEY F50 compression test system (Figure 2.7). The tests began 4 hours after casting or once adequate strength had been developed. The age of the specimen was recorded as the time elapsed from the end of casting to the start of testing.

#### **2.3.4.2 Compression Test Results and Discussion**

The compressive strength development of various mixes are summarized in Tables 2.5, 2.6, and 2.7 and plotted in Figures 2.8, 2.9, 2.10, and 2.11. Three specimens were tested for each test series and the average values were plotted.

The replacement of Type I by Type III cement greatly improved the early age compressive strength gain rate (Figure 2.8). For example, the 12h and 24h compressive strengths both increased by more than 60%, even though the 14d and 28d compressive strengths exhibited little difference. However, Mix 2 containing Type III cement was unable to achieve the target high early strength. Its 4h compressive strength was 3.4 - 3.6 MPa, which is far below the target 17.2 MPa at 4h. The 6h compressive strength (17.3 –

19.1 MPa) also failed to meet the requirement of 20.7 MPa. The high content of fly ash was considered to be the factor that delayed the early-age compressive strength development. Therefore, fly ash was eliminated from the following mixes.

Lowering the water/cement (w/c) ratio was shown to be an effective way to improve early-age and late-age compressive strength. This is more effective for ECC mixes than regular concrete, as ECC mixes often contain higher content of cement. As shown in Figure 2.9, reduction of w/c from 0.53 to 0.36 leads to a greater than 100% increase in compressive strength at 4h and 28d. The curing time required to reach the 4h compressive strength target of 17.2 MPa was 24h, 8.5h, and 5.5h for w/c 0.53, 0.45, and 0.36 respectively. The curing time required to reach the 6h compressive strength target of 20.7 MPa was 36h, 11h, and 6h for w/c 0.53, 0.45, and 0.36 respectively. Mix 5, with w/c = 0.36, met the 6h, 24h, and 28d compressive strength requirements, but not the 4h compressive strength requirement.

The use of polycarboxylate based superplasticizer, e.g. GL3200, was crucial to achieve very high early strength when a reduced w/c ratio was used in a type III cement-based system. It was also noticed that a higher dosage has a strong retarding effect. The effectiveness of superplasticizer is not only dependent on its composition, but also the chemistry of the cementitious phase and the presence of other admixtures, e.g. accelerators, retarders, etc. The compatibility of commercially available superplasticizers and other admixtures with type III portland cement is one compelling driver of the preference toward portland cement based-systems over proprietary rapid hardening cement binder systems.

To further improve strength development within the first 6 hours, additional accelerator was incorporated (Mix 6). As shown in Figure 2.10, the use of calcium nitrate based accelerator NC534 at dosage of 4.0% reduced the age to reach 17.2 MPa compressive strength from 5.5h to less than 4h. The 6h, 24h, and 28d compressive strengths also satisfied the target strength requirements.

The curing condition was found to have a significant influence on the strength gain rate at early ages. As shown in Figure 2.11, Mix 6 developed strength much faster in the first 12 hours under insulated conditions, where the specimens were stored in plastic containers with insulation foam. The target 17.2 MPa at 4h compressive strength could be achieved as early as 3 hours. This can be explained by the temperature controlled hydration rate of  $C_3S$  and formation of C-S-H. It should also be noted that compressive strength was measured using relatively small cylinders in this experimental program. As hydration heat can be better preserved in larger volume, the compressive strength development of Mix 6 when processed in a larger volume should be between the non-insulated and insulated lab curing conditions.

Mix 6 remained workable for 20 minutes, which was considered sufficient for repair jobs. For larger-scale mixing that requires a longer working time, a hydration control agent can be used to retard the hydration process and retain workability. Delvo<sup>®</sup> stabilizer from Master Builders has been tested to work well for this purpose; the details of processing optimization for larger-scale mixing are described in Chapter 8.

As a conclusion, Mix 6 was initially selected as the mix proportion that satisfied the early-age and late-age compressive strength and workability requirements. Further

evolution of this mix is necessitated by tensile property demands, as described in the following sections.

## **2.3.5 Microstructure Tailoring for Tensile Ductility**

### **2.3.5.1 Initial Composite Testing in Uniaxial Tension**

With Mix 6 satisfying target compressive strength requirements, initial tensile testing was conducted to evaluate its tensile properties at different material ages. The direct uniaxial tensile test is considered the most convincing method for evaluating material strain-hardening behavior<sup>66</sup> because some quasi-brittle fiber reinforced concrete can also show apparent hardening behavior under flexural loading – a phenomenon known as “deflection hardening”. Figure 2.12 shows the uniaxial tensile test setup and Figure 2.13 illustrates the specimen dimensions. The plate specimens are 228.6 mm (9 in.) long, 76.2 mm (3 in.) wide and 12.7 mm (0.5 in.) thick. Before testing, four aluminum plates were glued to the four edges of the plate specimen to facilitate gripping. Tests were conducted on an MTS machine with 25 KN (5.62 kip) capacity, under a displacement control with rate of 0.005 mm/s ( $1.97 \times 10^{-4}$  in./s). Two external LVDTs (Linear Variable Displacement Transducers) were attached to the specimen surface, with a gage length of 101.6 mm (4 in.), to measure the displacement. The mixing procedure was the same as described in Section 2.3.4. Specimens were demolded at 4 hours, cured in air at room temperature ( $20 \pm 3^\circ\text{C}$ ), and tested at different ages from 4 hours to 28 days.

The tensile stress-strain curves of Mix 6 at ages of 4h, 24h, 3d, 7d, and 28d are shown in Figure 2.14. The age dependencies of the tensile strain capacity and tensile strength of Mix 6 are shown in Figure 2.15 and 2.16. Three specimens were tested for

each age. Mix 6 exhibited a rapid strain capacity decrease with age, accompanied by an increase in first cracking strength. The tensile strain capacity was around 4% at 4h, decreased to 3% at 24h, and further decreased to less than 1% after 3d. This reduction in tensile strain capacity at later ages is unfavorable for durable performance of this repair material when undergoing large deformation due to shrinkage, thermal effects, structural loading, and expansion of corroded reinforcement, under restrained conditions. Therefore, Mix 6 needs further tailoring to maintain tensile ductility at all ages.

### **2.3.5.2 Microstructure Tailoring of Mix 6 for Tensile Ductility**

To overcome the gradual loss of tensile ductility in Mix 6, it is necessary to investigate the fundamental micromechanisms responsible for this undesirable composite behavior, and to provide a pathway to minimize this tendency. Toward these goals, the age dependency of micromechanical parameters, including matrix and fiber/matrix interface properties, were measured at different ages and used to guide the tailoring process. Based on the conditions for strain-hardening and saturated multiple cracking, it is evident that high tensile strain capacity requires a high  $J_b'/J_{tip}$  ratio and sufficient number of pre-existing flaws larger than  $c_{mc}$ . The matrix toughness  $J_{tip}$  and flaw size distribution are matrix properties, while the complementary energy  $J_b'$  is mainly controlled by fiber and interface properties.

To measure the age dependency of  $J_{tip}$ , matrix toughness tests were conducted on the Mix 6 matrix (without fibers) at different ages. This test was similar to ASTM E399 “Standard Test Method for Plane-Strain Fracture Toughness of Metallic Materials”. The ASTM E399 allows one to use different geometry specimens, such as bending specimens

and compact tension specimens, to measure the  $K_m$  value. The Mix 6 matrix was prepared and cured as described in Section 2.3.4, except that fibers were not added. The fresh mix was cast into notched beam specimens measuring 305 mm (12 in.) in length, 76 mm (3 in.) in height, and 38 mm (1.5 in.) in thickness. The matrix fracture toughness  $K_m$  at different ages was measured by the three point bending test, as shown in Figure 2.17. The span of support is 254 mm (10 in.) and the notch depth to height ratio is 0.4. Three specimens were tested for each test series.  $J_{ip}$  was calculated from the measured  $K_m$  by use of Equations 2.1 and 2.2.

To calculate the age dependency of  $J_b'$  of Mix 6, single fiber pullout tests were conducted to measure three important interfacial parameters at different ages: chemical bond strength  $G_d$ , frictional bond strength  $\tau_0$ , and slip hardening coefficient  $\beta$ . As shown in Figure 2.18, single fiber pull-out tests were conducted on small-scale prismatic specimens with dimensions of 10 mm  $\times$  5 mm  $\times$  0.5 mm (0.4 in.  $\times$  0.2 in.  $\times$  0.02 in.). A single fiber was aligned and embedded into the center of a Mix 6 mortar prism with an embedment length of 0.5 mm (0.02 in.). Three specimens were tested for each test series. The load  $P$  versus displacement  $\delta$  curve was obtained through quasi-static testing and used to determine the interfacial parameters. These interfacial parameters, along with fiber volume fraction, length and diameter, were then used to calculate the fiber bridging law  $\sigma(\delta)$ . (More details on  $\sigma(\delta)$  are given below). The snubbing coefficient is closely related to fiber surface frictional coefficient, which decreases significantly with increase of oiling coating content<sup>65</sup>. The snubbing coefficient  $f = 0.2$  was assumed in this study for PVA fiber with 1.2% oiling coating, and decreases significantly with increase of oiling coating content. The fiber strength reduction coefficient  $f' = 0.33$  was measured

by single fiber in-situ strength test<sup>67</sup>. The resulting complimentary energy  $J'_b$  calculated from the  $\sigma(\delta)$  curve combined with the matrix fracture toughness  $J_{tip}$  obtained from the  $K_m$  measurement were used as inputs to evaluate composite material behavior (i.e. strain-hardening or tension-softening) and to calculate the PSH index as defined in Equation 2.4.

The general profile of a single fiber pullout curve (P vs.  $\delta$ ) can be decomposed into three major regimes as shown in Figure 2.19<sup>68</sup>. Initially, a stable fiber debonding process occurs along the fiber/matrix interface (Figure 2.17 a). While the load carried by the fiber increases up to  $P_a$ , the fiber embedded end,  $l = l_e$ , does not become displaced. The debond length,  $l_d$ , increases towards  $l_d = l_e$ . During this “debonding” stage, the displacement of the fiber end is the sum of the elastic stretching of the debonded fiber segment and of the fiber free length (the portion of the fiber outside the matrix). This debonding process results in a tunnel-like crack that propagates stably from the free end towards the embedded end of the fiber. This tunneling process is stable until the tunnel crack tip approaches the embedded end of the fiber at which stage it loses stability and the load suddenly drops from  $P_a$  to  $P_b$ . At this moment the fiber is held in the matrix only by friction. The chemical debonding energy value,  $G_d$ , is calculated from the  $P_a$  to  $P_b$  difference using Equation 2.5:

$$G_d = \frac{2(P_a - P_b)^2}{\pi^2 E_f d_f^3} \quad (2.5)$$

where  $E_f$  is the fiber Young's modulus, and  $d_f$  is the fiber diameter.

At the point  $P_b$ , the embedded fiber end is just debonded and the frictional bond strength  $\tau_0$  at the onset of fiber slippage can be calculated using Equation 2.6:

$$\tau_0 = \frac{P_b}{\pi d_f l_e} \quad (2.6)$$

During the fiber slippage stage, the fiber can undergo sliding with slip hardening, constant friction, or slip-softening, characterized by the positive, zero or negative coefficient  $\beta$ , respectively<sup>69</sup>. Slip-hardening occurs often with polymer fibers including PVA fibers used in this study. Because polymer fibers are less hard than the surrounding matrix, they tend to be damaged during pullout process and therefore a jamming effect can take place inside the matrix, leading to an increasing load. Conversely, constant friction or slip-softening are often observed when the fiber hardness is higher than that of the surrounding matrix. The  $\beta$  value is calculated from the initial ( $S'$  approaching 0) slope of the P versus  $S'$  curve using:

$$\beta = (d_f / l_f) [1 / \tau_0 \pi d_f] (\Delta P / \Delta S') \Big|_{S' \rightarrow 0} + 1 \quad (2.7)$$

Lin et al.<sup>69</sup> proposed the formulation of the crack bridging stress versus opening relationship  $\sigma(\delta)$  based on single fiber pullout  $P(\delta)$  relation

$$\sigma_B(\delta) = \frac{4V_f}{\pi d_f^2} \int_{\phi=0}^{\pi/2} \int_{z=0}^{(L_f/2)\cos\phi} P(\delta) e^{f\phi} p(\phi) p(z) dz d\phi \quad (2.8)$$

where  $V_f$  is the fiber volume fraction,  $d_f$  is the fiber diameter,  $\phi$  is the orientation angle of the fiber relative to a crack plane,  $L_f$  is the fiber length,  $z$  is the centroidal distance of a fiber from the crack plane,  $f$  is a snubbing coefficient, and  $p(\phi)$  and  $p(z)$  are probability density functions of the fiber orientation angle and centroidal distance from the crack plane, respectively.  $P(\delta)$  is the pullout load versus displacement relation of a single fiber aligned normal to the crack plane, as experimentally measured in this study from the single fiber pullout test. It should be noted that during fiber debonding and pullout stages (Figure 2.17), the fiber may rupture if the load  $P$  exceeds the fiber strength,  $\sigma_f$ , which is often the case in the PVA-ECC system when the interfacial chemical bond and frictional bond are strong.

Figure 2.20 presents the age dependency of matrix fracture toughness  $K_m$  determined from the notched beam bending test. The development of  $K_m$  at early age is fastest during the first 24 hours, and the  $K_m$ -age curve becomes relatively flat after 3 days.

Figures 2.21, 2.22, and 2.23 present the age dependency of  $G_d$ ,  $\tau_0$  and  $\beta$  measured from the single fiber pullout test. Despite the scattering of data, the trend clearly shows that the development of interface chemical bond  $G_d$  and frictional bond  $\tau_0$  remained relatively slow during the first 24 hours, accelerated considerably after 24 hours, and finally reached a plateau after 7 days.

Compared with  $K_m$ , the development of interface bonding strength was much lower at the early age until about 3 days. The different development rates between fracture toughness and interfacial properties can be due to the accelerated hydration at early ages in the cementitious matrix, and development of the fiber/matrix interfacial bond is less affected by the accelerated hydration process. These findings were different from the age-dependent development of interfacial properties of polyethylene (PE) fibers, which are hydrophobic, in a cementitious matrix<sup>70</sup>. It was found that the interfacial bond strength of PE fibers matured much faster, in less than 7 days, in comparison with the development of matrix bulk properties that typically took 14-28 days. The difference between the present study and Chan and Li<sup>70</sup> can be attributed to the adoption of a rapid-strength-gain binder system and different type of fibers (PVA fibers instead of PE fibers) in Mix 6.

It was the difference between the development rates of matrix toughness and matrix/fiber interface properties that resulted in the quick change of the pseudo strain-hardening (PSH) performance index, defined by the  $J_b'/J_{tip}$  ratio. PVA fibers form strong

chemical and frictional bonds with the cementitious matrix because of their hydrophilic nature. Moreover, PVA fiber has strong slip-hardening behavior during the pullout process. Therefore, the fiber often ruptures instead of being pulled out from the surrounding matrix, leading to a reduction in complementary energy  $J_b'$ . For Mix 6, the rapid increase in  $G_d$ ,  $\tau_0$  and  $\beta$  after 24 hours led to more occurrences of fiber rupture than pullout, resulting in a significant decrease in  $J_b'$  (Figure 2.24). This was accompanied by an increasing  $J_{tip}$  (Figure 2.24) corresponding to increased matrix toughness  $K_m$ . As shown in Figure 2.24,  $J_b'/J_{tip}$  dropped from 39 at 4 hours to 5 at 24 hours, then to around 1 at 3 days, and flattened after 3 days, leading to the deteriorated composite tensile strain capacity. Tensile strain capacity of Mix 6 at different ages is also plotted in Figure 2.24. Strong correlation was found between the age dependent development of tensile strain capacity and the  $J_b'/J_{tip}$  ratio (PSH index).

The low tensile strain capacity of Mix 6 after 24 hours is due to a low value of the  $J_b'/J_{tip}$  ratio, resulting in unsaturated multiple cracking. When the margin between  $J_b'$  and  $J_{tip}$  is small, it becomes critical to control pre-existing flaw distribution in the matrix to retain high strain capacity. As discussed in Section 2.2.3, a large number of flaws slightly larger than  $c_{mc}$  are preferred for saturated multiple cracking and high tensile strain capacity. The critical flaw size  $c_{mc}$  is set such that only those flaws larger than  $c_{mc}$  can be activated before reaching  $\sigma_0$  and contribute to multiple cracking. The approach used in this study is to superimpose a prescribed flaw system to the pre-existing flaws in the Mix 6 matrix, as illustrated in Figure 2.25. The artificial flaws can be any inclusion with a weak bond to the cementitious matrix or with relatively low tensile strength compared to the tensile strength of the surrounding matrix, such as lightweight

aggregates, air bubbles, polymer foams and rubber powder. In this study, Polystyrene (PS) beads (Figure 2.26) with a size of 4 mm were added as artificial flaws at a dosage of 5% by volume. The size of 4 mm was chosen because it was slightly larger than the calculated critical flaw size  $c_{mc}^{71}$ , so that the PS beads are large enough to initiate cracking without significantly lowering the first cracking strength and interrupting fiber dispersion. Possessing a cylindrical shape with sharp edges and extremely weak bond with the surrounding cement binder, the PS beads serve as crack initiators. The modified mixing proportion - Mix 7 - is the same as Mix 6 except for the presence of PS beads (Table 2.8).

Figure 2.27 shows the tensile stress-strain curves of Mix 7 at the ages of 4h, 24h, 3d, 7d, 28d and 50d. Significant tensile strain-hardening behavior with strain capacity above 3% was observed at all ages up to 50d. Figure 2.28 compares the tensile strain capacity of Mix 6 and Mix 7 at different ages. Greatly improved tensile strain capacity was found in Mix 7 at all ages, especially at ages after 24h, compared to Mix 6. Moreover, introduction of 5 vol% artificial flaws does not seem to affect the first cracking strength and ultimate tensile strength. This is because of the small dosage, and the similarity of the artificial flaw size and pre-existing flaw size in Mix 6. The introduction of artificial flaws with prescribed size was shown to be an effective approach to improve tensile strain capacity through increased saturation of multiple cracking.

The effect of adding PS beads on ECC compressive strength was investigated and shown in Figure 2.27. Comparing the compressive strength development curves for Mix 6 and 7, this figure shows the minor effect of PS bead presence on the early compressive

strength gain rate, although inclusion of the beads greatly improves the multiple cracking behavior when the specimen is under tension. Specifically, small differences in the strength gain rate were observed in the first 6h, while compressive strength after 12h was reduced by approximately 10%. Even with this reduction, Mix 7 still satisfied the compressive strength requirements at early and late ages as well as the workability requirement. Up to now, HES-ECC (Mix 7) has been successfully developed with the target early-age compressive strength, workability, and high tensile ductility at all ages. Its mechanical properties will be characterized in detail in the next section.

### **2.3.6 HES-ECC Material Characterization**

In this section, the mechanical properties of the newly developed HES-ECC material, including tensile, compressive, and flexural properties, were tested with a larger number of specimens and documented in detail.

#### Materials

The mix proportion of the newly developed HES-ECC is shown in Table 2.9. It contains type III portland cement, fine silica sand F110, water, PVA fibers, PS beads, superplasticizer, accelerating admixture, and hydration control admixture (when a longer working time is needed). Mixes were prepared with a Hobart-type mixer with 13 liter capacity according to following mixing procedure:

- 1) Mix type III Portland cement and silica sand for approximately 1 minute;
- 2) Add water slowly and continue mixing for 1-2 minutes;
- 3) Add superplasticizer; continue mixing for 1-2 minutes until a consistent mixture is reached;

- 4) Add PVA fibers slowly and mix for 2 minutes until fibers are well distributed;
- 5) Add polystyrene beads and mix for 1-2 minutes;
- 6) Add hydration control admixture and mix for 1 minute unless casting will be completed within 15 minutes of completion of mixing;
- 7) Add accelerating admixture and mix for 1 minute before casting into molds.

The whole mixing procedure for each batch took 10-15 minutes. After mixing, the mixture was cast into tensile, compressive and flexural specimen molds with moderate vibration applied. The molds were then covered with plastic sheets, demolded in 4 hours, cured in air at room temperature ( $20\pm 3^{\circ}\text{C}$ ) and relative humidity (RH  $40\pm 5\%$ ), and tested at different ages.

#### Uniaxial Tensile Test and Results

Age-dependent uniaxial tension tests were conducted to measure the tensile strength, Young's modulus, tensile strain capacity, crack width and crack pattern of HES-ECC. Testing procedure and specimen preparation were the same as described in Section 2.3.5. Specimens were tested at ages of 4, 6, 12 and 24 hours, and 3, 7, 14, 28 and 60 days, measured as the time between the end of casting and start of testing. Ten to fourteen specimens each were tested at each age.

Under uniaxial tensile loading, HES-ECC specimens exhibit significant tensile strain-hardening behavior. HES-ECC first undergoes "elastic straining" until the first microcrack appears. Then, the material undergoes "strain-hardening" similar to the "plastic yielding" in metals. The strain-hardening stage is accompanied by the formation of many closely-spaced microcracks with controlled crack width. These cracks are unlike the localized fracture in concrete or other brittle materials as they continue to carry

increasing stress across the crack faces after formation. The multiple microcracks eventually “saturate” (reach the minimum spacing) along the specimen and a localized fracture occurs due to exhaustion of the local fiber bridging capacity. At this moment, the load starts dropping and the HES-ECC enters the “tension softening” stage until final failure. The peak stress prior to the tension-softening stage is defined as the tensile strength of the HES-ECC.

Table 2.10 and Figures 2.30, 2.31, 2.32 and 2.33 summarize the uniaxial tensile test results of HES-ECC. As shown in Figure 2.30, The tensile strength of HES-ECC increases rapidly during the first 24 hours, from  $3.5 \pm 0.1$  MPa ( $501 \pm 12$  psi) at 4 hours to  $4.7 \pm 0.1$  MPa ( $680 \pm 12$  psi) at 24 hours. It continues increasing at a lesser rate during later ages, and reaches  $5.8 \pm 0.2$  MPa ( $840 \pm 28$  psi) at 60 days.

The Young’s modulus (E) of HES-ECC is determined from its tensile stress-strain curve, defined as the slope of the line drawn between the starting point and the point corresponding to a strain of 0.015%. The 0.015% tensile strain is an approximate elastic strain capacity of ECC material<sup>32</sup>. The age dependency of the HES-ECC Young’s modulus is plotted in Figure 2.31. Young’s modulus of HES-ECC increases with age, from  $13.1 \pm 0.8$  GPa ( $1900 \pm 111$  psi) at 4 hour to  $23.8 \pm 0.7$  GPa ( $3452 \pm 103$  psi) at 60 days. The Young’s modulus of HES-ECC is generally lower than that of concrete materials, due to the absence of coarse aggregates in its mix. This lower Young’s modulus is in fact desirable for a concrete repair material because it lowers the induced tensile stress build-up caused by shrinkage restrained by the existing surrounding concrete<sup>72, 73, 74</sup>, thereby reducing the tendency toward cracking and repair/substrate material interface delamination.

The tensile strain capacity of each specimen was defined as the tensile strain value corresponding to tensile strength (prior to tension softening). Figure 2.32 shows the age-dependent development of HES-ECC tensile strain capacity that exceeds 5% at 4 hours, decreases to 4% at 3 days, and stabilizes to an average of 3.5% beyond 7 days (test data extend up to 60 days). This long-term high tensile strain capacity is several hundred times larger than the 0.01% assumed for normal concrete materials.

The crack width of HES-ECC microcracks at the strain-hardening stage was measured because it determines the HES-ECC's resistance to the penetration of aggressive agents. Research has shown that the narrow crack width of ECC reduces water permeability<sup>75</sup> and chloride diffusion penetration<sup>76</sup>; these issues will be discussed in detail in Chapter 6. Figure 2.33 shows the multiple microcracking behavior and crack width of HES-ECC at the ages of 4 hours, 24 hours, 3 days and 28 days. To enhance resolution of these microcrack images, epoxy glue was applied to the surfaces of the specimens before the photos were taken. Near-saturated multiple microcracks with crack width below 60  $\mu\text{m}$  were observed at all ages. It should be noted that the crack width at the very early age of 4h is as low as 10  $\mu\text{m}$  while the tensile strain capacity is as high as 6%. This high tensile ductility and very tight crack width at early age of the repair material are crucial for the repair's resistance to early-age cracking due to restrained shrinkage and chloride penetration, which start as soon as the repair is re-opened to service.

### Uniaxial Compressive Test and Results

Age dependent tests in uniaxial compression were conducted to establish a database of HES-ECC compressive strength development as a function of material age.

Compressive testing was conducted according to the procedure described in Section 2.3.4. Specimens were tested at ages of 4, 6, 12 and 24 hours, and 3, 7, 14, 28 and 60 days. Ten to fourteen specimens each were tested at each age.

Table 2.11 and Figure 2.34 summarize the compressive strength of HES-ECC at different ages. HES-ECC reaches compressive strengths of  $23.6 \pm 1.4$  MPa ( $3422 \pm 203$  psi) at 4 hours,  $34.2 \pm 1.4$  MPa ( $4963 \pm 182$  psi) at 6 hours, and  $42.3 \pm 1.4$  MPa ( $6130 \pm 202$  psi) at 24 hours. The increasing trend slows down at later ages, leveling off at  $55.6 \pm 2.2$  MPa ( $8063 \pm 315$  psi) at 28 days, and  $56.8 \pm 1.7$  MPa ( $8233 \pm 250$  psi) at 60 days. The compressive strength development of HES-ECC is shown in Figure 2.35 along with the target requirements, and requirements given by NJSDOT 1997<sup>32</sup>, MDOT QA/QC 2003<sup>40</sup>, Zia et al. 1991<sup>42</sup> and FHWA 1999<sup>43</sup>.

### Flexural Test and Results

A minimum flexural strength of the repair material, apart from its compressive strength, is usually specified as a requirement for reopening a roadway to traffic. NJDOT specified a target flexural strength of 350 psi (2.4 MPa) in 6 hours for the “Fast-track mix” developed in mid-90’s<sup>32</sup>. Caltran requires a minimum flexural strength of 400 psi (2.8 MPa) prior to opening to traffic for full depth pavement repairs<sup>33</sup>. FHWA<sup>43</sup> recommends a minimum flexural strength of 450 psi (3.1 MPa) for Rapid-setting Cementitious Concretes.

For high early strength concrete, the flexural strength requirements are more stringent than the compressive strength requirements because of the material’s brittle nature. In contrast, ECC materials feature very high flexural strength, or modulus of

rupture (MOR), because of its high ductility and strain-hardening behavior<sup>77</sup>. The flexural strength of ECC normally approaches three times the flexural strength of its matrix. It was expected, and verified in this study, that once the compressive strength and tensile ductility requirements are met, the flexural strength targets of HES-ECC can be easily attained.

A flexural test was conducted on HES-ECC prism specimens to measure the stress-deformation curves and material flexural strength (MOR) at different ages. Flexural testing procedures followed the ASTM C78<sup>78</sup> standard. Figure 2.36 shows the three-point bending test set-up and specimen dimensions. Each beam specimen measured 406.4 mm (16 in.) long, 76.2 mm (3 in.) wide and 101.6 mm (4 in.) thick, with a test span length of 304.8 mm (12 in.). Specimens for flexural testing were demolded at 4 hours, cured in air, and tested at different ages from 4 hours to 60 days. The air-curing condition was different from that specified in ASTM C78 because it was intended to simulate the curing condition in field applications, where the repair was expected to be exposed to air and open to traffic in 4 hours. The three-point bending test was conducted with an MTS 810 machine under displacement control at a loading rate of 0.02 mm/s ( $7.87 \times 10^{-4}$  in./s). Five specimens were tested at each age.

Table 2.12 summarizes the flexural strength (MOR) and deflection at failure of HES-ECC. Figure 2.37 shows the typical flexural stress versus deflection curves of HES-ECC at ages of 4 hours, 24 hours, and 28 days. Significant deflection hardening is observed at these ages. The flexural strength (MOR) of HES-ECC increases rapidly during the first 24 hours from  $9.8 \pm 0.2$  MPa ( $1422 \pm 34$  psi) to  $11.4 \pm 0.2$  MPa ( $1656 \pm 30$  psi). This increasing trend slows down at later ages and reaches  $15.1 \pm 0.4$  MPa (2188

$\pm 50$  psi) at 28 days. At the same time, specimen flexural ductility (defined as the maximum deflection when local failure starts) decreases after 6 hours, but approaches a constant after 3 days. It should be noted that HES-ECC attains a flexural strength of  $9.8 \pm 0.3$  MPa ( $1422 \pm 34$  psi) at 4 hours, which is significantly higher than the requirements of NJDOT, Caltran and FHWA. The 28-day flexural strength of HES-ECC is  $15.1 \pm 0.3$  MPa ( $2188 \pm 50$  psi), more than double the flexural strength of normal concrete with similar compressive strength.

## **2.4 Conclusions**

Material engineering for durable repair materials is possible through the application of micromechanical tools developed for ECC materials. This has been demonstrated through the development of the high early strength and ductile repair material HES-ECC. Micromechanics can be used as a tool for designing HES-ECC composites that meet the two strain-hardening criteria as well as conditions for saturated multiple cracking to achieve large tensile ductility above 3% and self-controlled crack widths below  $100 \mu\text{m}$  at both early and late ages. These properties are crucial for repair durability, as they prevent restrained volume change or stress concentration induced cracking and penetration of aggressive agents, which are typical deterioration causes in concrete repairs.

Through strategic combination of type III Portland cement, low water/cement ratio, polycarboxylate based superplasticizer and calcium nitrate based accelerator, the newly developed HES-ECC material is capable of attaining compressive strength of  $23.6 \pm 1.4$  MPa ( $3422 \pm 203$  psi) in 4 hours and  $55.6 \pm 2.2$  MPa ( $8062 \pm 315$  psi) in 28 days,

which exceeds HES-ECC design targets as well as federal and state transportation agency requirements. HES-ECC attains flexural strength of  $9.8 \pm 0.2$  MPa ( $1422 \pm 34$  psi) in 4 hours and  $15 \pm 0.3$  MPa ( $2187 \pm 50$  psi) in 28 days, which exceeds twice the flexural strength of concrete with similar compressive strength. Its tensile strength is  $3.5 \pm 0.1$  MPa ( $501 \pm 12$  psi) at the age of 4 hours and  $5.7 \pm 0.2$  MPa ( $823 \pm 20$  psi) at age of 28 days.

The age dependencies of micro-parameters and their effects on the age dependency of composite tensile strain capacity were investigated using experimental methods and micromechanics-based analytical tools. The significant increase of interfacial properties  $\tau_0$ ,  $G_d$  and  $\beta$  after 24 hours led to more fiber ruptures during the pullout process, resulting in a diminishing complementary energy  $J_b'$ . Meanwhile, the matrix fracture toughness increased at a faster pace within the first 24 hours and achieved a relatively high value after 24 hours. The micromechanics model revealed that the quick deterioration in composite tensile strain capacity after 24 hours was attributed to the rapid drop in complementary energy  $J_b'$  and continuous rise of  $J_{tip}$ , which leads to a significant reduction in the PSH index measured by  $J_b'/J_{tip}$ .

When there is a small margin of  $J_b'/J_{tip}$ , it is important to have large amounts of flaws in the matrix with sizes above  $c_{mc}$ , which can be activated during material strain-hardening stage before the maximum fiber bridging stress is reached. Introduction of artificial flaws (PS beads) with prescribed size distribution proved to be an effective approach to achieve saturated multiple cracking, therefore retaining large tensile strain capacity at late ages. The presence of small volume fraction (e.g. 5%) of PS beads did

not impair the early age compressive strength gain rate before 24 hours, although it did decrease the compressive strength at late ages by approximately 10%.

Detailed characterization of mechanical properties of HES-ECC further validated the material performance, and provided a database of the tensile, compressive, and flexural properties of the newly developed repair material for future engineering applications.

Table 2.1 – Three phases of ECC microstructure and corresponding micro-parameters.

<b>Phase</b>	<b>Micro-Parameters</b>
Fiber	Length $L_f$ , Diameter $d_f$ , Volume Fraction $V_f$ Tensile Strength $\sigma_f$ , Elastic Modulus $E_f$
Matrix	Fracture Toughness $K_m$ , Elastic Modulus $E_m$ , Initial Flaw Size Distribution $a_0$
Fiber/Matrix Interface	Chemical Bond $G_d$ , Frictional Bond $\tau_0$ , Slip Hardening Property $\beta$ , Snubbing Coefficient $f$ , Fiber Strength Reduction factor $f'$

Table 2.2 – List of materials used.

Category	Product Name	Manufacturer	Chemical Composition	Particle Size
Cementitious Material	Portland Cement Type I	LaFarge Co., USA	Ordinary Portland Cement (OPC)	Blaine Surface area: 3300 cm <sup>2</sup> /g
	Portland Cement Type III	Holcim Co., USA	Finely ground OPC	Blaine Surface area: 5000 cm <sup>2</sup> /g
	Normal Fly Ash	Boral Material Tech. Inc., USA	ASTM C618 Class F	Mean size: 10-20 μm
Accelerating Admixture	Pozzolith <sup>®</sup> NC 534	Master Builders, Inc., USA	Calcium nitrate <43%, Sodium thiocyanate <5%	Specific weight: 1.39g/ml
Aggregate	Silica sand F110	U.S. Silica Co.	Silica	Mean size: 110 μm, Max. size: 250 μm
	PS Beads	Dow Chemical Co., USA	Polystyrene	Size: 4mm, Density: 1.4g/cm <sup>3</sup>
Superplasticizer	Glenium <sup>®</sup> 3200 HES	Master Builders, Inc. USA	Polycarboxylate Based	Specific weight: 1.05 g/ml
Hydration Control	Delvo <sup>®</sup> Stabilizer	Master Builders, Inc. USA		
Fiber	REC15	Kuraray, Co, Japan	Polyvinyl Alcohol (PVA) Fiber	

Table 2.3 – Mixing proportions for initial material composition selection based on strength requirements.

Mix	Cement	Silica Sand	Fly Ash	Water	Admixtures	Fiber, $V_f(\%)$
1	Type I 1.0	0.8	1.2	0.53	GL3200 0.75%	2.0
2	Type III 1.0	0.8	1.2	0.53	GL3200 0.75%	2.0
3	Type III 1.0	1.0	-	0.53	-	2.0
4	Type III 1.0	1.0	-	0.45	GL3200 0.35%	2.0
5	Type III 1.0	1.0	-	0.33	GL3200 0.75%	2.0
6	Type III 1.0	1.0	-	0.33	GL3200 0.75%, NC534 4.0%	2.0

Table 2.4 – Properties of REC 15 PVA fiber from Kuraray, Co, Japan.

Fiber Type	Nominal Strength (MPa)	Apparent Strength (MPa)	Fiber Diameter ( $\mu\text{m}$ )	Fiber Length (mm)	Young's Modulus (GPa)	Elongation (%)
REC15	1620	1092	39	12	42.8	6.0

Table 2.5 – Compressive strength of Mix 1 and 2 at different ages.

Age (Hour)	Compressive Strength (MPa)					
	Mix 1			Mix 2		
4				3.4	3.4	3.6
5				7.1	8.2	9.4
6				17.3	18.8	19.1
10				24.3	25.5	28.3
12	17.8	17.9	18.3	28.8	30.4	32.3
24	22.0	22.6	24.4	35.4	38.5	38.6
48	31.1	32.3	32.6	41.6	42.6	44.8
72	40.9	44.3	46.9	44.5	46.8	48.4
144	55.9	57.9	60.2	55.1	56.6	57.7
672	62.7	65.5	66.7	59.7	62.0	65.7

Table 2.6 – Compressive strength of Mix 3, 4 and 5 at different ages.

Age (Hour)	Compressive Strength (MPa)								
	Mix 3			Mix 4			Mix 5		
4				1.8	1.9	2.0	4.7	5.0	5.3
5				5.2	5.2	5.4	8.9	10.2	11.7
6				5.9	5.9	6.3	23.1	26.1	26.4
7				9.7	11.2	12.8	30.3	31.1	31.6
8	1.4	1.9	2.5	14.0	15.2	17.1	32.8	34.0	35.7
9	3.2	3.4	4.1	18.6	20.0	20.0	33.1	36.0	38.3
10	4.0	4.7	5.5	18.8	20.0	21.1	37.3	37.7	39.0
12	9.7	10.9	12.4	21.4	22.3	22.8	36.7	38.8	41.0
24	16.4	17.7	19.2	29.3	30.3	30.8	41.9	43.5	44.5
48	24.8	25.5	26.9	31.8	33.1	34.1	47.9	50.2	51.9
72	24.8	26.7	28.1	33.1	34.2	34.7	52.6	55.3	56.2
96	25.7	27.0	28.0	35.6	36.4	37.7	53.7	55.2	56.4
120	27.6	28.6	28.7	37.2	38.5	39.9	56.3	57.4	58.2
144	27.1	29.1	30.6	40.1	43.0	43.5	55.8	57.9	60.0
168	27.7	29.4	29.8	42.7	43.7	45.1	56.9	58.7	61.4
336	28.3	29.7	30.7	46.1	47.2	48.0	59.9	62.3	63.8
480	29.2	30.3	29.6	48.0	49.3	49.6	62.3	64.3	64.5
672	29.0	30.3	31.8	47.6	49.0	50.6	62.9	65.4	66.7

Table 2.7 – Compressive strength of Mix 6 (w/ and w/o insulation) at different ages.

Age (Hour)	Compressive Strength (MPa)					
	Mix 6 (w/ insulation)			Mix 6 (w/o insulation)		
2.7				12.4	12.5	12.6
3	7.6	7.7	8.7	21.3	22.0	22.7
4	17.4	17.9	18.0	26.6	28.1	29.3
5	28.6	29.7	31.7	34.3	34.6	34.6
6	33.0	34.3	34.7	38.3	40.1	41.0
7	34.8	36.4	37.4	39.5	40.8	41.7
8	37.1	38.6	39.8	40.4	41.5	42.5
9	39.3	40.2	40.5	41.8	43.3	44.5
10	39.5	40.0	41.1	42.5	43.9	45.6
12	39.9	41.1	42.3	44.8	44.8	45.1
24	44.5	45.7	47.5	45.7	48.0	50.5
48	47.6	49.3	50.0	51.0	51.8	53.2
72	51.8	53.0	54.2	53.2	56.4	57.8
96	52.9	54.1	55.9	54.7	56.6	58.3
120	54.4	55.2	56.0	56.2	57.2	57.4
144	54.3	55.9	56.9	56.5	58.6	59.0
168	57.0	58.1	58.9	57.2	58.5	58.9
336	59.8	60.7	61.0	59.5	60.0	60.6
480	60.7	62.2	63.4	62.7	63.2	64.0
672	61.6	63.0	64.4	62.4	63.7	65.3

Table 2.8 – Mixing proportion of HES-ECC before / after adding artificial flaws.

Mix	Cement	Silica Sand	Water	Other Aggregates	Admixtures (wt% of cement)	Fiber $V_f$ (%)
6	Type III, 1.0	1.0	0.33	-	GL3200 0.75%, NC534 4.0%	2.0
7	Type III, 1.0	1.0	0.33	PS Beads 0.064	GL3200 0.75%, NC534 4.0%	2.0

Table 2.9 – Mix proportion of HES-ECC.

HES-ECC Mix Design Parameter	Value (kg/m <sup>3</sup> )
Portland Cement, Type III	918
Silica sand, F110	918
Water	301
Poly-vinyl-alcohol Fiber	26.1
Polystyrene Beads	58.8
Superplasticizer, Glenium <sup>®</sup> 3200HES	6.89
Accelerating Admixture, Pozzolith <sup>®</sup> NC 534	36.7
Hydrating Control Admixture, Delvo <sup>®</sup> Stabilizer	Optional

Table 2.10 – HES-ECC tensile properties at different ages (mean ± standard deviation).

Age	Young's Modulus, ×10 <sup>3</sup> MPa (ksi)	Tensile Strength, MPa (psi)	Strain Capacity, %
4 h	13.10 ± 0.77 (1900.12 ± 111.44)	3.46 ± 0.08 (501.23 ± 11.64)	5.97 ± 0.22
6 h	14.98 ± 0.79 (2173.37 ± 114.11)	4.21 ± 0.13 (610.41 ± 19.42)	4.97 ± 0.38
12 h	16.05 ± 1.02 (2328.26 ± 147.29)	4.57 ± 0.17 (662.27 ± 25.18)	4.41 ± 0.33
24 h	18.30 ± 0.59 (2654.19 ± 84.87)	4.69 ± 0.08 (680.35 ± 11.50)	3.99 ± 0.27
3 d	19.10 ± 0.81 (2770.22 ± 116.91)	5.09 ± 0.16 (738.32 ± 23.62)	3.61 ± 0.28
7 d	20.59 ± 0.70 (2986.32 ± 100.90)	5.56 ± 0.11 (806.82 ± 16.42)	3.52 ± 0.29
14 d	22.18 ± 1.02 (3216.27 ± 147.47)	5.88 ± 0.16 (852.42 ± 23.01)	3.64 ± 0.37
28 d	23.20 ± 0.96 (3364.88 ± 139.77)	5.98 ± 0.14 (867.33 ± 20.39)	3.47 ± 0.62
60 d	23.80 ± 0.71 (3451.90 ± 103.45)	5.99 ± 0.19 (868.78 ± 28.11)	3.52 ± 0.57

Table 2.11 – HES-ECC compressive properties at different ages (mean ± standard deviation).

Age (h)	Compressive Strength , MPa (psi)
3h	9.82 ± 0.56 (1424.82 ± 81.54)
4 h	23.59 ± 1.40 (3422.16 ± 203.33)
6 h	34.22 ± 1.40 (4963.22 ± 181.51)
12 h	37.01 ± 1.84 (5367.54 ± 266.43)
24 h	42.26 ± 1.39 (6129.62 ± 201.55)
3 d	44.70 ± 2.37 (6482.65 ± 343.99)
7 d	47.47 ± 1.89 (6884.56 ± 274.83)
14 d	50.79 ± 2.38 (7366.43 ± 344.71)
28 d	55.59 ± 2.17 (8062.90 ± 315.03)
60 d	56.76 ± 1.72 (8233.13 ± 250.08)

Table 2.12 – HES-ECC flexural properties at different ages (mean ± standard deviation).

Age (h)	Flexural Strength / MOR, MPa (psi)	Deflection at Failure, mm (in)
4 h	9.81 ± 0.24 (1422.19 ± 34.22)	14.73 ± 0.50 (0.58 ± 0.02)
6 h	11.02 ± 0.36 (1598.67 ± 51.94)	15.49 ± 0.50 (0.61 ± 0.02)
24 h	11.41 ± 0.21 (1655.54 ± 29.78)	12.45 ± 0.50 (0.49 ± 0.02)
3 d	12.96 ± 0.35 (1879.63 ± 50.79)	10.67 ± 0.50 (0.42 ± 0.02)
7 d	13.55 ± 0.43 (1965.28 ± 62.61)	9.91 ± 0.30 (0.39 ± 0.01)
28 d	15.08 ± 0.34 (2187.64 ± 49.87)	9.91 ± 0.50 (0.39 ± 0.02)

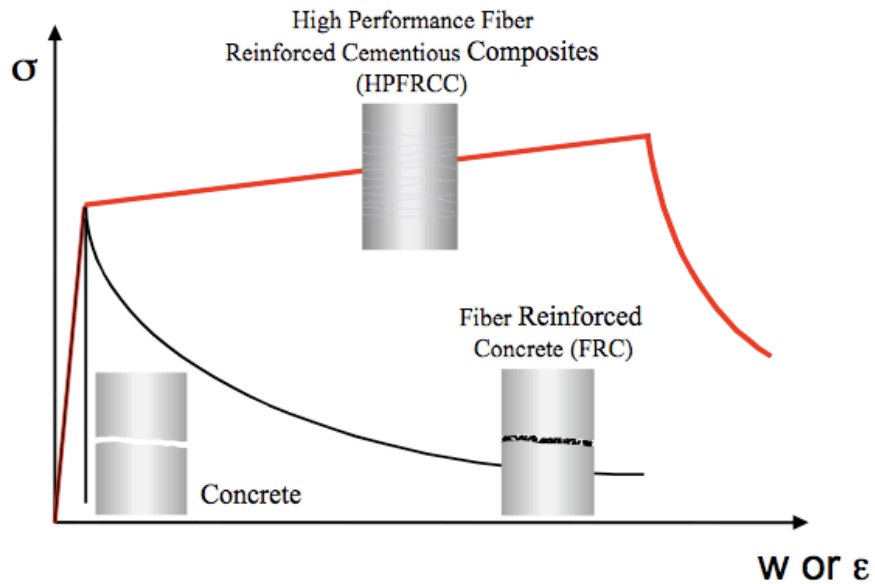


Figure 2.1 – Uniaxial tensile stress-deformation relation of concrete, FRC, and HPFRCC. For concrete, formation of the crack corresponds to the sudden drop of tensile load carrying capacity. For FRC, after a crack is formed, deformation is associated with crack opening  $\delta$ . Tensile load capacity drops at a slower rate (compared to concrete) as a single crack enlarges. This is a typical “tension softening” behavior. For HPFRCC, deformation during the elastic and strain-hardening stages is described as straining. After the first crack forms, tensile load capacity continues to rise with increasing strain through multiple micro-cracking behavior. The strain capacity of HPFRCC is defined as the strain value at which peak tensile load is reached.

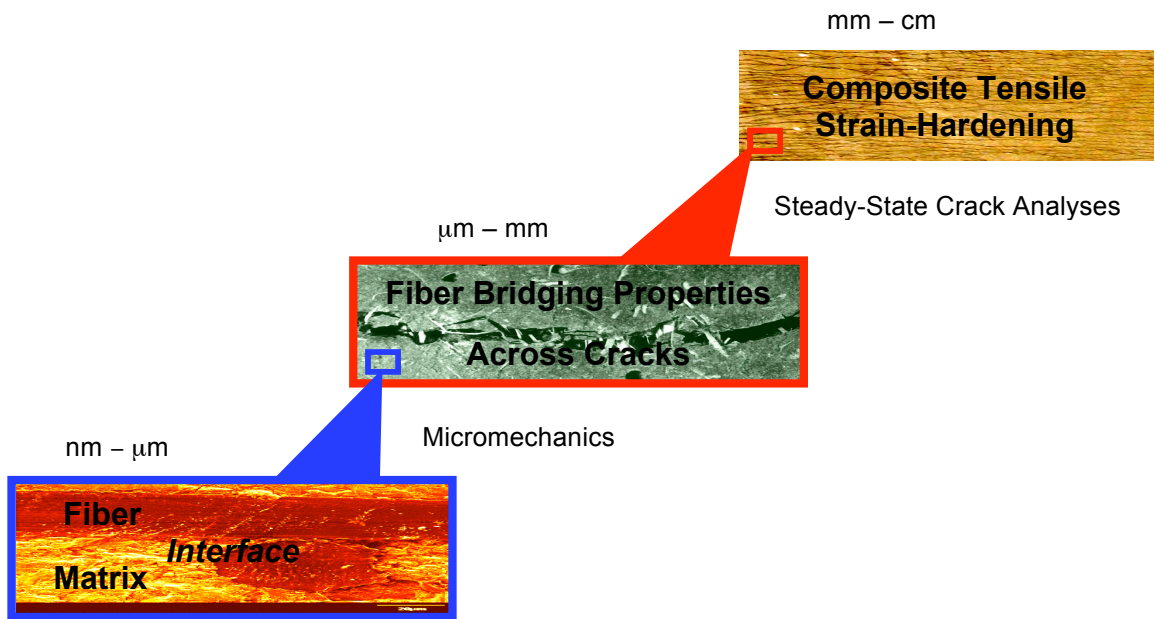


Figure 2.2 – Scale linking in ECC material development.

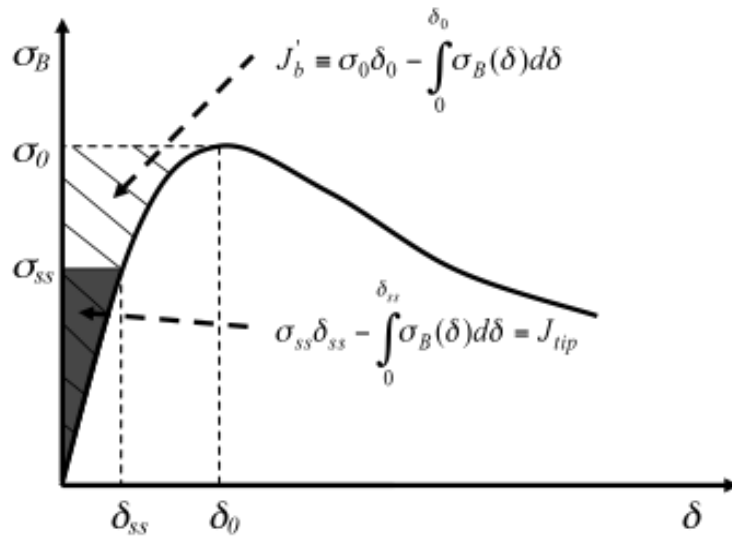


Figure 2.3 – Typical fiber bridging stress vs. crack opening  $\sigma(\delta)$  curve for a tensile strain-hardening composite. Hatched area represents complimentary energy  $J'_b$ . Shaded area represents crack tip toughness  $J_{tip}$ .

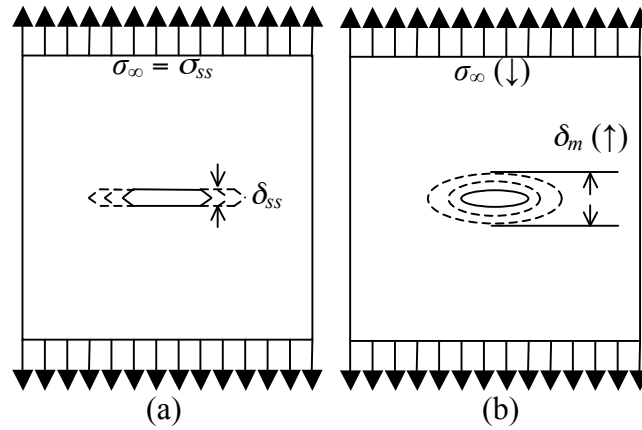


Figure 2.4 – (a) Steady-state cracking with a constant crack opening  $\delta_{ss}$  accompanied by a constant ambient load  $\sigma_{ss}$ ; (b) Griffith cracking with a widening crack opening  $\delta_m$  accompanied by a descending ambient load.

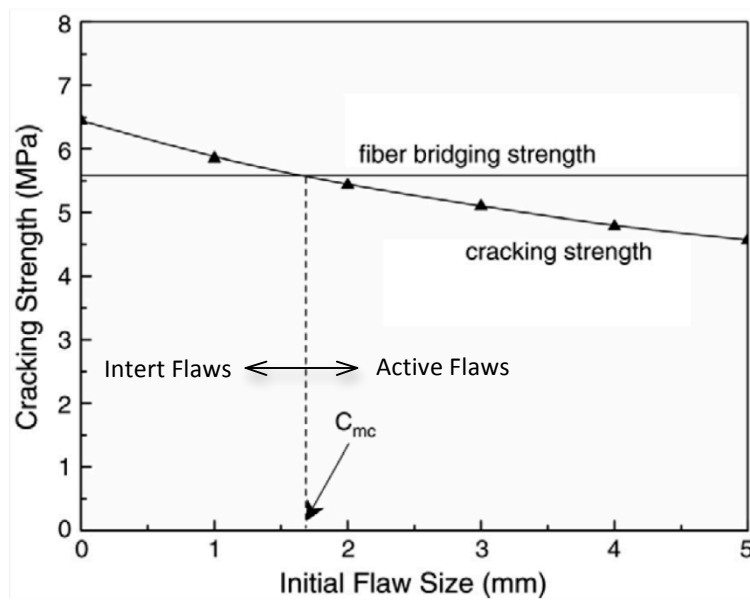


Figure 2.5 – Theoretically predicted effect of initial flaw size on the cracking strength of PVA-ECC containing 2% by volume PVA fiber. The maximum fiber bridging strength is also shown in the plot. The critical flaw size ( $c_{mc}$ ) separates inert and active flaws.

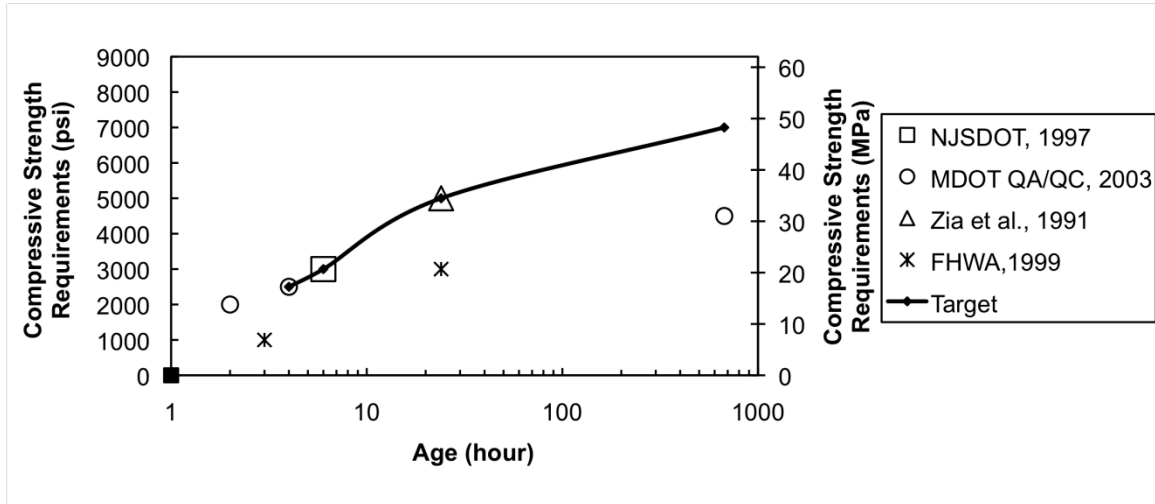


Figure 2.6 – State and federal compressive strength requirements, and target compressive strength at different ages for HES-ECC.

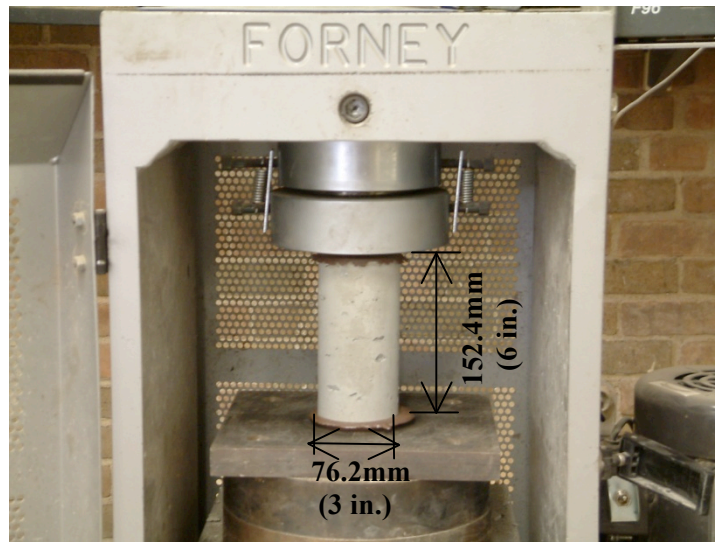


Figure 2.7 – Uniaxial compressive test setup.

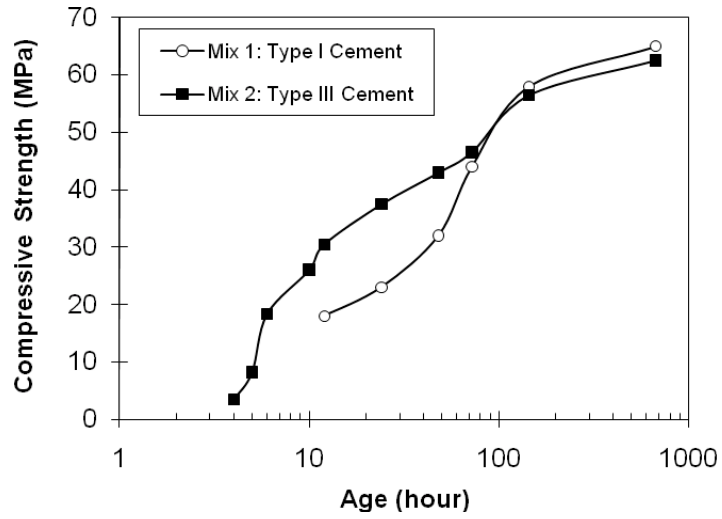


Figure 2.8 – Effect of cement type on compressive strength development.

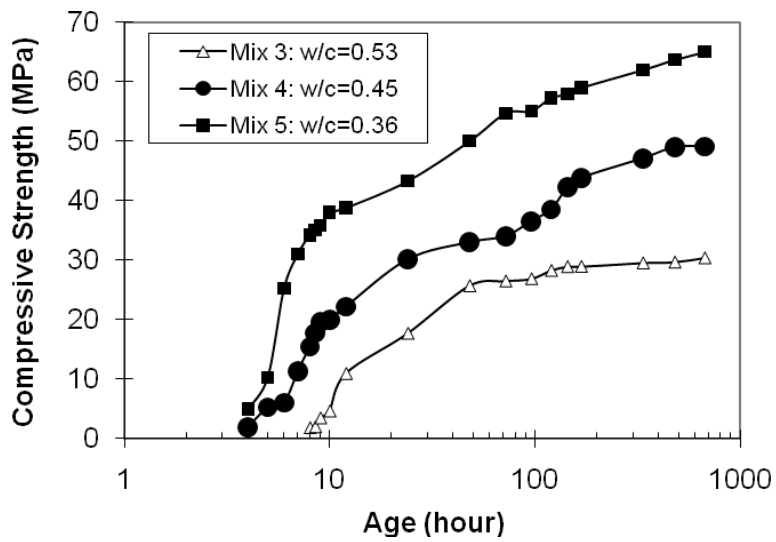


Figure 2.9 – Effect of water/cement ratio on compressive strength development.

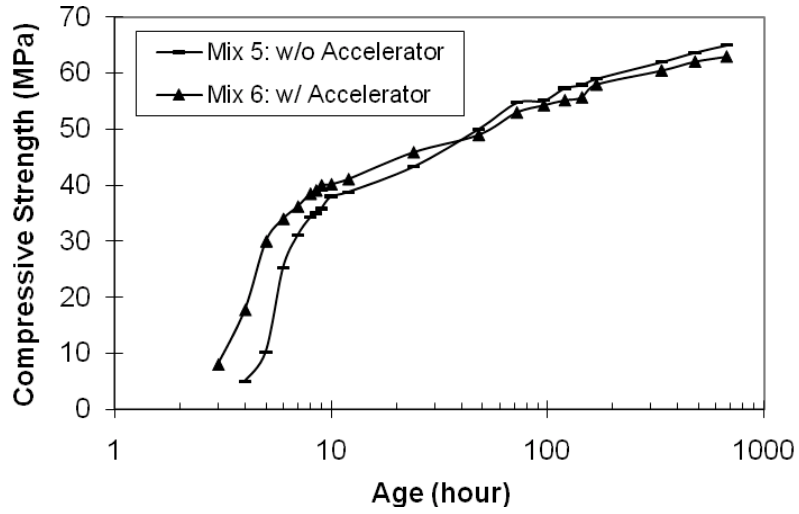


Figure 2.10 – Effect of accelerator on compressive strength development.

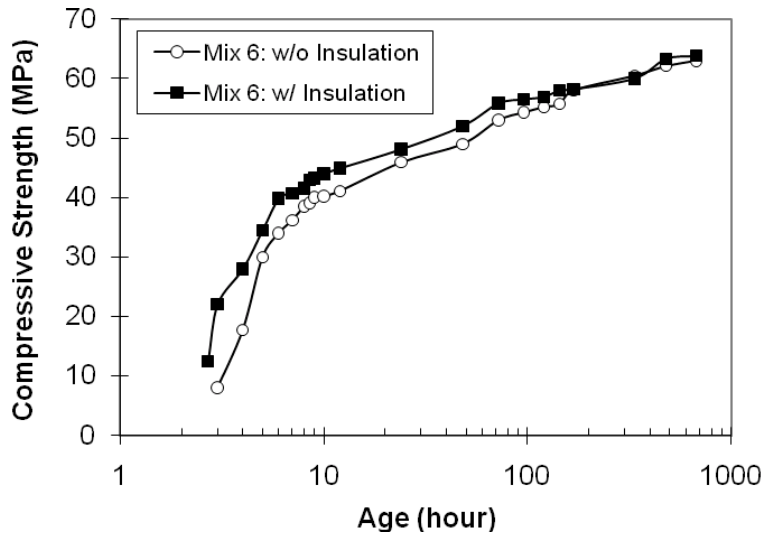


Figure 2.11 – Effect of curing condition on compressive strength development.



Figure 2.12 – Uniaxial tensile test setup.

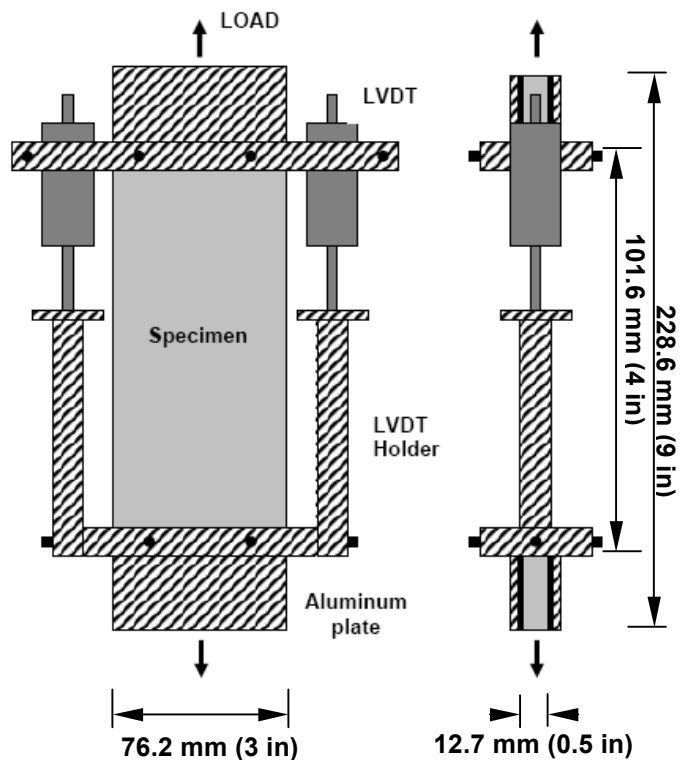
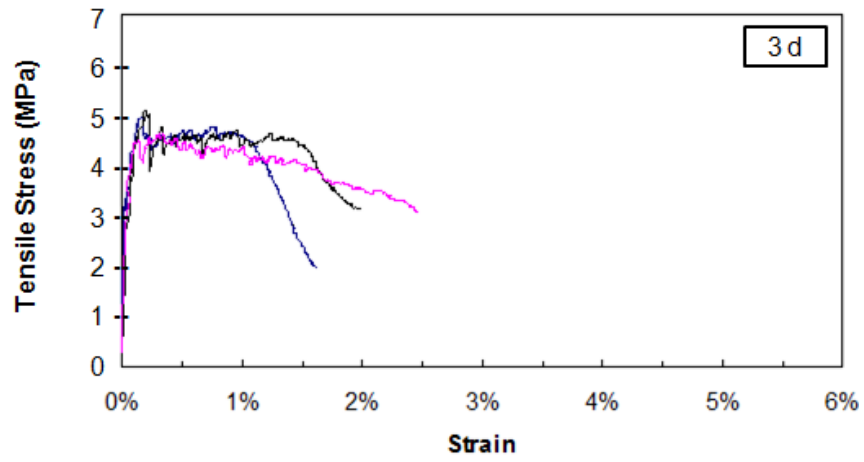
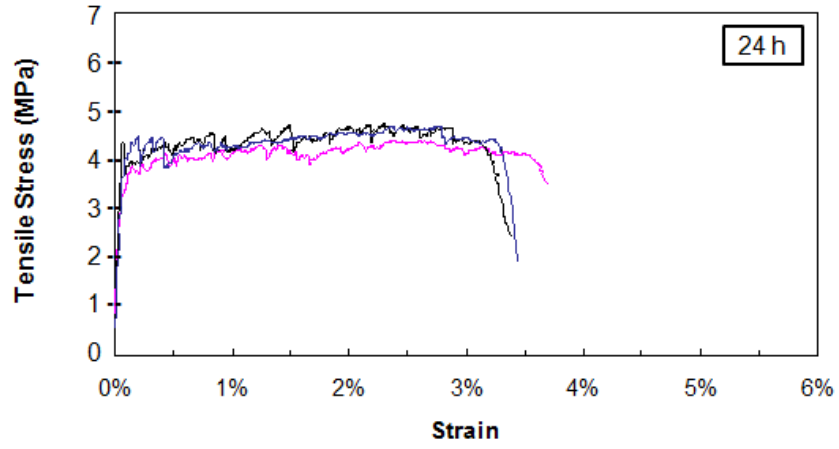
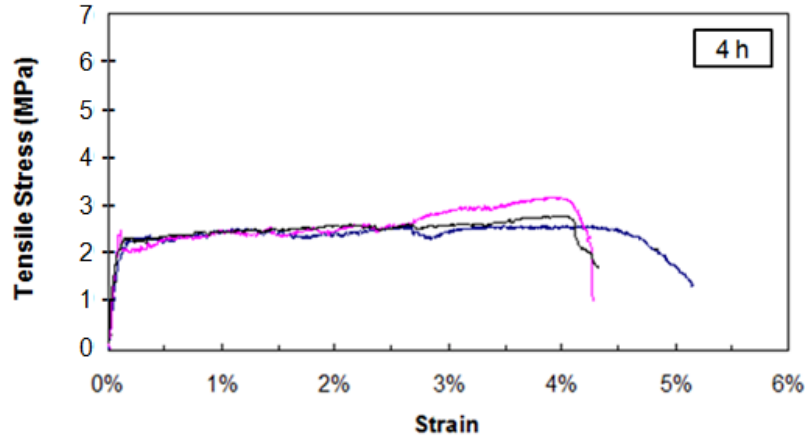


Figure 2.13 – Dimensions of tensile test specimen.



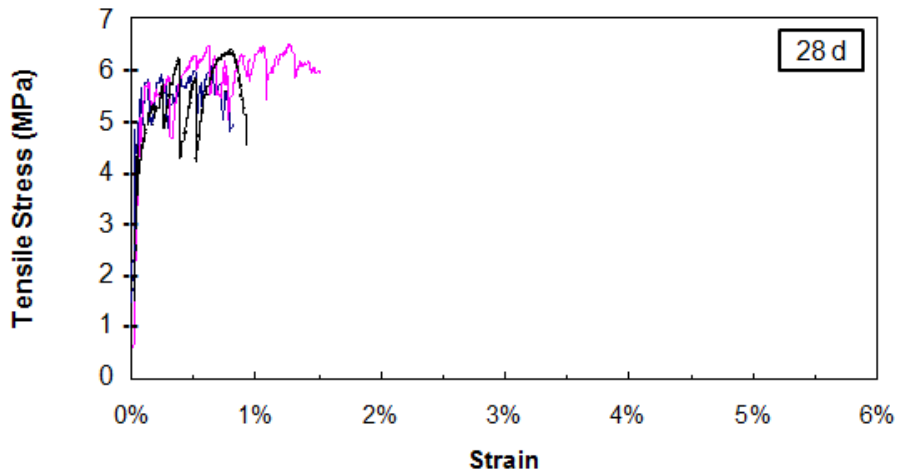
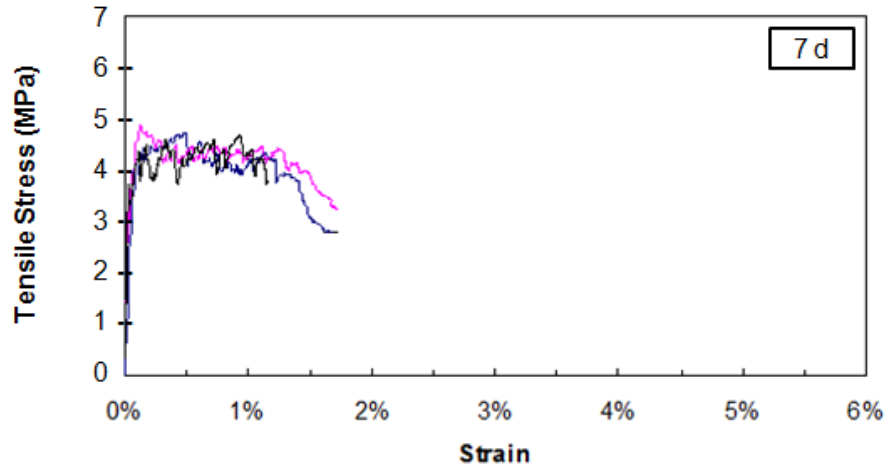


Figure 2.14 – Tensile stress - strain curves of Mix 6 at ages of 4h, 24h, 3d, 7d, and 28d.

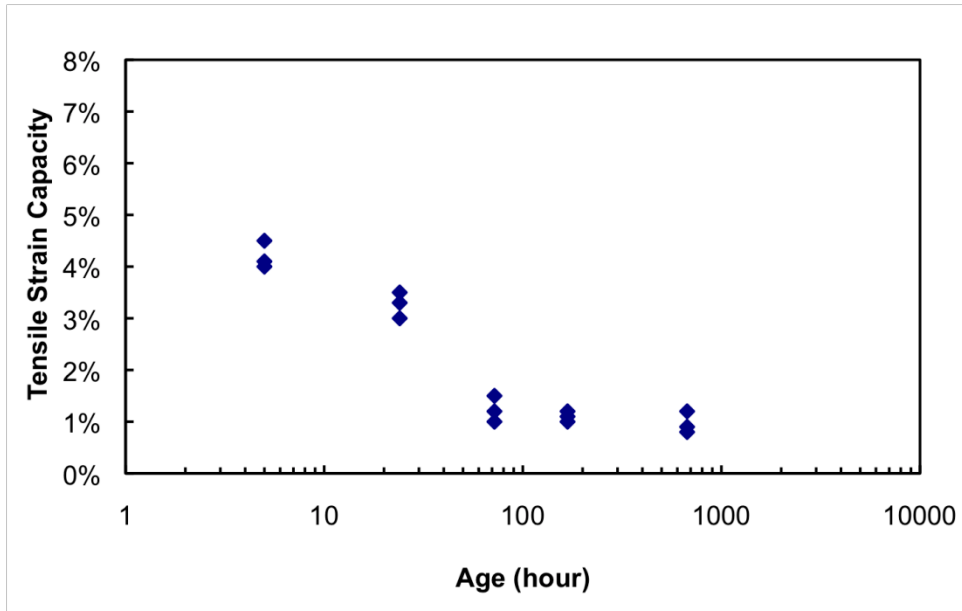


Figure 2.15 – Age dependency of tensile strain capacity of Mix 6.

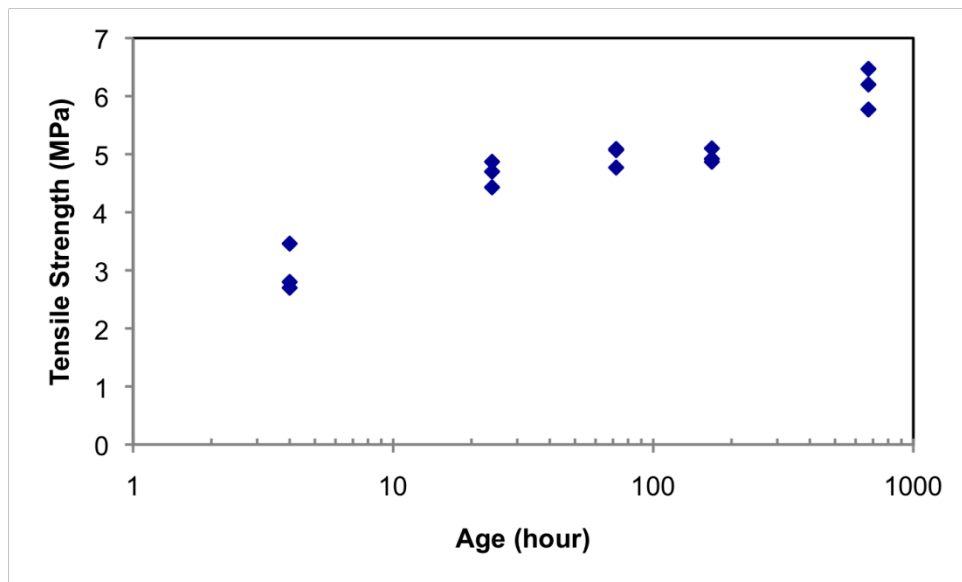


Figure 2.16 – Age dependency of tensile strength of Mix 6.

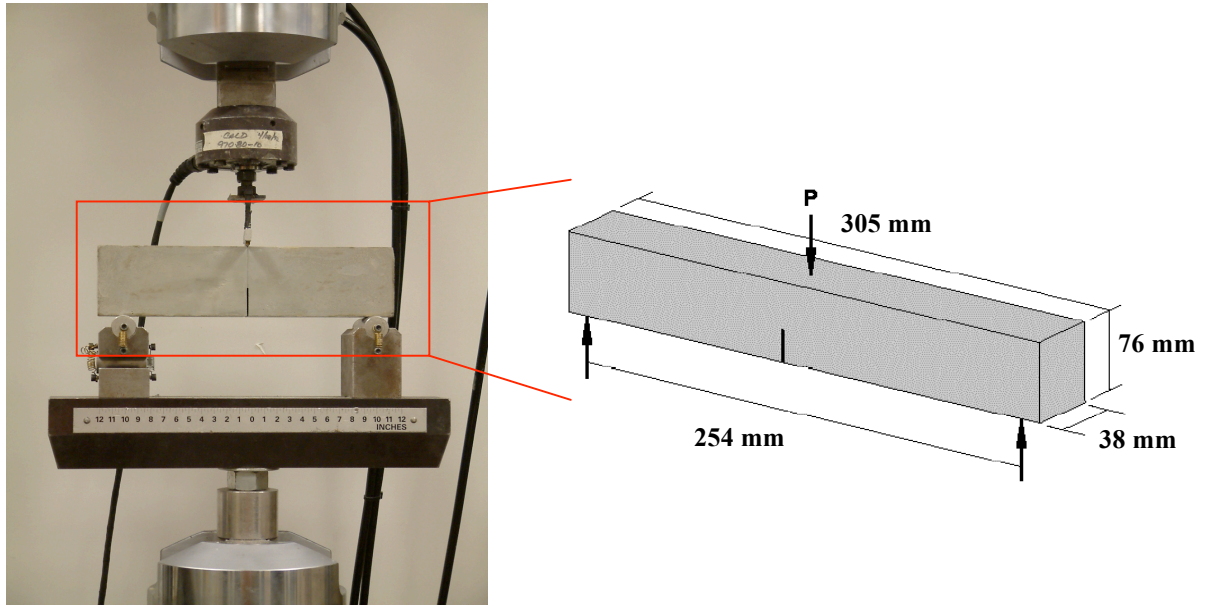


Figure 2.17 – Matrix fracture toughness test set-up.

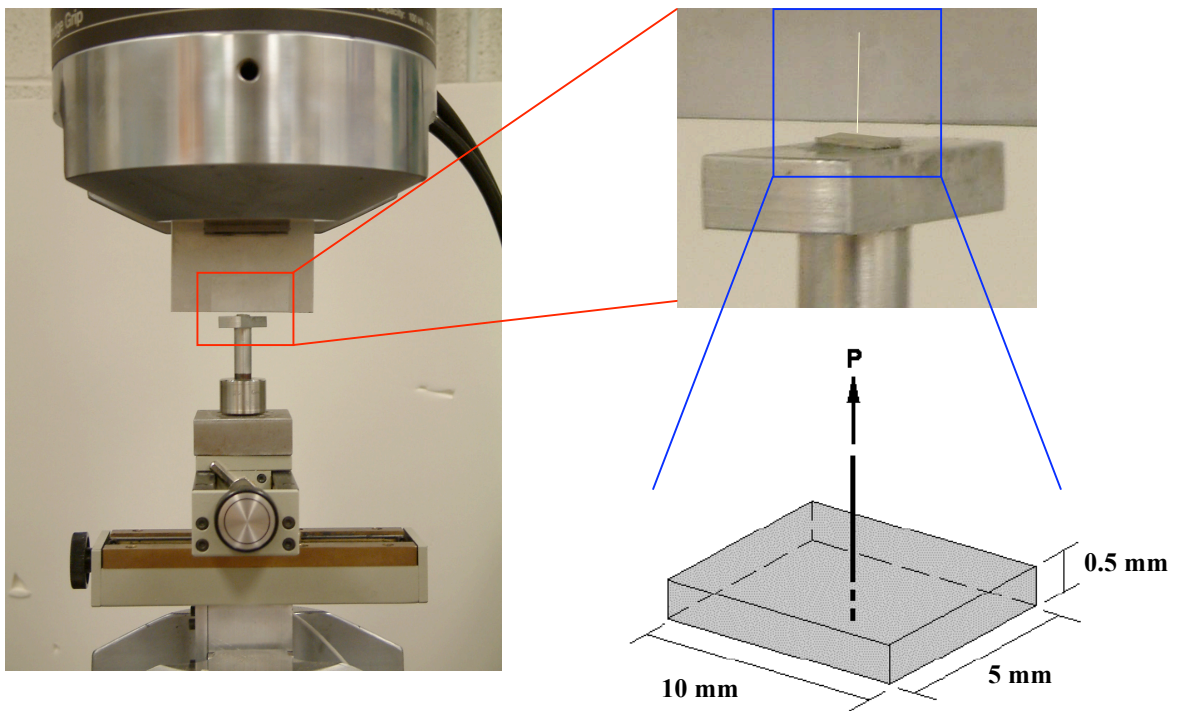


Figure 2.18 – Single fiber pull-out test set-up.

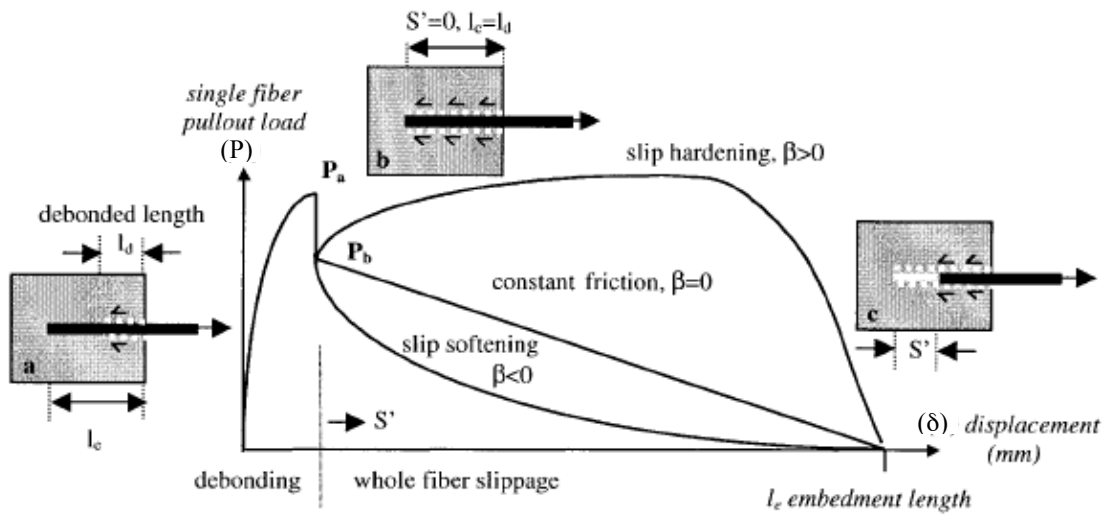


Figure 2.19 – General profile of a single fiber pullout curve.

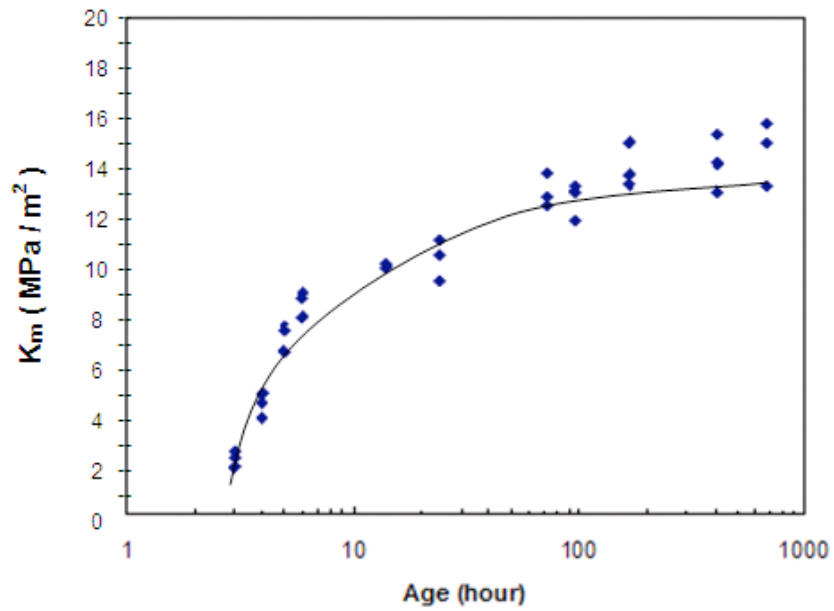


Figure 2.20 – Age dependency of matrix fracture toughness.

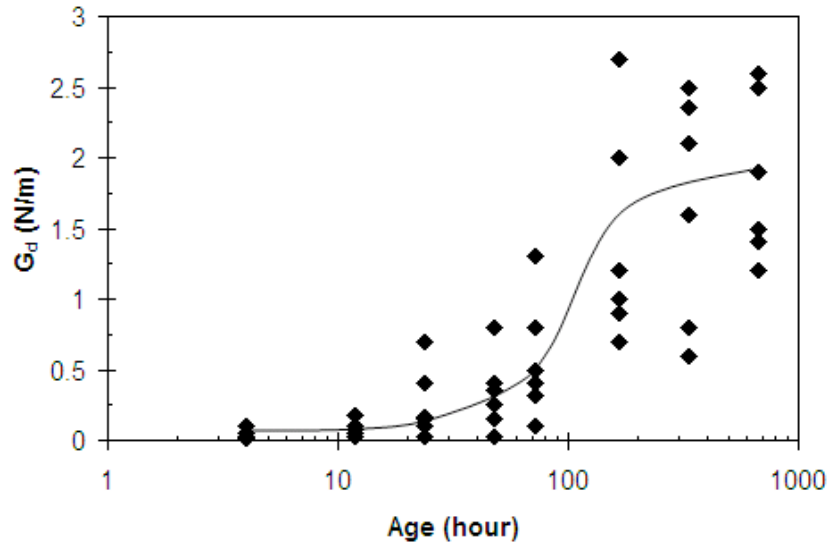


Figure 2.21 – Age dependency of matrix/fiber interface chemical bond.

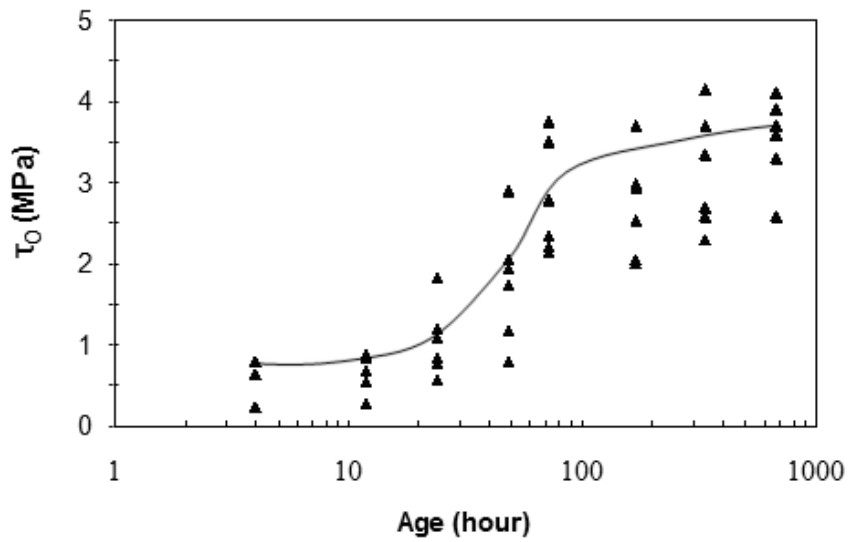


Figure 2.22 – Age dependency of matrix/fiber interface frictional stress.

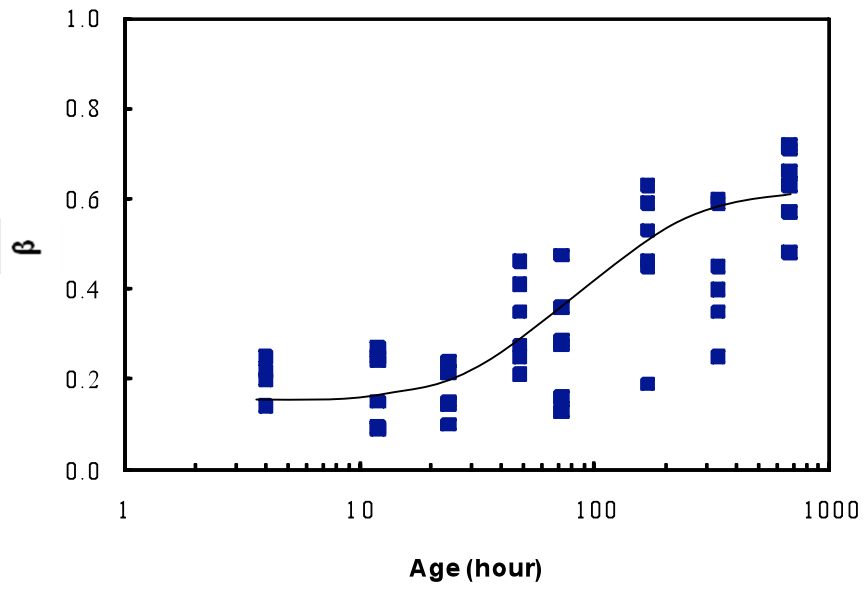


Figure 2.23: Age dependency of slip hardening coefficient.

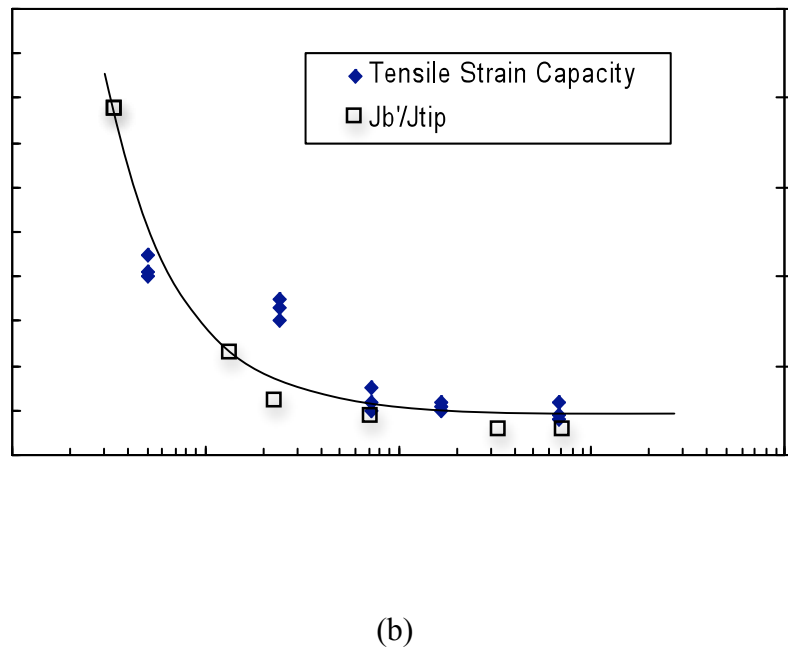
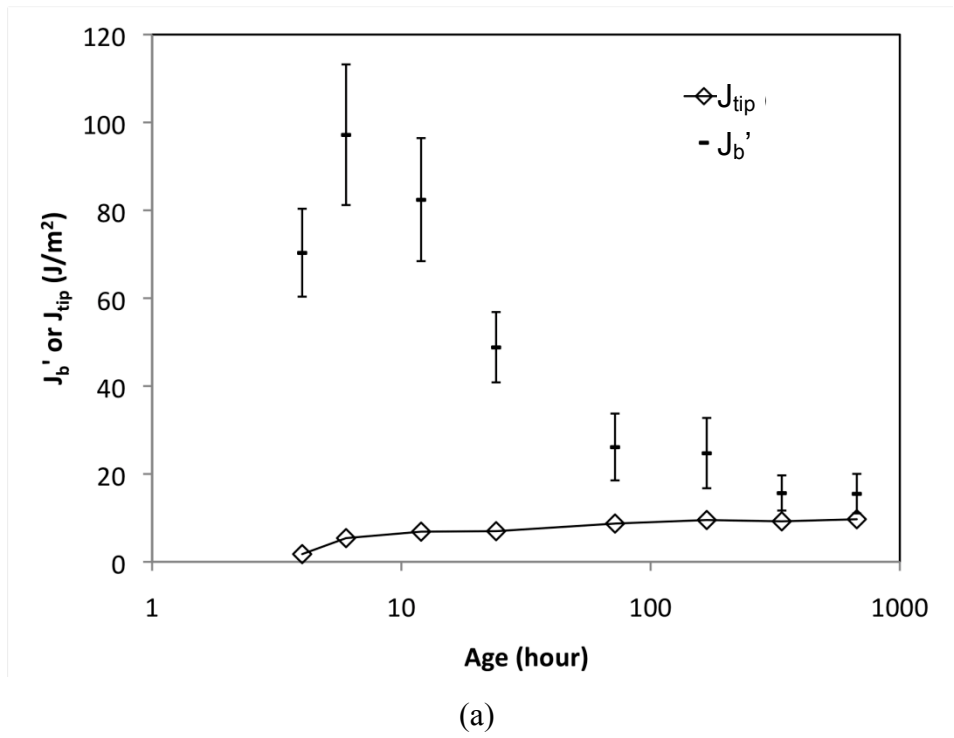


Figure 2.24: Evolution of (a)  $J_b'$  and  $J_{tip}$ , (b)  $J_b'/J_{tip}$  ratio and tensile strain capacity with age (Mix 6).

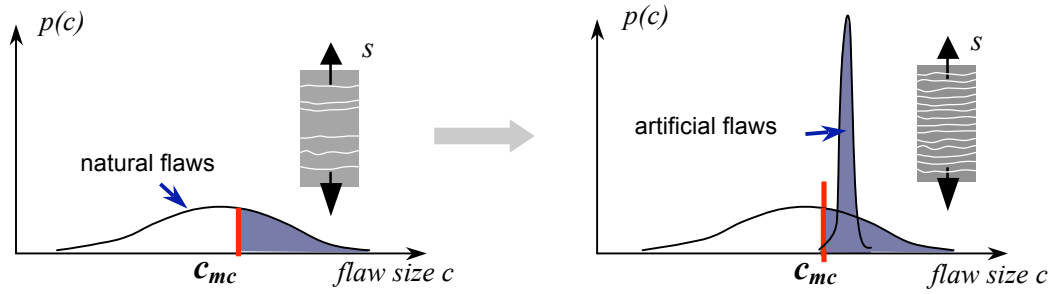
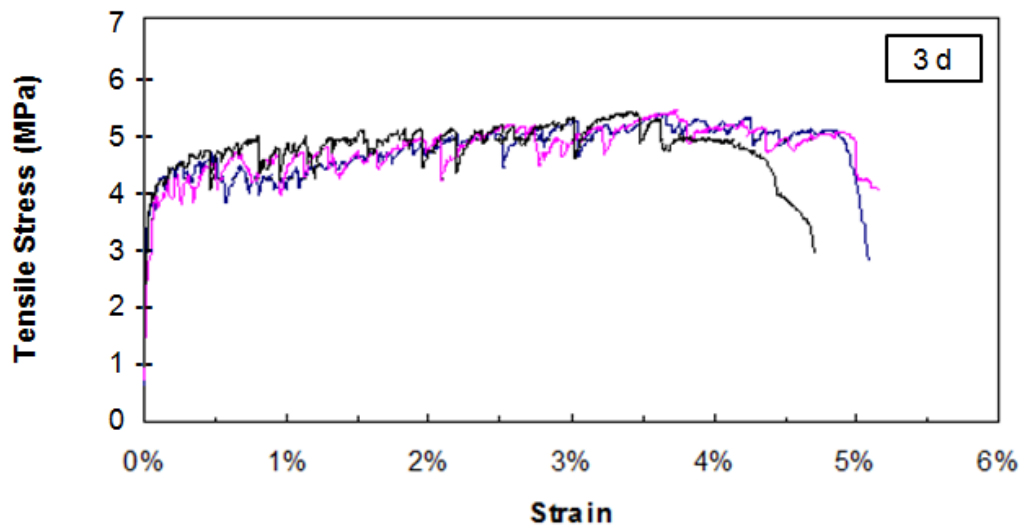
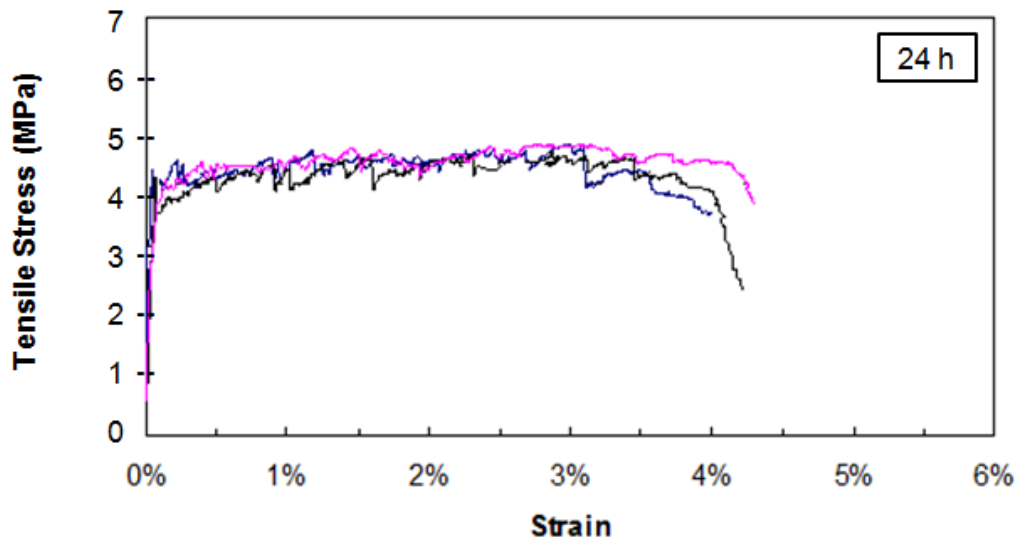
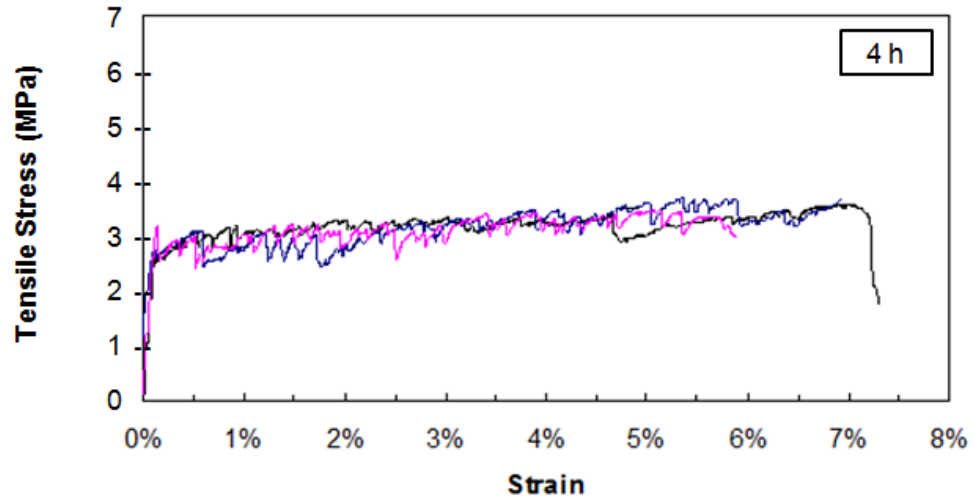


Figure 2.25 – Optimization scheme for pre-existing flaw size distribution in matrix: (a) natural flaw size distribution with random nature inherent from processing; (b) artificial flaws larger than critical size  $c_{mc}$  imposed to ensure saturation of multiple-cracking (Wang and Li, 2004).



Figure 2.26: Aggregates used as artificial flaws: polystyrene (PS) beads.



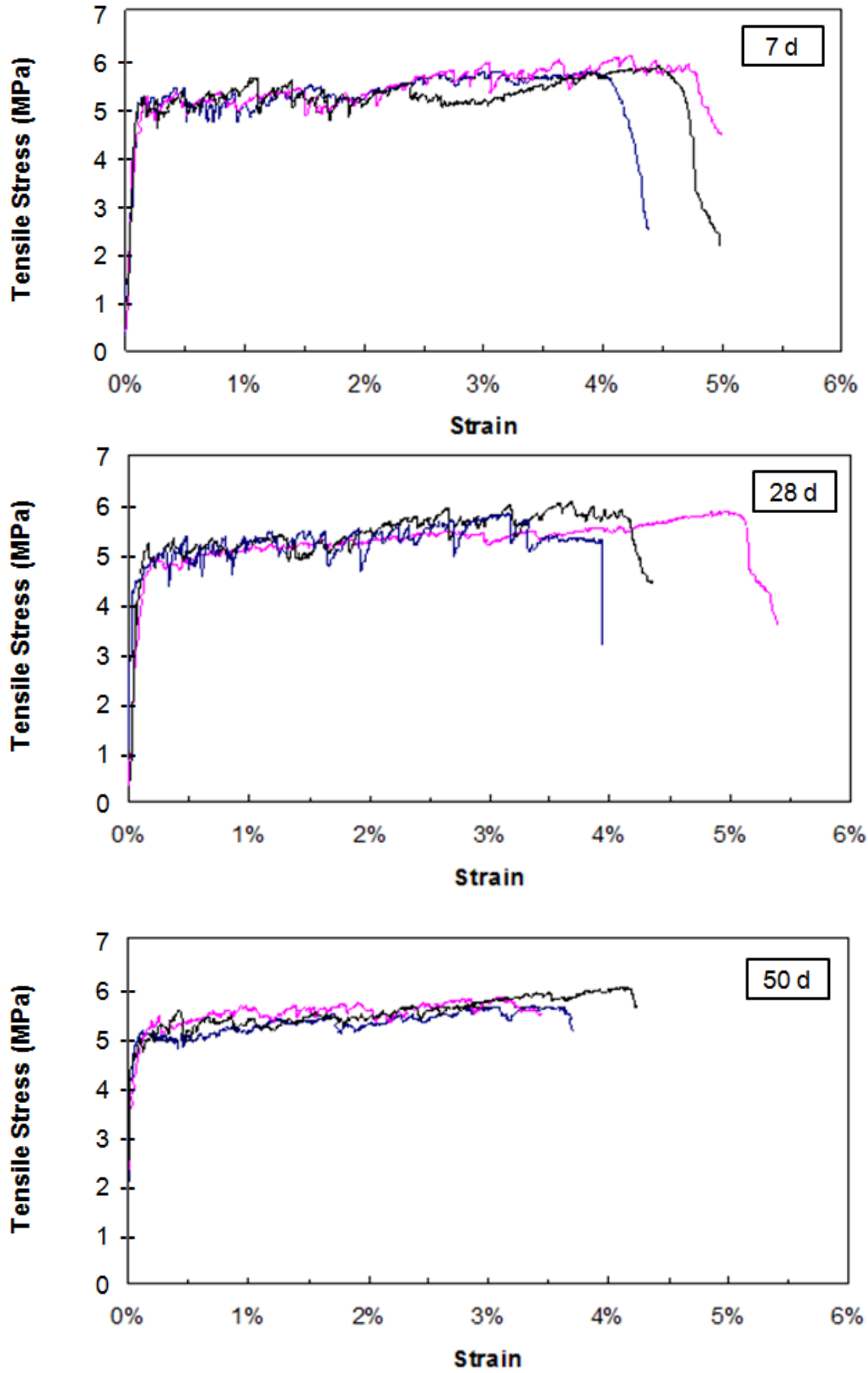
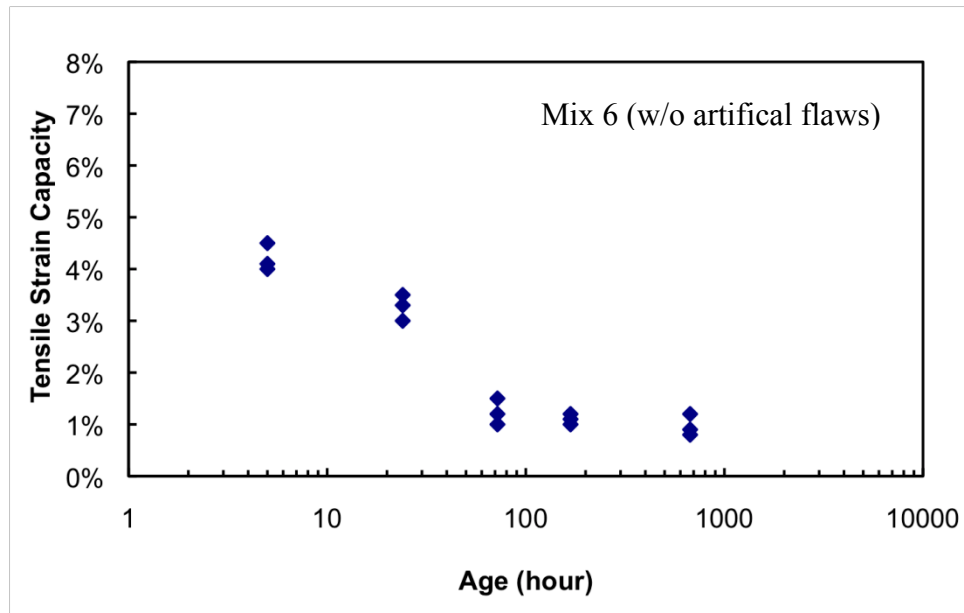
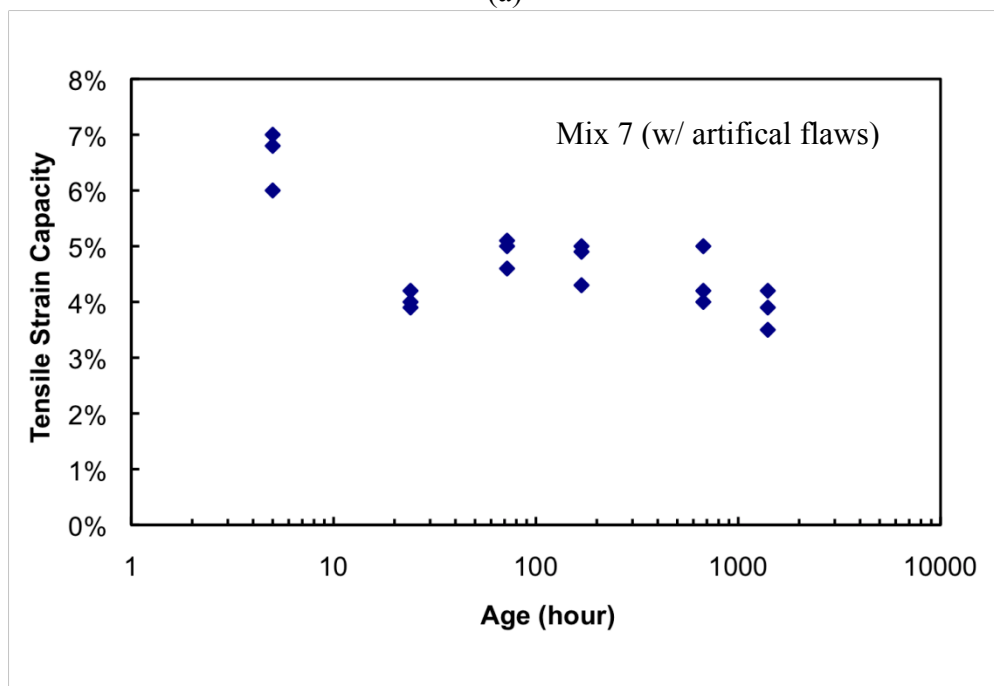


Figure 2.27 – Age dependent tensile stress vs. strain curve of Mix 7.



(a)



(b)

Figure 2.28 – Age dependency of tensile strain capacity: (a) before adding artificial flaws (Mix 6); (b) after adding artificial flaws (Mix 7).

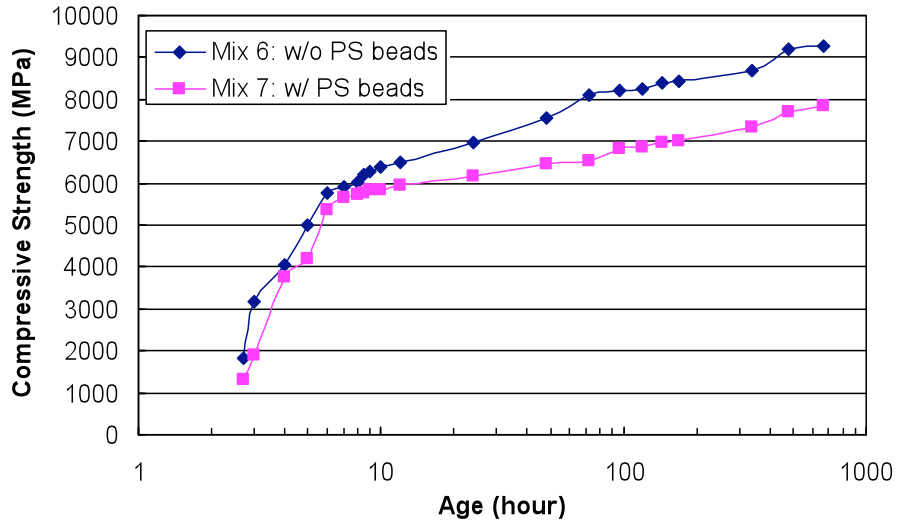


Figure 2.29 – Effect of PS beads on compressive strength development.

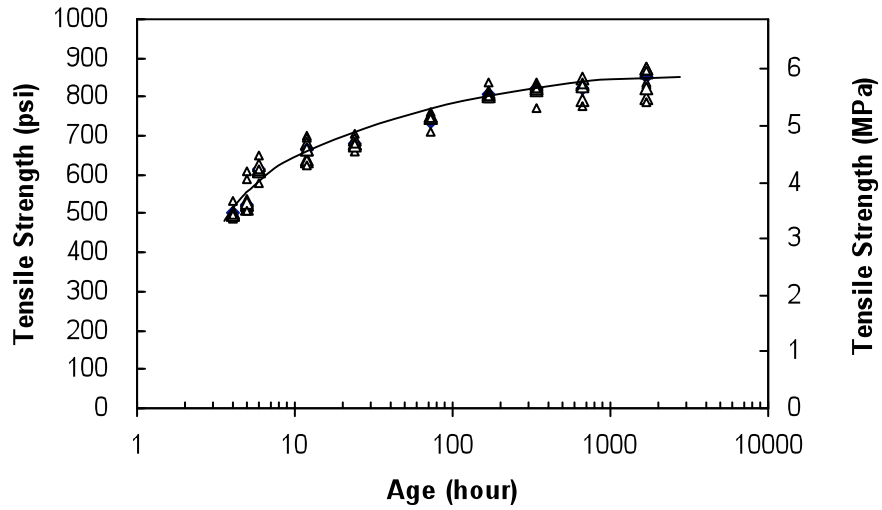


Figure 2.30 – HES-ECC tensile strength development with ages.

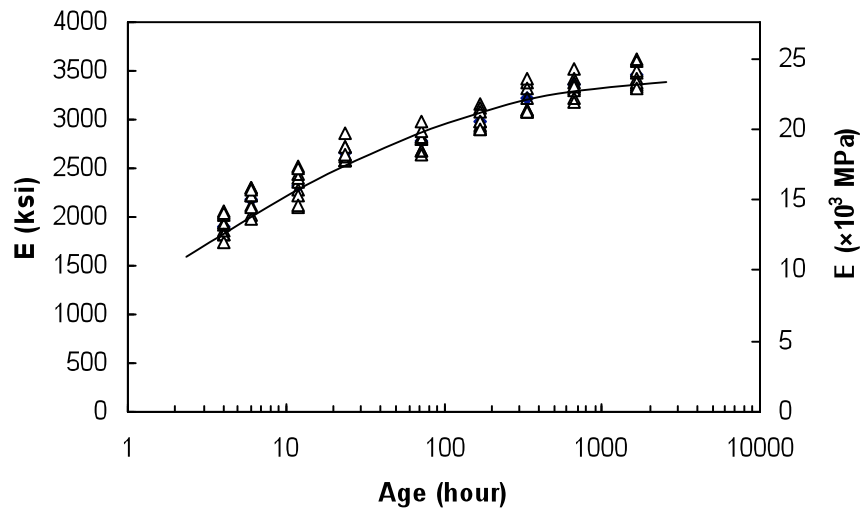


Fig. 2.31 – HES-ECC Young's modulus (E) development with ages.

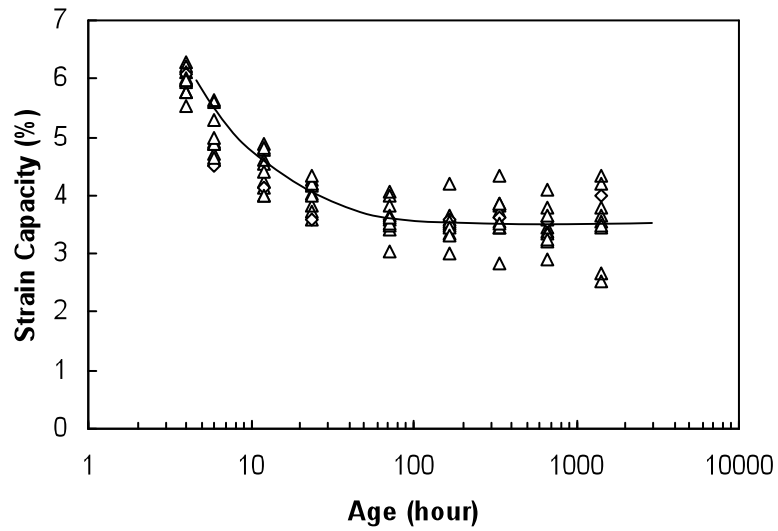


Figure 2.32 – HES-ECC tensile strain capacity development with ages.

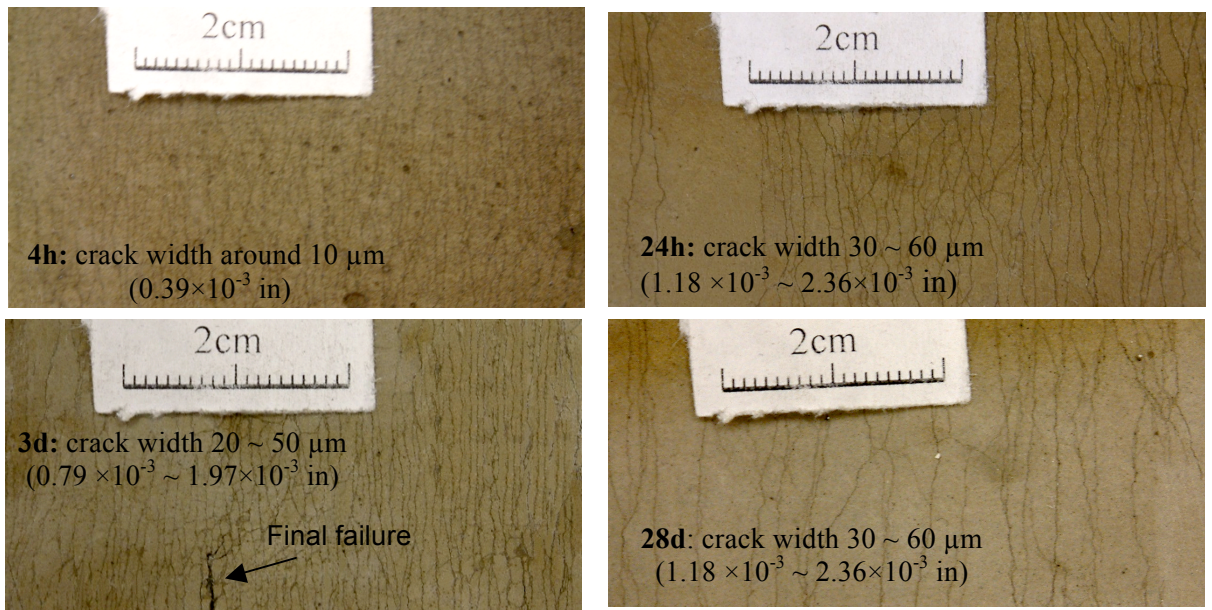


Figure 2.33 – HES-ECC multiple microcracking pattern at different ages.

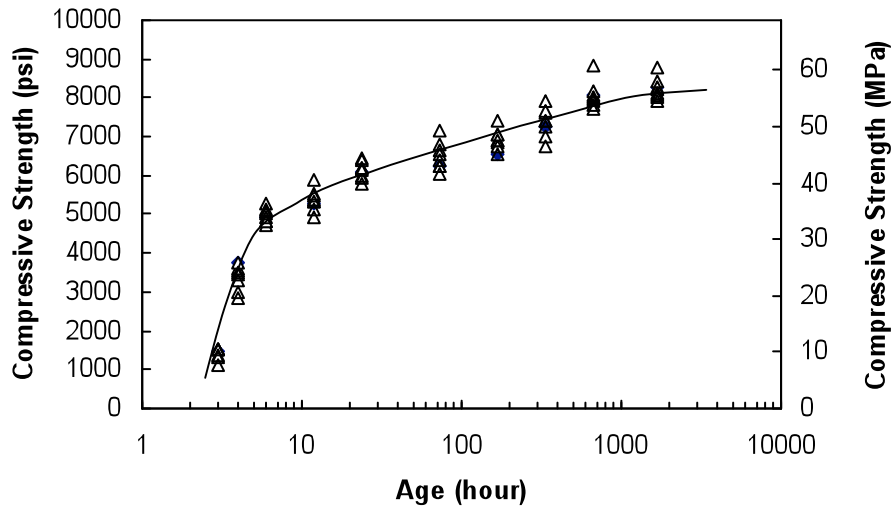


Figure 2.34 – HES-ECC compressive strength development with age.

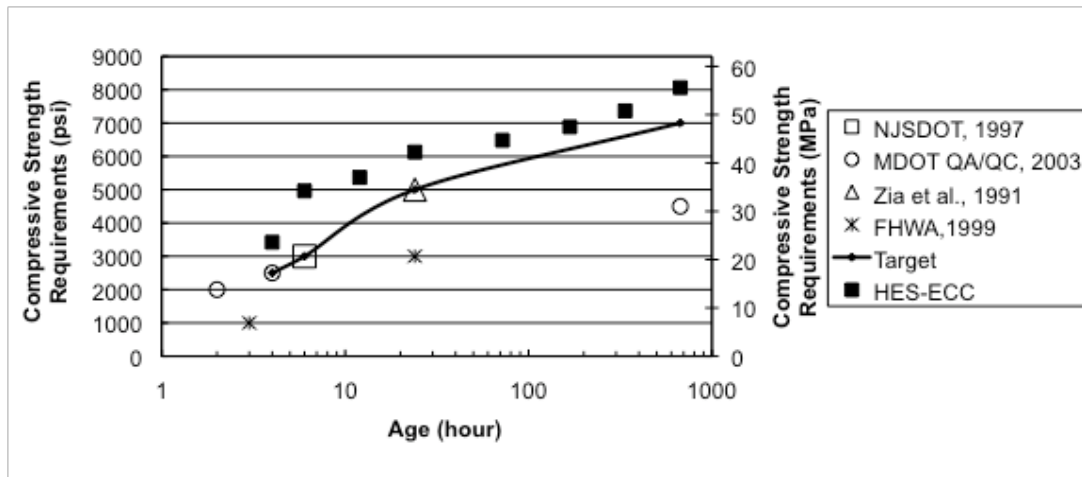


Figure 2.35– Compressive strength (average value) development of HES-ECC compared with requirements by DOTs and FHWA.

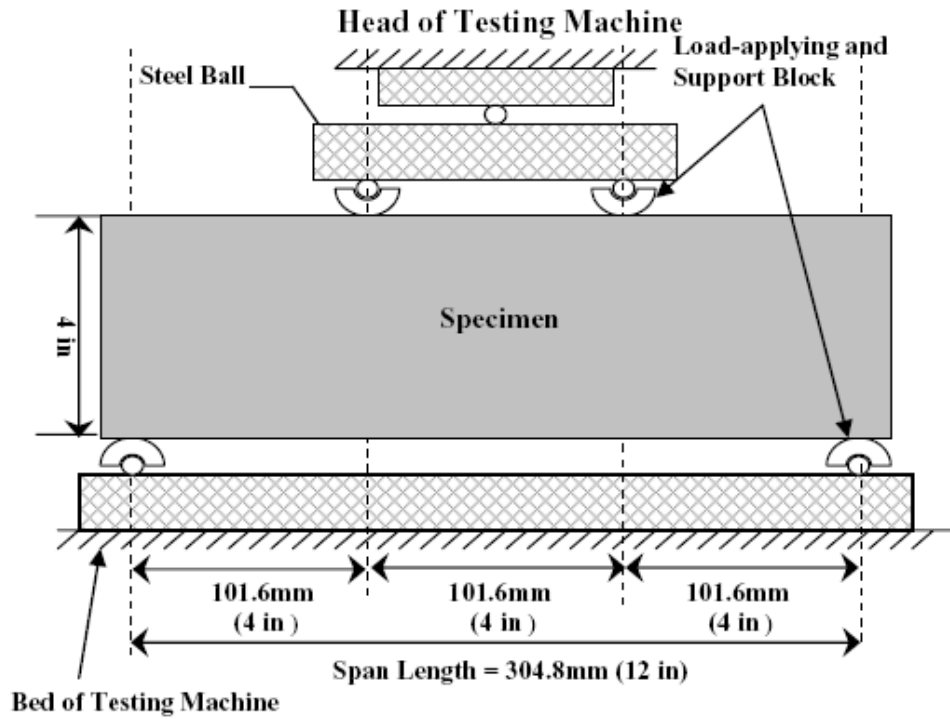


Figure 2.36 – Third-point bending test setup and specimen dimensions.

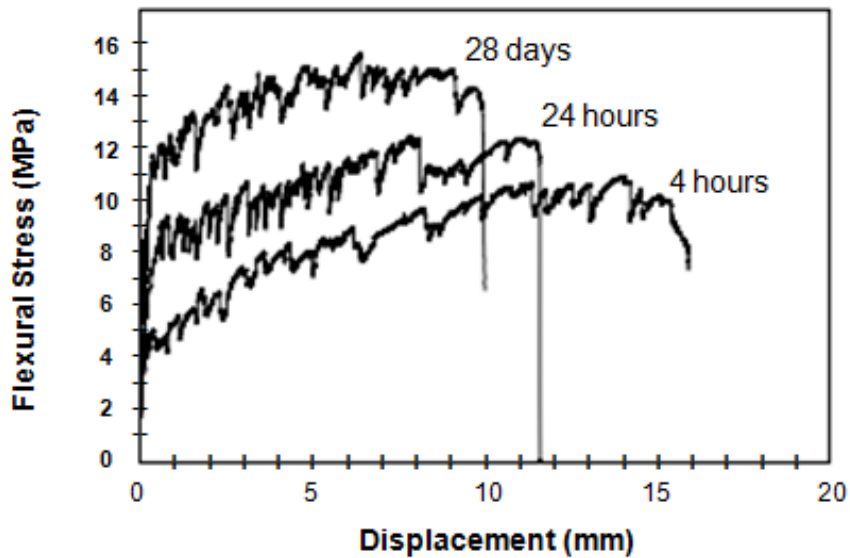


Fig 2.37 – HES-ECC flexural stress – displacement curves at 4 hours, 24 hours, and 28 days.

## References:

- 
- <sup>1</sup> Wang, S., and Li, V. C., “High Early Strength Engineered Cementitious Composites,” *ACI Materials Journal*, Vol. 103, No. 2, 2006, pp. 97-105.
- <sup>2</sup> Naaman, A. E., and Reinhardt, H. W., “Characterization of High Performance Fiber Reinforced Cement Composites HPRCC,” *High Performance Fiber Reinforced Cementitious Composites*, RILEM Proceeding 31, Eds. A. E. Naaman and H. W. Reinhardt, 1996, pp. 1-23.
- <sup>3</sup> Li, V.C., and Wang, S., “On High Performance Fiber Reinforced Cementitious Composites,” *Proc. of the JCI Symposium on Ductile Fiber Reinforced Cementitious Composites (DFRCC)*, Tokyo, Japan, pp. 13-23, 2003.
- <sup>4</sup> Aveston, J., Cooper, G., and Kelly, A., “Single and Multiple Fracture,” *Properties of Fiber Composites*, Guildford, UK, 1971, pp. 15-24.
- <sup>5</sup> Krenchel, H. and Stang, H., “Stable microcracking in cementitious materials,” In *Brittle Matrix Composites 2*. A.M. Brandt and J.H. Marshall, eds., 1989, pp. 20-33.
- <sup>6</sup> Curbach, M. and Jesse, F., “High-Performance Textile-Reinforced Concrete,” *Structural Engineering International*, Vol. 9, No. 4, 1999, pp. 289-291.
- <sup>7</sup> Reinhardt, H.W., Krüger, M. and Große, C.U., “Concrete prestressed with textile fabric,” *Journal of Advanced Concrete Technology*, Vol. 1, No. 3, 2003, pp. 231-239.
- <sup>8</sup> Mobasher, B., Peled, A. and Pahilajani, J., “Distributed cracking and stiffness degradation in fabric-cement composites,” *Materials and Structures*, Vol. 39, No. 3, 2006, pp. 317-331.
- <sup>9</sup> Allen, H.G., “Stiffness and strength of two glass-fiber reinforced cement laminates,” *Journal of Composite Materials*, Vol. 5, No. 2, 1971, pp. 194-207.
- <sup>10</sup> Lankard, D.R., “Preparation, properties and applications of cement based composites containing 5-20 percent steel fiber reinforcement,” *Steel Fiber Concrete*, S.P. Shah, S.P. and A. Skarendahl, eds. Elsevier Publishers, 1986.
- <sup>11</sup> Naaman, A.E., “SIFCON: Tailored properties for structural performance,” *Proceedings of the International Workshop on High Performance Fiber Reinforced Cement Composites*, H.W. Reinhardt and A.E. Naaman, eds., Published by E & FN Spon, London, 1992, pp. 18-38.
- <sup>12</sup> Li, V.C., “From Micromechanics to Structural Engineering – the design of cementitious composites for Civil Engineering applications,” *JSCE J. of Struc. Mechanics and Earthquake Engineering*, Vol. 10, No. 2, 1993, pp. 37-48.

- 
- <sup>13</sup> Li, V. C., and Leung, C. K. Y., "Theory of Steady State and Multiple Cracking of Random Discontinuous Fiber Reinforced Brittle Matrix Composites," *Journal of Engineering Mechanics*, ASCE, Vol. 118, No. 11, 1992, pp. 2246-2264.
- <sup>14</sup> Li, V. C., and Wu, H. C., "Conditions for Pseudo Strain-Hardening in Fiber Reinforced Brittle Matrix Composites," *Journal of Applied Mechanics Review*, Vol. 45, No. 8, August, 1992, pp. 390-398.
- <sup>15</sup> Marshall, D.B., and Cox, B. N., "A J-Integral Method for Calculating Steady-State Matrix Cracking Stresses in Composites," *Mechanics of Materials*, Vol. 7, No. 2, 1988, pp. 127-133.
- <sup>16</sup> Griffith, A. A., "The phenomena of rupture and flow in solids," *Philosophical Transactions of the Royal Society of London*, A 221, 1921, pp. 163-198, <http://www.cmse.ed.ac.uk/AdvMat45/Griffith20.pdf>.
- <sup>17</sup> Wang, Y., Backer, S., and Li, V.C., "A Statistical Tensile Model of Fiber Reinforced Cementitious Composites," *Journal of Composites*, Vol. 20, No. 3, 1990, pp.265-274.
- <sup>18</sup> Aveston, J., Cooper, G. A., and Kelly, A., "Single and Multiple Fracture," *Proceedings of Properties of Fiber Composites*, National Physical Laboratory, IPC Science and Technology Press, Buildford, UK, 1971, pp. 15-24.
- <sup>19</sup> Wu, H. C., and Li, V. C., "Stochastic Process of Multiple Cracking in Discontinuous Random Fiber Reinforced Brittle Matrix Composites," *International Journal of Damage Mechanics*, Vol. 4, No. 1, 1995, pp. 83-102.
- <sup>20</sup> Li, V. C., and Wang, S., "Microstructure Variability and Macroscopic Composite Properties of High Performance Fiber Reinforced Cementitious Composites," *Probabilistic Engineering Mechanics*, Vol. 21, No. 3, 2006, pp. 201-206.
- <sup>21</sup> American Concrete Pavement Association, "How do I obtain "high early strength" concrete?", [http://www.pavement.com/Concrete\\_Pavement/Technical/FATQ/Design/High\\_Early\\_Strength\\_Concrete.asp](http://www.pavement.com/Concrete_Pavement/Technical/FATQ/Design/High_Early_Strength_Concrete.asp).
- <sup>22</sup> Delatte, N. J., *Concrete Pavement Design, Construction, and Performance*, 2007, 372pp.
- <sup>23</sup> Portland Cement Association, [http://www.cement.org/pavements/pv\\_cp\\_airports.asp](http://www.cement.org/pavements/pv_cp_airports.asp), accessed on August 15, 2009.
- <sup>24</sup> Elhindy, E., Chevalier, F. and Khayat, K. H., "Airfield Pavement Repair Using High Early Strength Concrete: Experience of the Aeroports De Montreal," *Concrete for Infrastructure and Utilities* by Ravindra, L, D. and Henderson, N. A., 1996, pp. 601-603.

- 
- <sup>25</sup> Kohn, S. D., Tayabji, S., and Okamoto, P., *Best Practices for Airport Portland Cement Concrete Pavement Construction Rigid Airport Pavement*, American Concrete Pavement Association, Washington, D. C., 2003, 146 pp.
- <sup>26</sup> Seehra, S. S., Gupta, S., and Kumar, S., “Rapid Setting Magnesium Phosphate Cement for Quick Repair of Concrete Pavements – Characterization and Durability Aspects,” *Cement and Concrete Research*, Vol. 23, No. 2, 1993, pp. 254-266.
- <sup>27</sup> Knofel, D., and Wang, J. F., “Properties of Three Newly Developed Quick Cements,” *Cement and Concrete Research*, Vol. 24, No. 5, 1994, pp. 801-812.
- <sup>28</sup> Whiting, D., and Nagi, M., “Strength and Durability of Rapid Highway Repair Concretes,” *Concrete International*, Vol. 16, No. 9, 1994, pp. 36-41.
- <sup>29</sup> Sprinkel, M. M., “Very-Early-Strength Latex-Modified Concrete Overlay,” *Report No. VTRC99-TAR3*, Virginia Department of Transportation, Richmond, Virginia, 1998, 11pp.
- <sup>30</sup> Baraguru, P. D., and Bhatt, D., “Rapid Hardening Concrete,” *Report No. FHWA NJ 2001-3*, New Jersey Department of Transportation, Trenton, New Jersey, 2000, 22pp.
- <sup>31</sup> Parker, F., and Shoemaker, M. L., “PCC Pavement Patching Materials and Procedures,” *ASCE Journal of Materials in Civil Engineering*, Vol. 3, No. 1, 1991, pp. 29-47.
- <sup>32</sup> Kurtz, S., Balaguru, P., Consolazio, G., and Maher, A., “Fast Track Concrete for Construction Repair,” *Report No. FHWA 2001-015*, New Jersey Department of Transportation, Trenton, New Jersey, 1997, p. 67.
- <sup>33</sup> Anderson, J., Daczko, J., and Luciano, J., “Producing and Evaluating Portland Cement-Based Rapid Strength Concrete,” *Concrete International*, Vol. 25, No. 8, 2003, pp. 77-82.
- <sup>34</sup> Bentz, D. P., and Peltz, M. A., “Reducing Thermal and Autogeneous Shrinkage Contributions to Early-Age Cracking,” *ACI Materials Journal*, Vol. 105, No. 4, July-August 2008, pp. 414-420.
- <sup>35</sup> Mehta, P. K., and Burrows, R. W., “Building Durable Structures in the 21<sup>st</sup> Century,” *Concrete International*, Vol. 23, 2001, pp. 57-63.
- <sup>36</sup> Mihashi, H., Nishiyama, N., Kobayashi, T., and Hanada, M., “Development of a Smart Material to Mitigate Thermal Stress in Early Age Concrete,” *Control of Cracking in Early Age Concrete*, Eds. H. Mihashi & F. H. Wittmann, Balkema, Rotterdam, 2002, pp. 385 – 392.
- <sup>37</sup> Wang, K., Jansen, D., Shah, S., and Karr, A., “Permeability Study of Cracked Concrete”, *Cement and Concrete Research*, Vol. 27, No. 3, 1997, pp. 381-393.

- 
- <sup>38</sup> Anderson, J., "Paving Repair Finds a Four-Hour Champion," *Concrete Construction*, Vol. 46, No. 12, 2001, pp. 69-70.
- <sup>39</sup> Kurtz, S., Balaguru, P., Consolazio, G., and Maher, A., "Fast Track Concrete for Construction Repair," *Report No. FHWA 2001-015*, New Jersey Department of Transportation, Trenton, N.J., 1997, p. 67.
- <sup>40</sup> Michigan Department of Transportation (MDOT), "Qualification Procedure For Prepackaged Hydraulic Fast-Set Materials for Patching Structural Concrete," MDOT Quality Assurance and Quality Control (QA/QC), 2003.
- <sup>41</sup> Parker, F., and Shoemaker, M. L., "PCC Pavement Patching Materials and Procedures," *ASCE Journal or Materials in Civil Engineering*, Vol. 3, No.1, 1991, pp. 29-47.
- <sup>42</sup> Zia, P., Leming, M. L., and Ahmad, S. H., "High Performance Concretes, a State-of-the-Art Report," *Report No. SHRP-C/FR-91-103*, Strategic Highway Research Program, National Research Program, Washington, DC, 1991.
- <sup>43</sup> Federal Highway Administration (FHWA), "Manual of Practice: Materials and Procedures for Rapid Repair of Partial-Depth Spalls in Concrete Pavements," Federal Highway Administration (FHWA), 1999, p. 135.
- <sup>44</sup> Neville, A. M., and Brooks, J. J., *Concrete Technology*, Longman Scientific and Technical, 1987.
- <sup>45</sup> Smith, K. L., Peshkin, D.G., Rmeili, E. H., Dam, T. V., Smith, K. D., Darter, M. I., "Innovative materials and Equipment for Pavement Surface Repairs", Strategic Highway Research Program (SHRP), National Highway research Council, Washington D.C., 1991, 205 pp.
- <sup>46</sup> Stingley, W. M., "NCHRP Synthesis of Highway Practice No. 45: Rapid Setting Materials for Patching of Concrete," National Cooperative Highway research Program (NCHRP), Transportation Research Board, Washington D.C., 1977, 13 pp.
- <sup>47</sup> Collepardi, M., "Water Reducers/Retarders", *Concrete Admixtures Handbook*, ed. V. S. Ramachandran, Noyes Publications, Park Ridge, NJ, 1984, pp. 116-210.
- <sup>48</sup> Malhotra, V. M., Berry, E. E., and Wheat, T. A., "Superplasticizers in Concrete", *Proceedings of International Symposium, Ottawa, 1988* (2 vols.), CANMET, Department of Energy, Mines and Resources, Ottawa, Canada, also published in part as ACI SP-62, American Concrete Institute, Detroit, MI, 1989.
- <sup>49</sup> Nmai, C. K., Schlagbaum, T., and Violetta, B., "A History of Mid-Range Water Reducing Admixtures", *Concrete International*, Vol. 20, No.4, 1998, pp. 45-50.

- 
- <sup>50</sup> Ramachandran, V. S., Malhotra, V. M., Jolicoeur, C. and Spriato, N., "Superplasticizer: Properties and Applications in Concrete," Publ. No. MTL-14 (TR), CANMET National Resources Canada, Ottawa, Canada, 1998.
- <sup>51</sup> Edmeades, R. M. and Hewlett, P. C., "Cement Admixtures", *Lea's Chemistry of Cement and Concrete*, (4<sup>th</sup> ed.), ed. P. C. Hewlett, Arnold, London, 1998, pp. 837-902.
- <sup>52</sup> Mindess, S., Young, J. F., and Darwin, D., *Concrete (2nd Ed.)*, 2003.
- <sup>53</sup> ACI Committee 212, "Admixtures for Concrete (ACI 212.3R-91)", *ACI Manual of Concrete Practice, Part I*, American Concrete Institute, Detroit, MI, 2001.
- <sup>54</sup> Ramachandran, V. S., *Calcium Chloride in Concrete Science and Technology*, Applied Science Publishers, London, 1986.
- <sup>55</sup> Rear, K., and Chin, D., "Non-Chloride, Accelerating Admixtures for Early Compressive Strength", *Concrete International*, Vol. 12, No.10, 1990, pp. 55-58.
- <sup>56</sup> Hewlett, P. C., and Young, J. F., "Physico-chemical Interactions between Chemical Admixtures and Portland Cement", *Journal of Materials Education*, Vol. 9, No. 4, 1989, pp. 389-433.
- <sup>57</sup> Ramachandran, V. S., *Concrete Admixtures Handbook*, Noyes Publications, Park Ridge, NJ, 1984.
- <sup>58</sup> Rixom, M. R., and Mailvaganam, N. P., *Chemical Admixtures for Concrete (2nd ed.)*, E & FN Spon, London, 1986.
- <sup>59</sup> Rear, K., and Chin, D., "Non-Chloride, Accelerating Admixtures for Early Compressive Strength", *Concrete International*, Vol. 12, No.10, 1990, pp. 55-58.
- <sup>60</sup> Ramachandran, V. S., *Concrete Admixtures Handbook*, Noyes Publications, Park Ridge, NJ, 1984.
- <sup>61</sup> Rixom, M. R., and Mailvaganam, N. P., *Chemical Admixtures for Concrete (2nd ed.)*, E & FN Spon, London, 1986.
- <sup>62</sup> Shao, Y. and Shah, S. P., "Mechanical Properties of PVA Fiber Reinforced Cement Composites Fabricated by Extrusion Processing," *ACI Material Journal*, Vol. 94, No. 6, 1997, pp. 555-564.
- <sup>63</sup> Kanda, T., and Li, V. C., "Interface Property and Apparent Strength of a High Strength Hydrophilic Fiber in Cement Matrix," *ASCE Journal of Materials in Civil Engineering*, Vol. 10, No. 1, 1998, pp. 5-13.

- 
- <sup>64</sup> Redon C., Li, V. C., Wu, C., Hoshiro, H., Saito, T., and Ogawa, A., "Measuring and Modifying Interface Properties of PVA Fibers in ECC Matrix," *ASCE Journal of Materials in Civil Engineering*, Vol. 13, No. 6, 2001, pp. 399-406.
- <sup>65</sup> Li, V. C., Wu, C., Wang, S., Ogawa, A., and Saito, T., "Interface Tailoring for Strain-hardening PVA-ECC," *ACI Materials Journal*, Vol. 99, No. 5, Sept.-Oct., 2002, pp. 463-472.
- <sup>66</sup> Stang, H., "Scale Effects in FRC and HPRFCC Structural Elements," *High Performance Fiber Reinforced Cementitious Composites*, RILEM Proceedings Pro 30, Eds. Naaman, A.E. and Reinhardt, H.W., 2003, pp. 245-258.
- <sup>67</sup> Kanda, T., Design of Engineered Cementitious Composites for Ductile Seismic Resistant Elements, Ph.D. Dissertation, University of Michigan, 1998, 329 pp.
- <sup>68</sup> Redon, C., Li, V.C., Wu, C., Hoshiro, H., Saito, T., and Ogawa, A., "Measuring and Modifying Interface Properties of PVA Fibers in ECC Matrix," *Journal of Materials in Civil Engineering*, Vol. 13, No. 6, 2001, pp. 399-406.
- <sup>69</sup> Lin, Z., Kanda, T., and Li, V. C., "On Interface Property Characterization and Performance of Fiber Reinforced Cementitious Composites," *Journal of Concrete Science and Engineering, RILEM*, Vol. 1, 1999, pp. 173-184.
- <sup>70</sup> Chan, Y. W., and Li, V. C., "Age Effect on the Characteristics of Fibre/Cement Interfacial Properties," *Journal of Materials Science*, Vol. 32, 1997, pp. 5287-5292.
- <sup>71</sup> Wang, S., "Micromechanics Based Matrix Design for Engineered Cementitious Composites," *Ph.D. Dissertation*, University of Michigan, 2005.
- <sup>72</sup> Vaysburd, A. M., Brown, C. D., Bissonnette, B., and Emmons, P. H., "'Realcrete' Versus 'Labcrete'", *Concrete International*, Vol. 26, No. 2, 2004, pp. 90-94.
- <sup>73</sup> Li, M., and Li, V. C., "Durability of HES-ECC Repair Under Mechanical and Environmental Loading Conditions," *Proc., High Performance Fiber Reinforced Cement Composites*, Eds. H.W. Reinhardt & A.E. Naaman, Mainz, Germany, 2007, pp. 399-408.
- <sup>74</sup> Li, M., and Li, V. C., "Influence of Material Ductility on the Performance of Concrete Repair," submitted to *ACI Structural Journal*, June, 2008.
- <sup>75</sup> Lepech, M., and Li, V. C., "Water Permeability of Cracked Cementitious Composites," *Paper 4539 of Compendium of Papers CD ROM*, ICF 11, Turin, Italy, March 2005.
- <sup>76</sup> Sahmaran, M., Li, M., and Li, V. C., "Transport Properties of Engineered Cementitious Composites Under Chloride Exposure," *ACI Materials Journal*, Vol.104, No. 6, 2007, pp. 604-611.

---

<sup>77</sup> Qian, S., and Li, V. C., “Simplified Inverse Method for Determining the Tensile Strain Capacity of Strain Hardening Cementitious Composites,” *J. Advanced Concrete Technology*, Vol. 5, No. 2, 2007, pp. 235-246.

<sup>78</sup> ASTM C78 - 08 Standard Test Method for Flexural Strength of Concrete (Using Simple Beam with Third-Point Loading).

## **CHAPTER 3**

### **ECC Processing and Quality Control for Optimized Material Properties and Robustness**

The capability of consistently processing and producing robust ECC materials plays a crucial role in its ascendancy as a new construction material in various structural applications. ECC strain-hardening behavior and tensile strain capacity are closely related to fiber dispersion uniformity. Non-uniform fiber dispersion within ECC can result in huge variation in its tensile properties, and even switch ECC from a strain-hardening material to a tension-softening normal fiber reinforced concrete (FRC) material. This can lead to material properties less than originally designed for based on the micromechanical theory described in Chapter 2; this theory assumes uniform fiber dispersion.

This study focuses on the development of a simple and practical quality control method for ECC processing. Through measuring ECC mortar rheological parameters, fiber dispersion, and ECC tensile properties, the correlation between the three was established. The optimal range of Marsh cone flow rate, which is an indicator of plastic

viscosity of ECC mortar, was then identified and used to guide ECC quality control. Based on these experimental findings, it is proposed that ECC material can achieve maximized fiber dispersion and hardened tensile properties, as well as improved robustness, through plastic viscosity control of ECC mortar within this optimal range. With this method, more widespread adoption of ECC material in structural applications as well as laboratory testing can be realized with confidence. A material with more robust properties will also lead to enhanced reliability in structural design, and more complete utilization of the material performance (e.g. by use of a smaller factor of safety).

Within the material engineering phase of the Integrated Material and Structural Engineering framework, the material processing technique developed in this chapter, together with the microstructure tailoring emphasized in Chapter 2, converge to ultimately produce composite materials with desired combinations of properties and robustness.

### **3.1 Introduction**

The laboratory and on-site processing and mixing capacities of ECC play a crucial role in its ascendancy as a construction material for structural applications. The ability to produce robust ECC materials with controlled quality in laboratories and on construction sites using existing equipment is essential for standardized testing of this new material and its successful introduction to the construction industry. Variation in ECC tensile behavior has been observed in laboratory small-scale and on-site large-scale production depending on the type of mixers, mixing procedure, source of local ingredients, and mixing personnel's experience. This variation is reflected in the standard deviation of

measured material tensile strain capacity, ultimate tensile strength, and width and density of microcracks. Figure 3.1 shows an extreme example of such variation in tensile stress-strain curves of one ECC mix produced from different batches using a gravity mixer with capacity of 0.6 m<sup>3</sup> (2 ft.<sup>3</sup>). Although the mixing proportion is identical, the specimens showed tensile strain capacity ranging from 0.6% to 3.4%. Some specimens formed closely spaced “saturated” microcracks during the strain-hardening stage, and therefore had larger tensile strain capacity before the tension-softening stage started. Other specimens reached the tension-softening stage soon after a limited number of microcracks formed, leading to a lower tensile strain capacity. Although this example reveals a somewhat exaggerated variation, it serves to illustrate the need for a simple and effective quality control methodology in ECC processing for consistent and optimized properties.

The variation in ECC tensile ductility is mainly due to the influence of processing details on composite microstructure that governs ECC material properties<sup>1</sup>. Notably, ECC utilizes short, randomly distributed polymer fibers at a moderate volume fraction (2% or less in general). During ECC mixing, fibers are added after the other ingredients, i.e. cementitious and pozzolanic ingredients, water, and admixtures are all mixed and have achieved a consistent mortar state. Based on past experience, it is known that processing details such as mixer type, mixing speed, time and sequence, and mixing personnel’s experience level can influence the rheological properties of ECC mortar (before adding fibers) while in fresh state, which in turn can strongly affect fiber dispersion uniformity, size distribution of entrapped air pores in the cementitious matrix, and bonding properties at the fiber/matrix interface in the hardened state. Using ECC

ingredients from different sources can also lead to a change in ECC rheological properties and composite microstructure.

Research has been conducted on the influence of rheological characteristics on the fiber dispersion in cementitious materials. Ozyurt et al, 2006<sup>2</sup> found that fresh rheological properties affect segregation of steel fibers and mechanical properties of steel fiber reinforced concrete. Standard deviation of the steel fiber contents throughout the specimen decreases when viscosity increases. Chung 2005<sup>3</sup> assessed the degree of dispersion of short microfibers, e.g. carbon and steel fibers, in cement mortar or paste through measuring the volume electrical resistivity, and found that the degree of dispersion is improved by the use of silica fume, acrylic particle dispersion, methylcellulose solution, silane, and use of fiber surface treatment. Yang et al<sup>4</sup> investigated the effects of fly ash type, water-binder ratio, and chemical admixtures on the fresh and hardened properties of ECC by means of design of experiments. Test results indicated that ECC tensile properties correlated well with the viscosity of fresh ECC mortar.

Within this chapter, a simple and effective quality control approach is presented for the production of robust ECC materials with optimized tensile properties and minimized material variation. To achieve this goal, we build on the findings of Yang et al<sup>4</sup>. Specifically, a systematic experimental framework is designed in this study to establish the correlation between ECC mortar rheological properties in fresh state, fiber dispersion in hardened state, and composite tensile properties in hardened state. Based on this correlation, the desired range of ECC mortar rheological properties is identified. Through controlling ECC mortar rheology within this range, it is confirmed that

optimized composite properties can be achieved through more uniform fiber dispersion. Intended applications for this quality control approach are standardized laboratory production of ECC for research purposes, as well as ECC factory precast, truck mixing, and on-site processing for various construction projects.

### **3.2 Effect of Processing on ECC Micromechanical Parameters**

As discussed in Chapter 2, tensile strain-hardening behavior of ECC is realized by tailoring the synergistic interaction between fiber, matrix, and fiber/matrix interface based on micromechanics theory. As a fiber-reinforced brittle mortar matrix composite, ECC's pseudo strain-hardening behavior is achieved through sequential formation of matrix multiple cracking. The fundamental requirement for matrix multiple cracking is that steady-state flat crack propagation prevails under tension, which was first characterized by Marshall and Cox<sup>5</sup> for continuous aligned fiber-reinforced ceramics, and extended to discontinuous fiber-reinforced cementitious composites by Li and Leung<sup>6</sup>. To ensure steady-state cracking, the crack tip toughness  $J_{tip}$  must be less than the complementary energy  $J_b'$  calculated from the fiber bridging stress  $\sigma$  versus crack opening  $\delta$  curve, as illustrated in Figure 3.2. This energy-based criterion determines whether the crack propagation mode is steady-state flat crack or Griffith crack<sup>7</sup>, as illustrated in Figure 2.4.

The fiber bridging stress versus crack opening relationship  $\sigma(\delta)$ , which can be viewed as the constitutive law of fiber bridging behavior, is analytically derived based on fracture mechanics, micromechanics, and probabilistics tools. In particular, the energetics of tunnel crack propagation along fiber/matrix is used to model the debonding

process of a single PVA fiber from the surrounding cementitious matrix. After debonding is completed, the fiber pullout stage begins, and is modeled as slip-hardening behavior assuming a non-linear frictional stress increase with slip distance. By these means, the full debonding-pullout process of a single fiber with given embedment length is quantified as the fiber bridging force vs. fiber displacement relation<sup>6</sup>. Probabilistics is then introduced to describe the randomness of fiber location and orientation with respect to a crack plane, with the assumption of uniform random fiber distribution<sup>8</sup>. The random orientation of the fibers also necessitates the accounting of the mechanics of interaction between an inclined fiber and the matrix crack. In addition, snubbing coefficient  $f$  and strength reduction factor  $f'$  are introduced to account for the interaction between fiber and matrix as well as the reduction of fiber strength when pulled at an inclined angle. As a result, the  $\sigma(\delta)$  curve is expressible as a function of micromechanics parameters, including fiber volume content  $V_f$ , fiber diameter  $d_f$ , fiber length  $L_f$ , fiber Young's modulus  $E_f$ , matrix Young's modulus  $E_m$ , interface chemical bond  $G_d$ , interface frictional bond  $\tau_0$ , and slip-hardening coefficient  $\beta$ , as well as  $f$  and  $f'$ .

Apart from the energy criterion (1), another condition for pseudo strain-hardening is that the matrix tensile cracking strength  $\sigma_c$  must not exceed the maximum fiber bridging strength  $\sigma_0$ .

For ECC materials with pseudo strain-hardening behavior, high tensile strain capacity results from saturated formation of multiple microcracks. Material tensile strength increases as the number of microcracks increases. While the steady-state cracking criteria ensure the occurrence of multiple-cracking, it is not directly related to the intensity of multiple cracking. Once the steady-state cracking criteria is satisfied, the

number of microcracks that can be developed before reaching the maximum bridging stress  $\sigma_0$  is determined by (i) the maximum fiber bridging stress  $\sigma_0$ , and (ii) the matrix properties, in particular the pre-existing flaw size distribution, and the matrix fracture toughness. Considering that ECC is a non-homogenous brittle-matrix composite, first-cracking strength is determined by the largest flaw size in the section where the first microcrack is initiated. Its ultimate tensile strength is determined by the "weakest" section, where the fiber bridging capacity (maximum bridging stress  $\sigma_0$ ) is the lowest among all sections subjected to the same level of stress. Therefore, the maximum fiber bridging stress  $\sigma_0$  at the "weakest" section imposes a lower bound of critical flaw size  $c_{mc}$  so that only those flaws larger than  $c_{mc}$  can be activated and contribute to multiple cracking. There also exists a minimum crack spacing controlled by interface properties, which imposes an upper bound for the density of multiple cracking.

Rheologic characteristics of fresh ECC during processing affect fiber dispersion, which influences the possibility and density of multiple-cracking. During ECC material design through microstructure tailoring, determination of the fiber bridging stress versus crack opening relationship  $\sigma(\delta)$  from single fiber pullout test results is based on the assumption of uniform random fiber distribution, which can hardly be ensured in actual processing. The uniformity of fiber dispersion in reality determines the maximum bridging stress  $\sigma_0$ , the shape of the  $\sigma(\delta)$  curve at the "weakest" section, and the critical flaw size  $c_{mc}$ , as illustrated in Figure 3.2. Non-uniform fiber dispersion leads to a reduction of the value of  $\sigma_0$  at the "weakest" section, which increases the critical flaw size  $c_{mc}$ . Therefore, less pre-existing flaws with sizes larger than  $c_{mc}$  can be triggered and contribute to multiple cracking, resulting in a relatively lower tensile strain capacity.

Non-uniform fiber dispersion also shifts the  $\sigma(\delta)$  curve downwards, and may reduce complementary energy  $J_b'$  to less than  $J_{tip}$ . In this case, the steady-state criteria are violated and tension-softening behavior results. Therefore, ECC loses its ductile behavior and becomes a regular FRC material. Ideally, processing of ECC should optimize fiber dispersion to achieve a uniform random distribution state, therefore minimizing the probability of creating “weak” sections with lower fiber content. By these means, the largest possible tensile strain capacity can be achieved through maximizing multiple cracking behavior.

In the following experimental study, the correlation between fiber dispersion uniformity and tensile strain capacity, as described above, is validated. The optimal range of ECC fresh properties that correspond to the largest fiber dispersion coefficient and tensile strain capacity are determined.

### **3.3 Experimental Program**

The experimental program contains four sets of investigations. First, fresh viscosity and flowability of seven ECC mortar mixes were measured using the Marsh cone flow test and mini slump test. Second, ECC tensile specimens made from the seven mixes were tested under uniaxial tensile load to measure their tensile stress-strain curves and tensile strain capacity. Third, fiber dispersion at the “weakest” section was measured using fluorescence imaging technology. Based on data from the three tests, the relationships between ECC fresh properties, tensile strain capacity, and fiber dispersion were established, and the optimal range of fresh properties was identified. Finally, to prove the effectiveness of this method, several versions of ECC were processed by

optimally controlling rheology to achieve improved and robust hardened material properties. The experimental program is shown in Figure 3.3.

### 3.3.1 Materials

Seven mixtures with the same mix proportion but increased viscosity were produced. The mix proportion was determined according to ECC micromechanics-based design theory described above for strain-hardening behavior. Increased viscosity of the seven mixtures was achieved by adding a Viscosity Modifying Agent (VMA), V-MAR®, with increased dosage of 0, 0.01%, 0.015%, 0.02%, 0.025%, 0.03% and 0.04% of cement weight. V-MAR® 3 is a high efficiency, milky white liquid admixture designed by W. R. Grace, which enables production of Self Consolidating Concrete by modifying the rheology of concrete<sup>9</sup>. It works by increasing the viscosity of the concrete while still allowing the concrete to flow without segregation. V-MAR® 3 is recommended for use in conjunction with ADVA® Cast 530, which is the common superplasticizer incorporated into different versions of ECC materials, to achieve self-consolidating properties.

The material mix proportions of the seven mixes are shown in Table 3.1. The cement is Ordinary Portland Cement (OPC) type I from Holcim Inc., USA, with Blaine Surface Area of 3300 cm<sup>2</sup>/g (2.320×10<sup>5</sup> in<sup>2</sup>/lb). The fly ash is ASTM standard type F fly ash with mean grain size of 10-20 μm (3.937×10<sup>-4</sup>-7.874×10<sup>-4</sup> in.) from Boral Material Tech. Inc., USA. F-110 fine silica sand from US silica, with 250 μm (9.843×10<sup>-3</sup> in.) maximum grain size and 110 μm (4.331×10<sup>-3</sup> in.) mean grain size, was used as fine aggregate. The superplasticizer is a polycarboxylate-based high range water reducer

(ADVA® Cast 530) from W.R. Grace & Co. Polyvinyl Alcohol (PVA) fiber REC-15 from Kuraray Co., Ltd., Japan, is used at a volume fraction of 2% in this study. This particular volume fraction and other fiber properties were determined by the ECC micromechanical model to satisfy strain-hardening criteria. The PVA fibers are 8 mm ( $3.150 \times 10^{-1}$  in.) long and 39  $\mu\text{m}$  ( $3.150 \times 10^{-4}$  in.) in diameter, with nominal tensile strength of 1600 MPa (232 ksi) and density of 1300  $\text{kg/m}^3$  (81.156  $\text{lb/ft}^3$ ). The fiber is surface-coated with oil (1.2% by weight) to reduce the interfacial bond with the surrounding cementitious matrix.

### **3.3.2 Mixing, Testing of Fresh Properties, and Casting**

In this study, all mixtures were prepared using the same 12 L (3.170 gallon) capacity Hobart mixer, and followed the same mixing sequence, speed, and time under controlled room temperature  $20 \pm 1$  °C (66-70 °F) and relative humidity conditions  $50 \pm 5$  % RH. By these means, the isolated effect of plastic viscosity could be investigated. Solid ingredients, including cement, fly ash, and silica sand, were first mixed at 100 rpm for one minute. Water and chemical admixtures, including superplasticizer and VMA, were then added into the dry mixture and mixed at 150 rpm for three minutes to produce a consistent and uniform ECC mortar (w/o PVA fiber). The fresh mortar was then measured for its workability and rheological parameters.

Mortar is generally assumed to be a non-Newtonian fluid, and the Bingham model is often used to describe its rheology<sup>10</sup>. According to this model, fresh mortar must overcome a yield stress before it can flow. Once the mortar starts to flow, shear stress increases linearly with an increase in strain rate, the slope of which defines the plastic

viscosity. The “plastic viscosity” measures how easily the material can flow, once the yield stress is overcome. The “deformability” measures the ultimate extent to which the material can flow. In this study, plastic viscosity of the seven mortars was measured using a rotational viscometer as a direct method, and Marsh cone flow time as an indirect method. While the direct method is more complicated and requires computer software to analyze data, the indirect method is simpler and the device is portable to mixing sites. The objective was to validate that the Marsh cone flow time correlates well with the plastic viscosity of ECC mortar measured using the rotational viscometer, so that the Marsh cone flow rate test can be adopted as a practical and reliable method for quality control during ECC processing on-site. The deformability of ECC mortar was measured using mini-slump flow test.

Fresh rheology test equipment is shown in Figure 3.4. A Viskomat-NT rotational viscometer<sup>11</sup> (Figure 3.4 (a)) was used to measure the plastic viscosity and yield stress of seven ECC mortars at a controlled temperature of  $20 \pm 1$  °C (66-70 °F). The material was stirred at a rotation rate  $N$ , generating shear resistance of torque  $T$ . A series of data points of  $T$  and  $N$  were recorded by a computer. Through linear regression, the relative yield stress  $g$  (N-mm) and relative plastic viscosity  $h$  (N-mm/rpm) can be determined<sup>12, 13</sup> by:

$$T = g + Nh \quad (3.1)$$

Relative plastic viscosity (N-mm/rpm) can be converted to plastic viscosity (Pa.s) using a calibration liquid<sup>14</sup>.

A Marsh cone (Figure 3.4 (b)), also called a “Marsh funnel” or “Marsh funnel viscometer”, is a simple device for measuring viscosity according to the time it takes a known volume of liquid to flow from the bottom of the cone through a short tube<sup>15,16</sup>. It is

often used in the concrete and oil industry to check the quality of cement grout mixtures or drilling mud. In this test, a funnel was filled completely with ECC mortar and then the bottom outlet was opened, allowing the mortar to start flowing. The Marsh cone flow time of mortar was determined as the elapsed time (t) in seconds between the opening of the bottom outlet until light first became visible at the bottom, when observed from the top.

The mini-slump test measures the consistency of mortar, and its results are correlated with the yield stress<sup>17</sup>. As shown in Figure. 3.4 (c), the mini-slump cone has a top diameter of 70 mm (2.76 in.), a bottom diameter of 100 mm (3.94 in.), and a height of 60 mm (2.36 in.). The cone was placed in the center of a square piece of glass and filled with ECC mortar. The cone was then lifted up to allow the mortar to flow. Once the flowing stopped, the spread of the mortar was recorded as the average of the diameters measured along two diagonals.

After these tests of the fresh properties of ECC mortar, another batch of the same mix was made following the same procedure, with the exception that fibers were added to the ECC mortar and mixed at 150 rpm for three more minutes. The mixtures were then cast into tensile plate molds, covered with plastic sheets, and demolded after 24 hours. The specimens were then moisture-cured in plastic bags at  $95\pm 5$  % RH and  $20\pm 1$  °C (66-70 °F) for 7 days, and air cured at  $50\pm 5$  % RH and  $20\pm 1$  °C (66-70 °F) for 21 days until the age of 28 days for testing. Five specimens were prepared for each mixture.

### **3.3.3 Testing of Hardened Tensile Properties**

At the age of 28 days, five specimens from each mixture were subjected to uniaxial tensile test. The direct uniaxial tensile test is considered the most convincing

method to evaluate material strain-hardening behavior<sup>18</sup>. Fig. 7 illustrates the test setup and specimen dimensions. The plate specimens were 228.6 mm (9 in.) in length, 76.2 mm (3 in.) in width and 12.7 mm (0.5 in.) in thickness. Before testing, four aluminum plates were glued to both ends of the plate specimen to facilitate gripping. Tests were conducted using an MTS machine with a 25 kN ( $5.620 \times 10^3$  lbf) capacity under a displacement control of rate of 0.0025 mm/s ( $9.843 \times 10^{-5}$  in./s) to simulate a quasi-static loading condition. Two external LVDTs (Linear Variable Displacement Transducers) were attached to the specimen surface with a gage length of 101.6 mm (4 in.) to measure the displacement. The tensile stress-strain curve of each specimen was recorded.

#### **3.3.4 Measurement of Fiber Dispersion Coefficient**

After the uniaxial tensile test, a 5 mm–thick small sample was cut from each tensile specimen at the final failure section, as shown in Figure 3.5. This failure section is considered as the “weakest section” where  $\sigma_0$  is the lowest (among all the multiple microcracks present at failure) for the specimen. Fluorescence imaging technique was used to quantify the fiber distribution at this section. It is known that many materials show fluorescence when irradiated with light<sup>19,20</sup>. Compared to the optical microscopic method and the X-ray method, fluorescence technology has a very high level of sensitivity to detect organic fibers from the surrounding cementitious matrix due to a low background signal<sup>21,22</sup>.

Figure 3.6 illustrates the fluorescence imaging technology, and Figure 3.7 shows the testing devices and setup. Without polishing, each of the forty-two samples from seven mixtures were observed through a fluorescence microscope (TE300 Nikon). The

light source of the fluorescence microscope was the mercury lamp, which generated light with a broad range of wavelengths. The sample was illuminated with light at a specific wavelength, which was absorbed by the fluorophores, causing them to emit longer wavelengths of light as the result of well-established physical phenomena described as fluorescence or phosphorescence. The emission of light through the fluorescence process is nearly simultaneous with the absorption of the excitation light due to less than a microsecond delay between photon absorption and emission<sup>23</sup>. The illumination light was separated from the much weaker emitted fluorescence through the use of a UV filter. Through this process, under the fluorescence microscope the fibers appeared brightly colored while the surrounding cementitious matrix appeared dark grey. The fluorescence image was then captured by a CCD camera (Hamamatsu 1394 ORCA-ER).

The whole cross sectional 76.2 mm × 12.7 mm (3 in. × 0.5 in.) image of each sample, with 23005 × 4186 pixels, was constructed by connecting 105 (21 × 5) images with image processing software.

### **3.4 Experimental Results and Discussion**

The Marsh cone flow time of the seven ECC mortar mixtures is shown in Figure 3.8. Through adding an increased dosage of VMA, ECC mortar mixtures with the same material composition but a broad range of plastic viscosity were achieved. From ECC\_0 (0% VMA content) to ECC\_0.04% (0.04% VMA content), the Marsh cone flow time increased from 9 seconds to 40 seconds due to increased plastic viscosity. The same trend was observed for the plastic viscosity measured using the rotational viscometer. A strong correlation ( $R = 0.95$ ) was found in this study between the Marsh cone flow time

and plastic viscosity, showing that the Marsh cone flow test should be a reliable indirect method for onsite or laboratory viscosity measurement.

The mini-slump flow diameters of these seven mixes before and after adding fibers are shown in Figure 3.9. For the same mix, adding 2% fibers reduced the mini-slump flow diameter. Increasing VMA content seems to have a very slightly or no effect on the mini-slump diameter, except for ECC\_0 that showed little change before and after adding fibers. These test results indicate that including VMA can adjust the plastic viscosity of ECC mortar without sacrificing ECC flowability, as indicated by the non-changing mini-slump flow diameter.

Figure 3.10 shows the tensile stress-strain curves of the seven ECC mixtures from the uniaxial tensile test. For ECC\_0, only one specimen shows slight strain-hardening behavior with 0.44% tensile strain capacity, while the other specimens show tension-softening behavior. Large variation exists not only in material tensile strain capacity, but also in the ultimate tensile strength. For ECC\_0.01%, although all of the specimens show tensile strain-hardening behavior, their tensile strain capacity is relatively low (0.32% – 1.19%). Large variation in tensile strain capacity and ultimate tensile strength was also found in ECC\_0.015%. While some specimens had improved tensile strain capacity up to 1.97%, others had tensile strain capacity lower than 1%. ECC\_0.02% exhibited more consistent tensile behavior as well as greatly improved tensile strain capacity, with an average value of 3.1%. Specimens from ECC\_0.025%, ECC\_0.03%, and ECC\_0.04% also all have tensile strain capacity around 3%, and greatly improved consistency in tensile test data.

Figure 3.11 plots the mean value and standard error (as described by the error bar)

of tensile strain capacity versus VMA/cement ratio. The trend contains two parts: (i) From VMA/cement ratio of 0 to 0.02%, tensile strain capacity increases while the standard error decreases. Note that the tensile strain capacity standard error of ECC\_0 is lower than ECC 0.01% because of its lower mean value (standard error is an absolute value); (ii) From VMA/cement ratio of 0.02% to 0.04%, there is no significant increase in tensile strain capacity and a decrease in the standard error.

Figure 3.12 shows the mean value and standard error (as described by the error bar) of tensile strength versus VMA/cement ratio. Again the trend contains two parts: (i) From VMA/cement ratio of 0 to 0.02%, tensile strength increases while the standard error decreases; (ii) From a VMA/cement ratio of 0.025% to 0.04%, tensile strength decreases while the standard error remains low. Microscopy of the failure section revealed that bigger air pores were entrapped during processing in ECC\_0.04% compared with other mixes due to a larger plastic viscosity. This effect, combined with less area of net cross section available for fiber bridging, resulted in the lowered first-cracking strength and ultimate tensile strength of ECC\_0.04%. Future research is needed for detailed study of the effect of plastic viscosity on ECC pore structure and tensile behavior.

Figures 3.11 and 3.12 together suggest an optimal VMA/Cement Ratio of 0.02% for maximizing the composite tensile strain capacity without reducing the tensile strength.

Figure 3.13 shows the assembled fluorescence image of the whole cross section of a sample specimen. Image processing software was used to increase the contrast of the image to better reveal the fibers. This whole image was then divided into  $6 \times 26$  unit areas. The number of fibers in each unit area was counted. The fiber dispersion uniformity of the whole cross section was quantified by a fiber dispersion coefficient,

which expresses the deviation of the number of fibers in a unit area from the average number of fibers. The fiber dispersion coefficient  $\alpha$  is calculated using Equations 3.2 and 3.3<sup>24</sup>:

$$\Psi(x) = \sqrt{\frac{\sum(x_i - \bar{x})^2}{n}} / \bar{x} \quad (3.2)$$

$$\alpha = \exp[-\psi(x)] \quad (3.3)$$

where  $\psi(x)$  is the coefficient of variation,  $x_i$  is the number of fibers in the unit area  $i$ ,  $\bar{x}$  is the average number of fibers in each unit area, and  $n$  is the number of unit area.  $\alpha$  equals to 1 when the fiber dispersion is uniform, and approaches 0 when the coefficient of variation of fiber dispersion becomes larger.

Table 3.2 summarizes the Marsh cone flow rate of fresh ECC mortar before adding fibers, fiber dispersion, and hardened tensile strain capacity of ECC after adding fibers. The relationships between the three parameters is illustrated in Figure 3.14. A strong positive correlation is found between the fiber dispersion coefficient and composite tensile strain capacity (Figure 3.14 (a)). This observation validates the concept discussed earlier that when the fibers are more-uniformly distributed in an ECC specimen, the fiber bridging capacity  $\sigma_0$  at the “weakest” section is larger, leading to a smaller critical flaw size  $c_{cm}$ . Therefore, more pre-existing flaws with size larger than  $c_{cm}$  can be activated to form microcracks before the fiber bridging capacity at the “weakest” section is exhausted, resulting in a larger tensile strain capacity.

Figure 3.14 (b) also shows that the fiber dispersion coefficient increases with Marsh cone flow time in ECC mortar. This increasing trend reaches a plateau after the Marsh cone flow time reaches 24 s. At the Marsh cone flow time of 39 s, a reduction in

the first cracking strength and ultimate tensile strength was found despite a high value for the fiber dispersion coefficient. This means that there exists an “optimal” range of Marsh cone flow time between 24 s and 33 s for desired good fiber distribution, but without the attendant larger air voids as discussed earlier. This Marsh cone flow time vs. fiber dispersion coefficient relation can be used as a guideline for quality control during ECC processing to achieve close-to-uniform fiber dispersion. It should be noted that mortar from different versions of ECC can have different plastic viscosities at fresh state due to variation in ingredients and composition. In this study, variation in VMA dosage was used to achieve various plastic viscosities for the same ECC mix (Figure 3.8). For this particular mix, an optimal dosage of 0.02-0.03% is suggested by this study. However, this optimal dosage value may not apply to other ECC mixes, which have different original viscosities (before viscosity control) due to different ingredients and composition. The optimal range of viscosity is the most important factor in achieving uniform fiber dispersion, which should not depend on the difference in mixes. In this sense, addition of various dosages of VMA, together with other potential viscosity control methods (e.g. modifying ingredient particle size distribution, adjusting water/cement ratio, using superplasticizer), are only tools to achieve the objective of controlling viscosity within the identified optimal range.

Figure 3.14 (c) shows the effect of ECC mortar Marsh cone flow rate on tensile strain capacity. Due to the strong positive correlation between tensile strain capacity and the fiber dispersion coefficient, the effect of Marsh cone flow time on tensile strain capacity is similar to its effect on the fiber dispersion coefficient. Tensile strain capacity increases with Marsh cone flow time, and reaches a plateau at 24 s. This trend indicates

that by controlling ECC mortar plastic viscosity so that its Marsh cone flow time falls into the range between 24 s and 33 s before adding fibers, the hardened ECC material can achieve maximum tensile strain capacity as originally designed, based on micromechanics tools which assume fiber dispersion uniformity.

### **3.5 Rheology Control Concept and Case Study**

Once the correlations between ECC mortar Marsh cone flow rate, fiber dispersion, and ECC tensile strain capacity were established, Figure 3.14 (b) became available as a guideline to control the plastic viscosity of ECC mortar before adding fibers so that maximized fiber dispersion and tensile strain capacity can be achieved. Plastic viscosity is indirectly quantified as the Marsh cone flow time (in seconds) in this figure, and the fiber dispersion coefficient is strongly correlated with tensile strain capacity. While the rheology control methodology was demonstrated using an ECC of the composition given in Table 3.1, the methodology itself is general and can be applied to other ECC compositions. This concept is illustrated with a case study of a newly developed pigmentable ECC for architectural applications, as described below.

WHITE ECC has the mix proportions shown in Table 3.3. This material was developed based on ECC strain-hardening theory, but was different from the ECC used to establish the rheology control methodology in terms of mix proportion and cement type. WHITE ECC contains type I white cement from Lehigh Cement Company instead of type I ordinary Portland cement. Also, fly ash was deliberately removed in its mix design. No VMA was used in this initial mix design. Using white cement and eliminating fly ash both reduce plastic viscosity of the mortar of WHITE ECC, making it challenging to

achieve robust composite properties due to the observed tendency of fiber clumping during mixing. As shown in Figure 3.15(a), tests on three specimens of WHITE ECC without rheology control showed large variation in tensile properties, with tensile strain capacity ranging from 1.1% to 2.7%.

To conduct rheology control on WHITE ECC, the Marsh cone flow rate test was performed on WHITE ECC mortar. Without any VMA, the Marsh cone flow rate for this mix was experimentally determined to be 12 s, corresponding to a fiber dispersion coefficient around 0.53 based on Figure 3.14 (b). This indicates that the fiber dispersion in this material was relatively poor. By adding VMA at a dosage of 0.05% cement content, the Marsh cone flow rate of WHITE ECC mortar was increased to 28 s, corresponding to a fiber dispersion coefficient of around 0.8 (Figure 3.14 (b)). As shown in Figure 3.15(b), this method greatly improved the average tensile strain capacity of WHITE-ECC from 2% to 3%, and reduced the variation in tensile properties. Adding more VMA, at a dosage of 0.1% of cement content, brought the Marsh cone flow rate up to 38 s, which was close to the upper bound of the optimal range of Marsh cone flow time. Tensile test results (Figure 3.15(c)) again showed greatly improved average tensile strain capacity as well as reduced variation. However, the first cracking strength and ultimate tensile strength were slightly reduced due to the higher value of plastic viscosity and likely entrapment of air. For this WHITE ECC mix, therefore, the optimal amount of VMA is 0.05% of cement content. This is more than twice the optimal amount recommended for the ECC mix discussed earlier (Table 3.1 ECC\_0), due to the substantially lower plastic viscosity of the WHITE-ECC mortar mix.

This case study verified the effectiveness of the rheology control methodology.

This methodology can be used for quality control of any fresh ECC mortar before adding fibers in order to achieve maximum fiber dispersion uniformity and composite tensile strain capacity. The findings above reiterate the fact that the optimal amount of VMA varies for different ECC mix compositions. However, the optimal plastic viscosity (or Marsh cone flow rate) is a universal parameter.

### **3.6 Conclusions**

Within this work, a simple and practical quality control method for ECC processing was developed. Seven ECC mixes with the same mix proportions but with viscosities varied by viscosity agent content were experimentally investigated to determine rheological properties, hardened tensile properties, and fiber dispersion at the final failure section. The following conclusions can be drawn:

A strong correlation, with  $R = 0.95$ , was found between the Marsh cone flow time and plastic viscosity measured using a Viskomat-NT rotational viscometer, showing that the simple Marsh cone flow test should serve as a reliable indirect method for onsite or laboratory viscosity measurement.

Through measurements of the ECC mortar plastic viscosity and Marsh cone flow rate, and ECC mini-slump flow diameter, it was found that incorporation of VMA can be an effective method to control plastic viscosity of ECC mortar without sacrificing ECC flowability after adding fibers.

Fluorescence imaging technique is a useful tool for quantifying the distribution of short discontinuous PVA fibers within a cementitious matrix. Fiber dispersion coefficient for the seven mixes was found to range from 0.29 to 0.89. This quantifies the

effectiveness of adding VMA as a rheology control method for achieving more uniform fiber dispersion in hardened ECC. This is the first time that fiber dispersion has been directly and quantitatively correlated with deliberate viscosity control for optimal composite tensile capacity performance.

Fiber uniformity as measured by the fiber dispersion coefficient was found to have a strong effect on ECC tensile strain capacity. A lower fiber dispersion coefficient not only reduces ECC tensile strain capacity and ultimate tensile strength, but also increases the variation in both properties. A very low value for the fiber dispersion coefficient can switch ECC from a strain-hardening material to a tension-softening material.

ECC mortar plastic viscosity is established experimentally as a fundamental rheological parameter that affects dispersion of PVA fibers in ECC mixes. An ECC mortar with low plastic viscosity and Marsh cone flow time tends to have poorly distributed fibers. Increasing plastic viscosity of ECC mortar improves fiber dispersion, and the improvement reaches a plateau once the Marsh cone flow time reaches 24 s. Further increasing viscosity can potentially lead to a reduction in ECC first cracking strength and ultimate tensile strength due to more larger-size entrapped air pores. Therefore, an optimal range of plastic viscosity (and corresponding optimal Marsh cone flow time) was revealed, which can be used to guide ECC rheology control during processing before fibers are added.

For ECC to achieve robust tensile strain-hardening behavior with designed tensile ductility, micromechanical material design should be combined with controlled material processing – neither of the two should be ignored. This is because material processing

strongly affects the composite microstructure, which in turn determines whether the strain-hardening criteria are satisfied in the produced material as originally designed. This concept was verified by the experimentally established relationship between ECC mortar Marsh cone flow rate and ECC composite tensile properties, accompanied by rheology control as demonstrated in this study.

Through the establishment of correlation between Marsh cone flow rate of ECC mortar, fiber dispersion at the “weakest” section, and ECC tensile strain capacity, the optimal range of Marsh cone flow time was identified. The present study results in a practical methodology to control the quality of ECC during laboratory or onsite large-scale processing for maximized material tensile properties and robustness, by simple use of a portable Marsh cone and adjustment of VMA content to result in a flow time between 24 s and 33 s. The effectiveness of this method was further confirmed using a special version of WHITE-ECC.

Table 3.1 – Mix proportion of materials.

Mix #	Cement	Silica Sand	Fly Ash	Water	Fiber, (V <sub>f</sub> )	Superplasticizer	VMA (%)
ECC_x	1.0	0.8	1.2	0.66	2.0%	0.013%	x

\* Content of PVA fibers is expressed as volume proportion of the mix, while all the other ingredients are expressed as weight proportion of cement content. Seven mixes were investigated, with x = 0, 0.01, 0.015, 0.02, 0.025, 0.03 and 0.04.

Table 3.2 – Material fresh and hardened properties.

ECC_0	Marsh Cone Flow Time (s)	9				
	Fiber Dispersion Coefficient	0.5	0.42	0.38	0.39	0.29
	Tensile Strain Capacity (%)	0.44	0.06	0.13	0.09	0.03
ECC_0.01%	Marsh Cone Flow Time (s)	12				
	Fiber Dispersion Coefficient	0.49	0.52	0.57	0.53	0.54
	Tensile Strain Capacity (%)	0.34	0.32	1.19	0.69	0.52
ECC_0.015%	Marsh Cone Flow Time (s)	17				
	Fiber Dispersion Coefficient	0.66	0.55	0.6	0.58	0.65
	Tensile Strain Capacity (%)	1.97	0.76	0.85	0.75	1.38
ECC_0.02%	Marsh Cone Flow Time (s)	24				
	Fiber Dispersion Coefficient	0.84	0.77	0.74	0.73	0.83
	Tensile Strain Capacity (%)	3.5	3.1	2.87	3.2	3.0
ECC_0.025%	Marsh Cone Flow Time (s)	30				
	Fiber Dispersion Coefficient	0.89	0.81	0.75	0.83	0.72
	Tensile Strain Capacity (%)	3.35	3.27	2.94	3.01	2.68
ECC_0.03%	Marsh Cone Flow Time (s)	33				
	Fiber Dispersion Coefficient	0.84	0.75	0.7	0.8	0.67
	Tensile Strain Capacity (%)	3.25	3.18	2.82	3.12	2.71
ECC_0.04%	Marsh Cone Flow Time (s)	39				
	Fiber Dispersion Coefficient	0.88	0.79	0.82	0.80	0.77
	Tensile Strain Capacity (%)	3.33	3.27	3.30	2.83	3.23

Table 3.3 – Mix proportion of WHITE ECC.

Material	Cement	Sand	Water	Superplasticizer	PVA Fiber, (V <sub>f</sub> )
WHITE ECC	1	0.5	0.31	0.003	2.0%

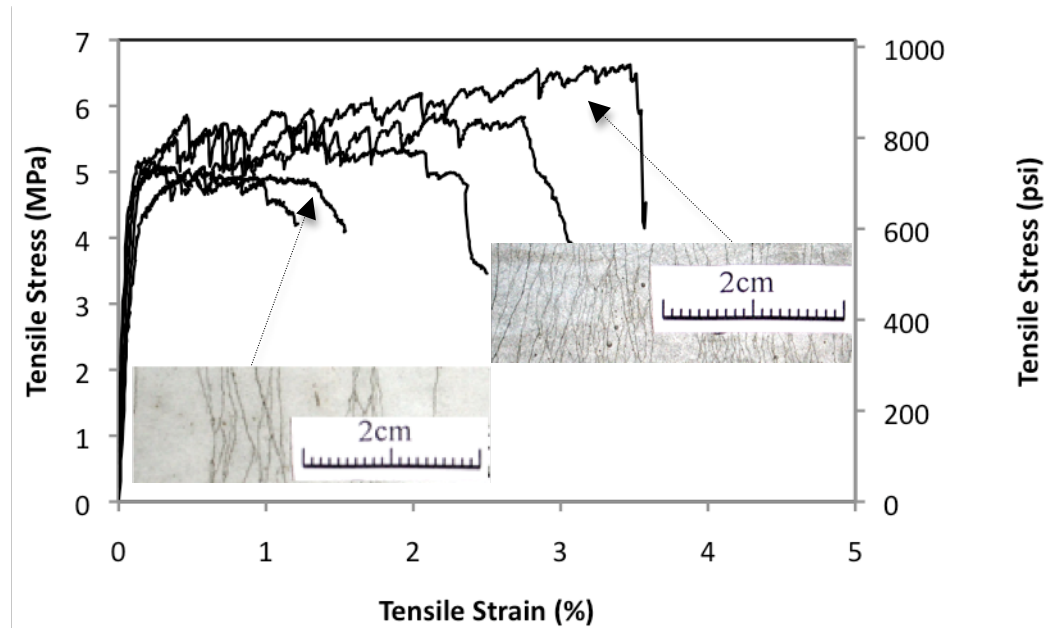


Figure 3.1 – Variation in tensile stress vs. strain curves of ECC with same mixing proportion.

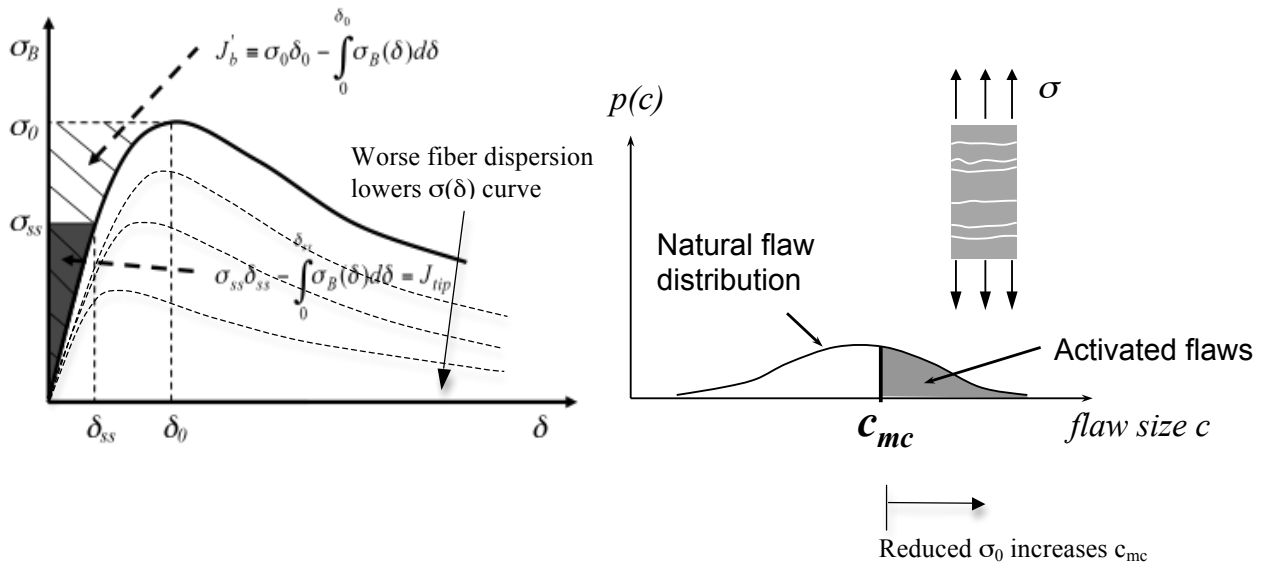


Figure 3.2 – Effect of fiber dispersion on  $\sigma(\delta)$  curve and  $c_{mc}$ .

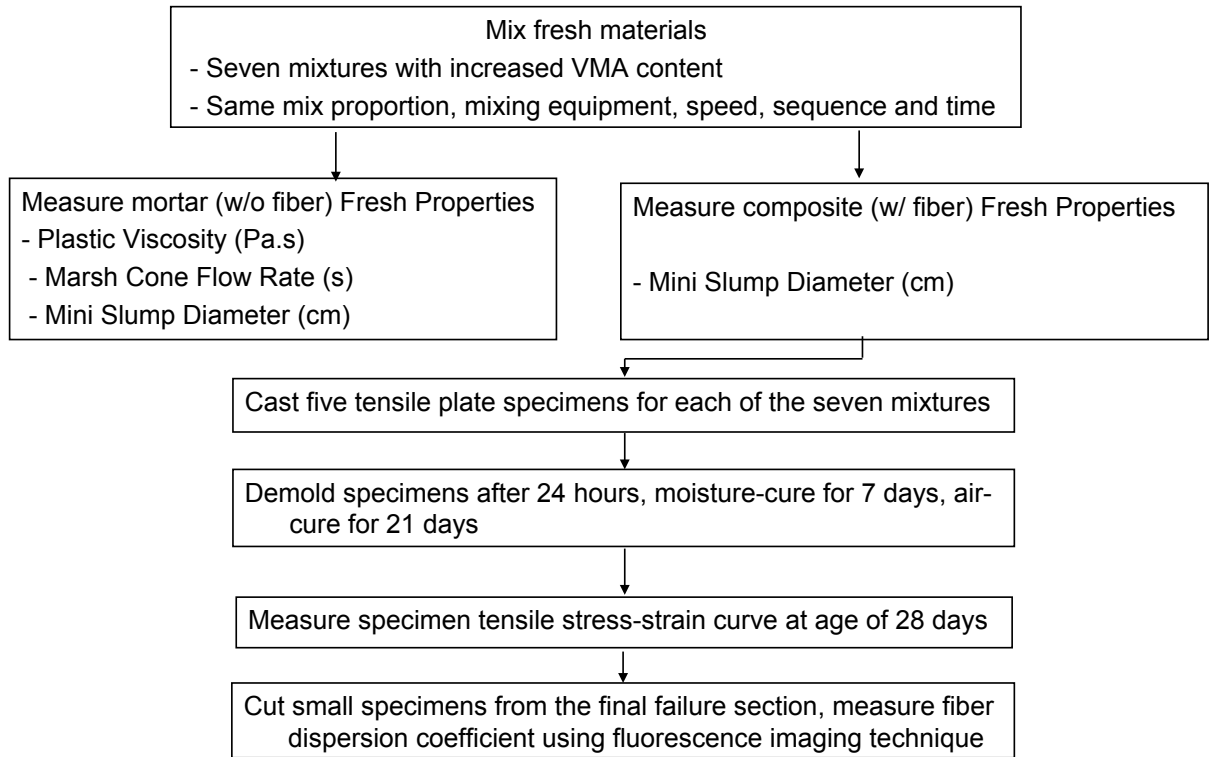


Figure 3.3 – Experimental program.

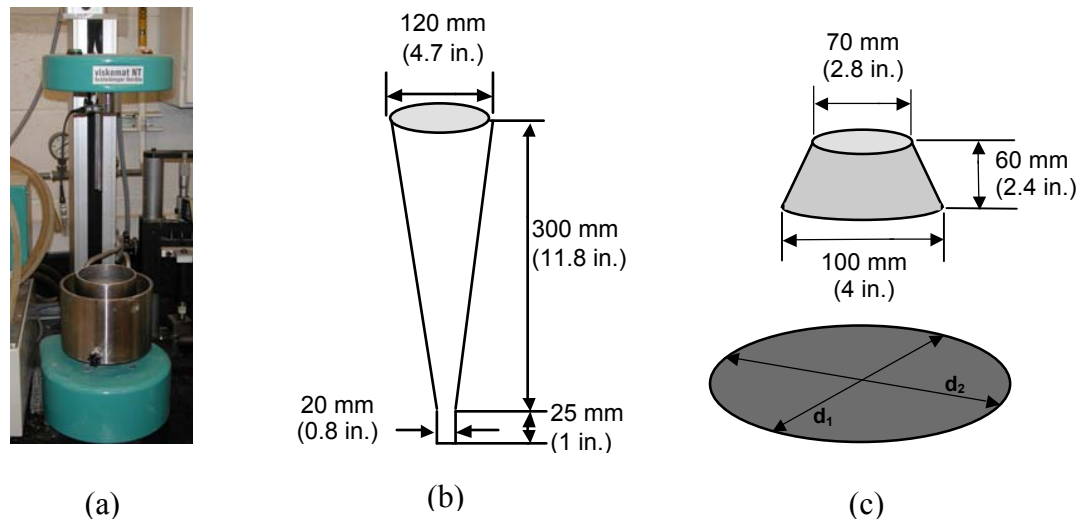


Figure 3.4 – Rheology properties tests: (a) Viskomat NT rotational viscometer (b) marsh cone flow rate test (c) mini-slump test.

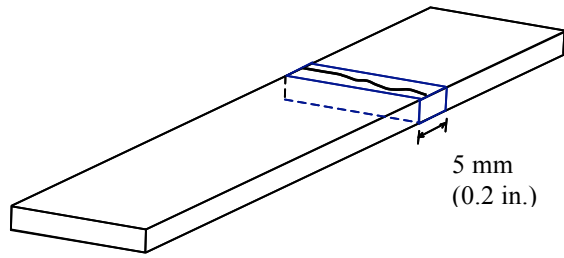


Figure 3.5 – Specimen preparation for measuring fiber dispersion at the final failure section.

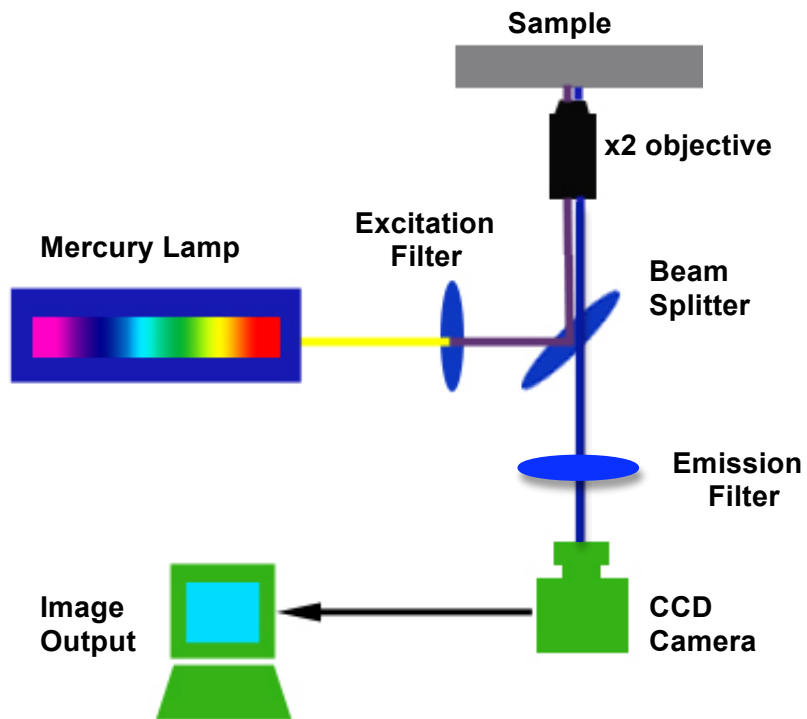


Figure 3.6 – Fluorescence imaging technology.

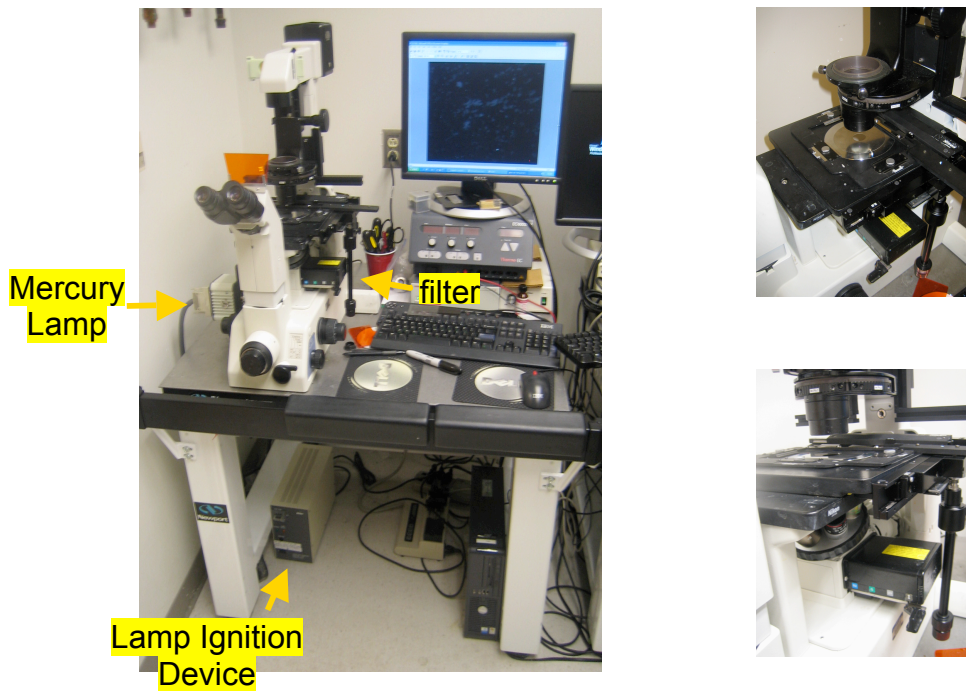


Figure 3.7 – Fluorescence imaging test setup.

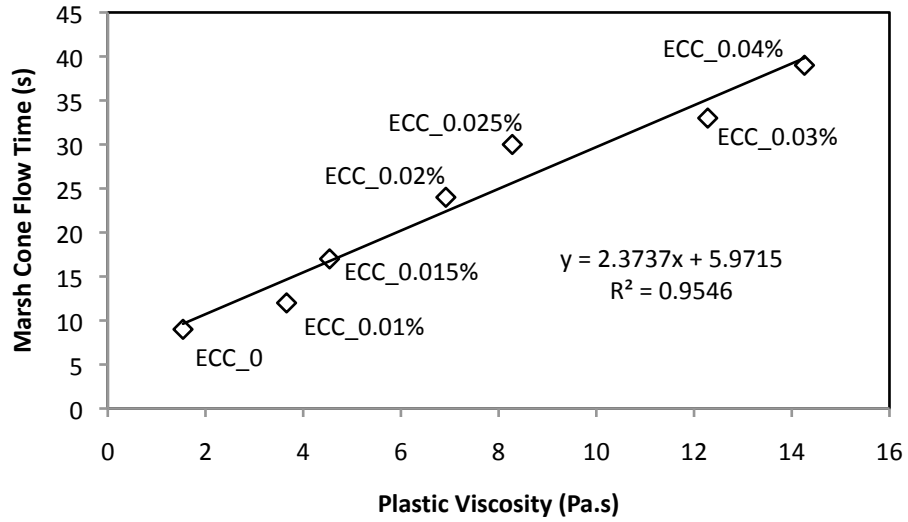


Figure 3.8 – Marsh cone flow time versus plastic viscosity.

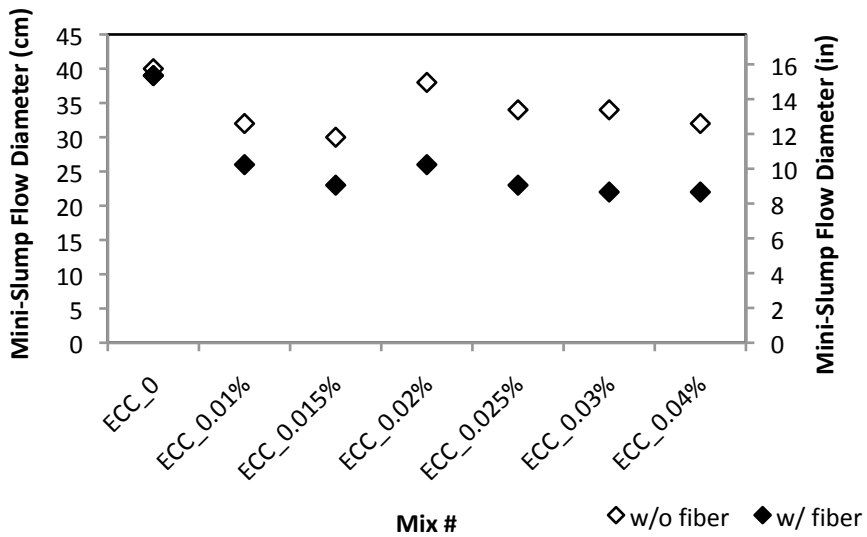


Figure 3.9 – Mini-slump flow diameter of the seven ECC mixes before/after adding fibers.

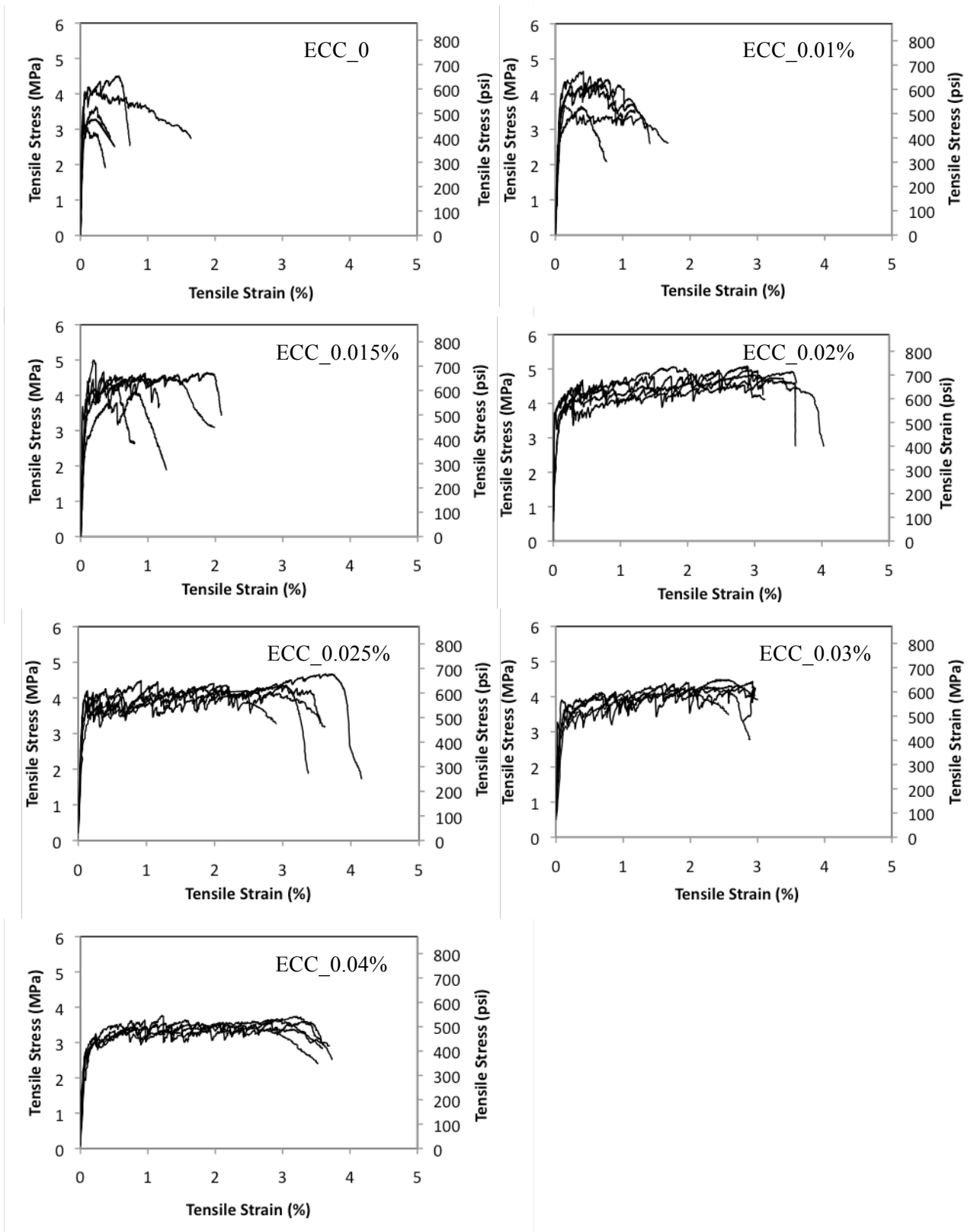


Figure 3.10 – Tensile stress versus strain curves of ECC with different VMA content.

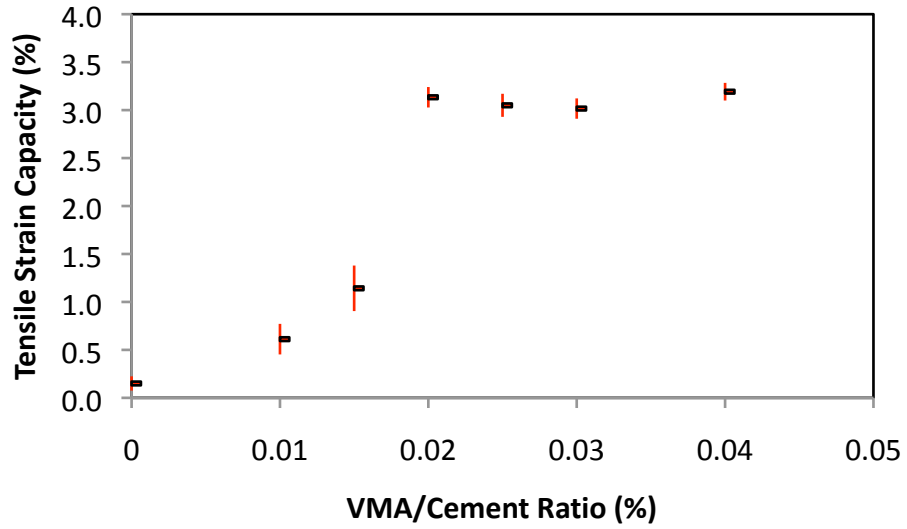


Figure 3.11 – Tensile strain capacity vs. VMA/cement ratio (error bars describe standard error of the data).

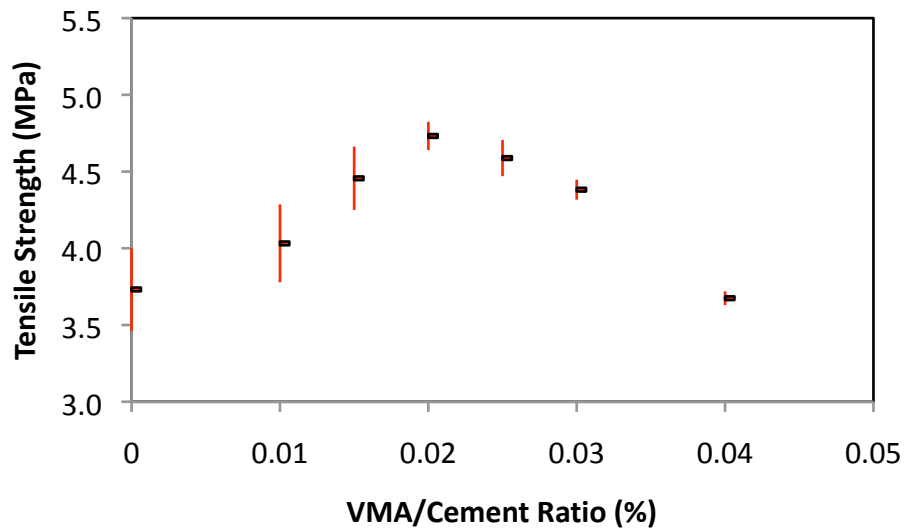


Figure 3.12 – Tensile strength vs. VMA/cement ratio (error bars describe standard error of the data).

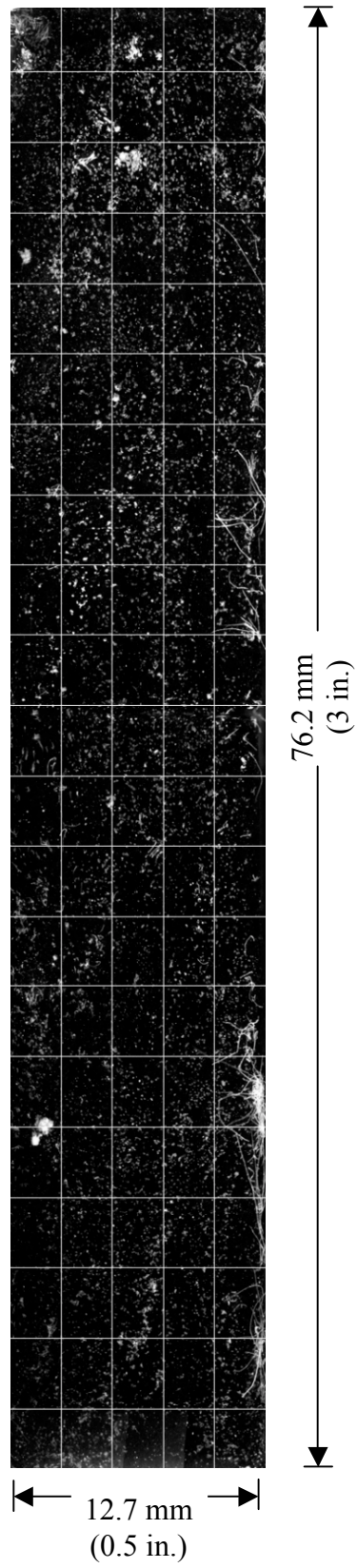


Figure 3.13 – Fluorescence image of a sample specimen.

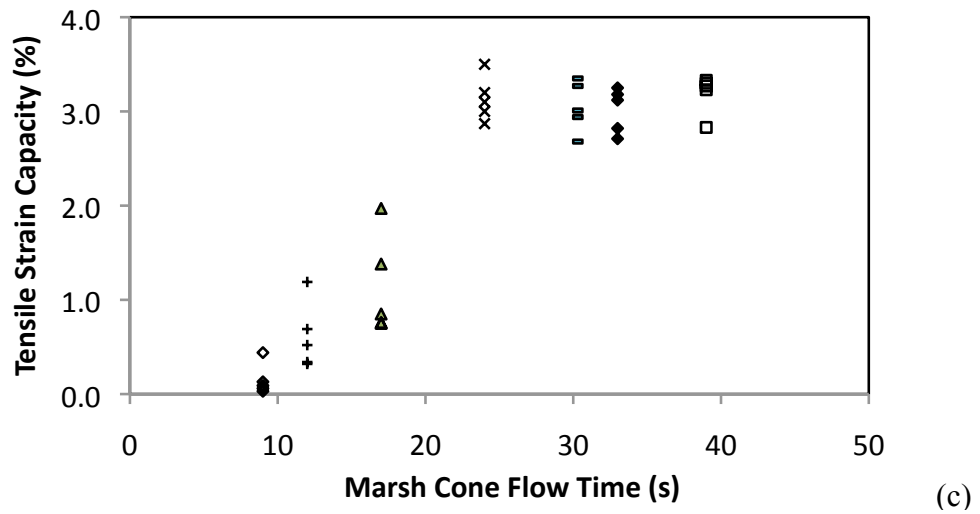
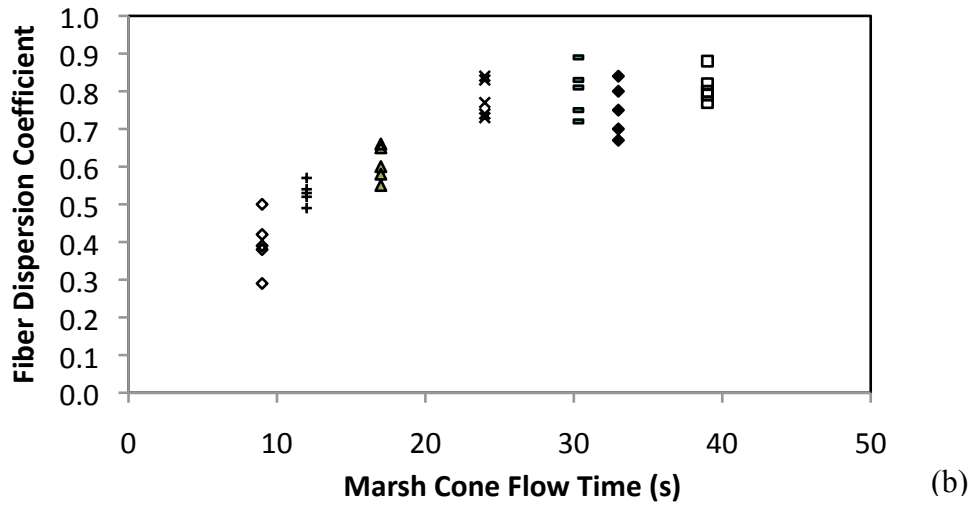
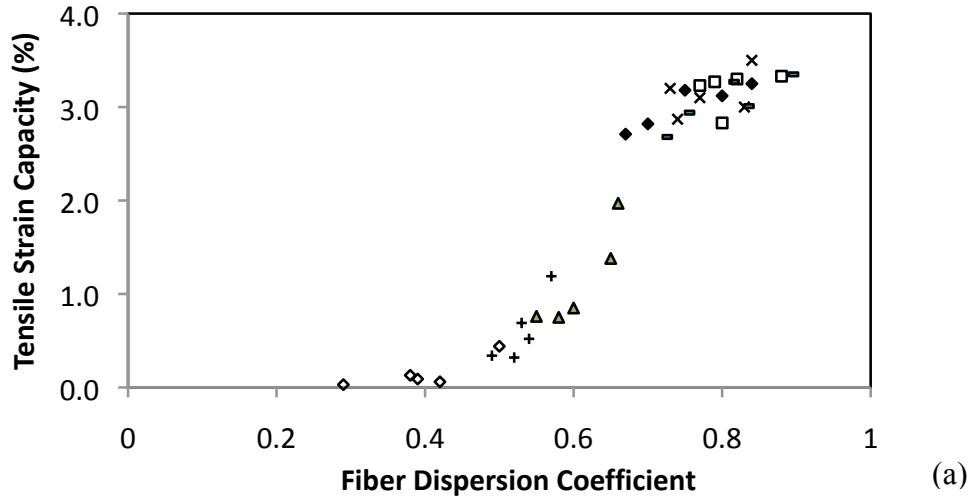


Figure 3.14 – Relation between marsh cone flow time before adding fiber, fiber dispersion coefficient, and tensile strain capacity.

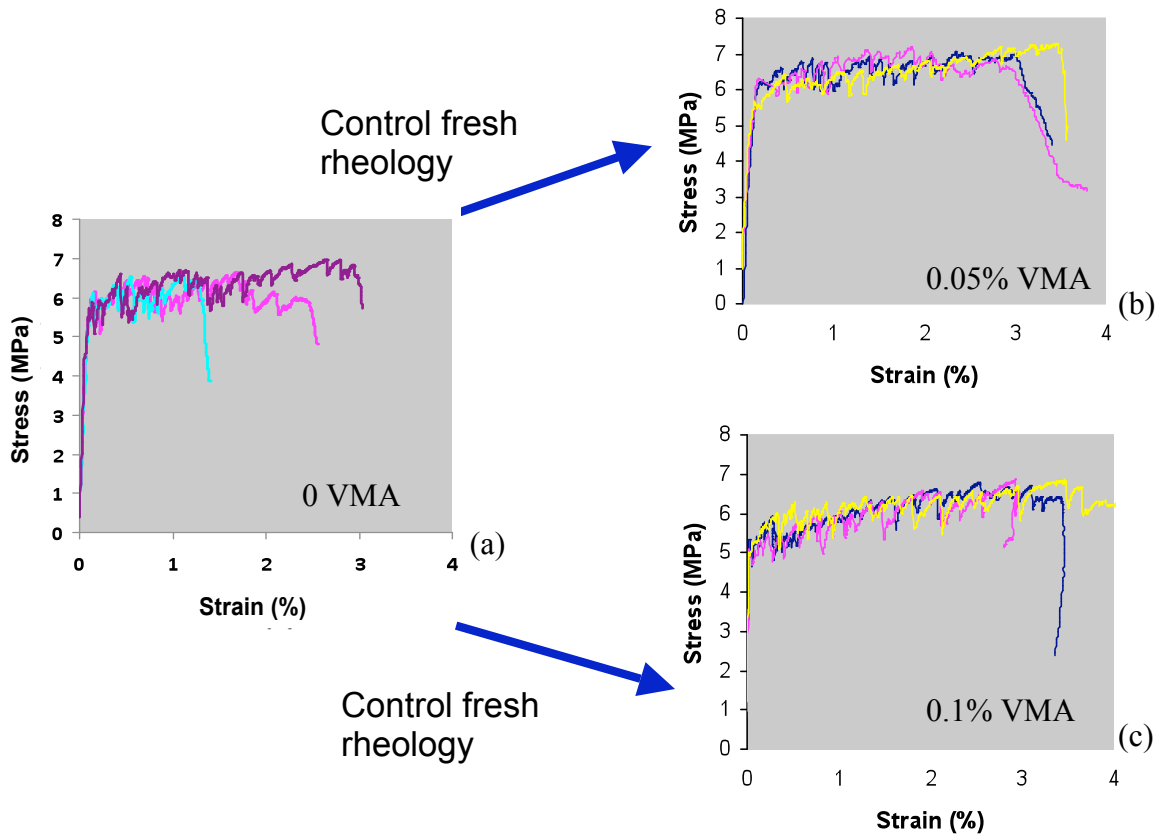


Figure 3.15 – Effect of rheology control on tensile properties of WHITE ECC: (a) A version of WHITE ECC - “MMX-ECC v4” with 0 VMA content and Marsh cone flow rate of 12 s in fresh state; (b) “MMX-ECC v4” with 0.05% VMA content and Marsh cone flow rate of 28 s in fresh state; (c) “MMX-ECC v4” with 0.1% VMA content and Marsh cone flow rate of 38 s in fresh state.

## References:

- 
- <sup>1</sup> Li, V. C., "Integrated Structures and Materials Design," *RILEM Journal of Materials and Structures*, Jan. 2006, pp. 1-10.
- <sup>2</sup> Ozyurt, N., Mason, T. Ol, and Shah, S. P., "Correlation of fiber dispersion, rheology and mechanical performance of FRCs," *Cement and Concrete Composites*, Vol. 29, No. 2, Feb. 2007, pp. 70-79.
- <sup>3</sup> Chung, D. D. L., "Dispersion of Short Fibers in Cement," *ASCE Journal of Materials in Civil Engineering*, Vol. 17, No. 4, Jul./Aug. 2005, pp. 379-383.
- <sup>4</sup> Yang, E.H., M. Sahmaran, Y. Yang and V.C. Li, "Rheological Control in the Production of Engineered Cementitious Composites," *ACI Materials Journal*, Vol. 106, No. 04, June-July 2009, pp. 357-366.
- <sup>5</sup> Marshall, D.B., and Cox, B. N., "A J-Integral Method for Calculating Steady-State Matrix Cracking Stresses in Composites," *Mechanics of Materials*, No. 8, 1988, pp. 127-133.
- <sup>6</sup> Li, V. C., and Leung, C. K. Y., "Theory of Steady State and Multiple Cracking of Random Discontinuous Fiber Reinforced Brittle Matrix Composites," *Journal of Engineering Mechanics*, ASCE, Vol. 118, No. 11, 1992, pp. 2246-2264.
- <sup>7</sup> Griffith, A. A., "The phenomena of rupture and flow in solids", *Philosophical Transactions of the Royal Society of London*, Vol. A 221, 1921, pp. 163–198, <http://www.cmse.ed.ac.uk/AdvMat45/Griffith20.pdf> .
- <sup>8</sup> Wang, Y., Backer, S., and Li, V.C., "A Statistical Tensile Model of Fiber Reinforced Cementitious Composites," *Journal of Composites*, Vol. 20, No. 3, 1990, pp. 265-274.
- <sup>9</sup> Grace Chemical Company, [www.grace.com](http://www.grace.com), accessed on August 14, 2009
- <sup>10</sup> Bingham, E. C. *Fluidity and Plasticity*. New York: McGraw-Hill, 1922.
- <sup>11</sup> Schleibinger Testing Systems, <http://www.schleibinger.com>. Accessed on August 13, 2009.
- <sup>12</sup> Banfill, P. F. G., "The Rheology of Fresh Mortar," *Magazine of Concrete Research*, Vol. 43, No. 154, 1991, pp. 13-21.
- <sup>13</sup> Ferrais, C. F., and de Larrard, F., "Testing and Modeling of Fresh Concrete Rheology," *Interagency Report 6094*, National Institute of Standards and Technology, 1998.
- <sup>14</sup> Flatt, R., Larosa, D., and Roussel, N., "Linking Yield Stress Measurements: Spread Test Versus Viskomat," *Cement and Concrete Research*, Vol. 36, No. 1, 2006, pp. 99-109.

- 
- <sup>15</sup> ASTM D6910-04 Standard Test Method for Marsh Funnel Viscosity of Clay Construction Slurries
- <sup>16</sup> Roussel, N., and Roy, R. L., "The Marsh Cone: a test or a rheological apparatus?" *Cement and Concrete Research*, Vol. 35, No. 5, May 2005, pp. 823-830.
- <sup>17</sup> Clayton, S., Grice, T. G., and Boger, D. V., "Analysis of The Slump Test for On-Site Yield Stress Measurement of mineral Suspensions," *International Journal of Mineral Processing*, Vol. 70, No. 1-4, 2003, pp. 3-21.
- <sup>18</sup> Stang, H., "Scale Effects in FRC and HPRCC Structural Elements," *High Performance Fiber Reinforced Cementitious Composites*, RILEM Proceedings Pro 30, A. E. Naaman and H. W. Reinhardt, eds., 2003, pp. 245-258.
- <sup>19</sup> Bradbury, S., and Evennett, P., "Fluorescence microscopy," *Contrast Techniques in Light Microscopy*, BIOS Scientific Publishers, Ltd., Oxford, United Kingdom, 1996.
- <sup>20</sup> Rost, F. and Oldfield, R., "Fluorescence microscopy," *Photography with a Microscope*, Cambridge University Press, Cambridge, United Kingdom, 2000.
- <sup>21</sup> Torigoe, S., Horikoshi, T., Ogawa, A., and Saito, T., "Study on Evaluation Method for PVA Fiber Distribution in Engineered Cementitious Composites," *Journal of Advanced Concrete Technology*, Vol. 1, No. 3, 2003, pp. 265-268.
- <sup>22</sup> Lee, B. Y., Kim, J. K., Kim, J. S., and Kim, Y. Y., "Quantitive Evaluation Technique of Polyvinyl Alcohol (PVA) Fiber Dispersion in Engineered Cementitious Composites," *Cement and Concrete Composites*, Vol. 31, No. 6, July 2009, pp. 408-417.
- <sup>23</sup> Spring, R. S., and Davidson, M.W., "Introduction to Fluorescence Microscopy," Nikon MicroscopyU – The Resource for Microscopy Education, <http://www.microscopyu.com/articles/fluorescence/fluorescenceintro.html>, Retrieved on June 6, 2009.
- <sup>24</sup> Torigoe, S., Horikoshi, T., Ogawa, A., Saito, T., and Hamada, T., "Study on Evaluation Method for PVA Fiber Distribution in Engineered Cementitious Composite," *Journal of Advanced Concrete Technology*, Vol. 1, No. 3, 2003, pp. 265-268.